THE UNIVERSITY OF HULL

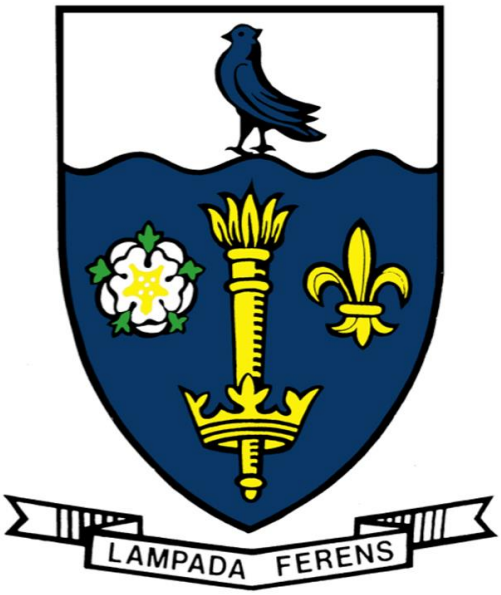

Electrical Detection of Spin State Switching in Electromigrated Nanogap Devices

Being a thesis submitted for the Degree of Doctor of Philosophy

in the University of Hull

by

Alex Gee MPhys (Hons.)

January 2020

To my family

Declaration

I declare that the work presented in this thesis is my own and has not been submitted previously for examination in any form. The experimental work throughout this thesis is my own work and has been presented at conferences and in journals. These are listed in this thesis. The literature review and theory sections contain figures and equations reproduced from journals and books and are cited where appropriate.

Acknowledgements

The work in this thesis would not have been possible without the help and support of many people. First and foremost, I wish to thank my supervisor Dr Neil Kemp for his help and advice throughout my time at Hull. He has always made time to listen and help with problems throughout my PhD and has taught me the skills necessary to become an experimental physicist. I also wish to thank Dr Šalitroš, Dr Brachňaková and Dr Kuppusamy for providing the spin crossover compounds for use in this work and Dr Massey for carrying out SQUID magnetometry for me.

An equally large amount of gratitude is given to my family and friends who have supported me through the duration of this work. My fellow PhD students deserve a big thanks. I have had many fantastic times over the course of the PhD and I wish them all the best for their future work, both in academia and industry. An extra special thanks is given to Rachel, my long-suffering girlfriend, who has had to listen to me talk about nanoimprint lithography and electromigration on a regular basis. For enduring several years of this I can only apologise!

I also wish to thank the technical and academic staff at Hull. In particular Garry Robinson and Tony Sinclair for their excellent skills with the SEM and for training me to use the microscope. I wish to thank the University of Hull for their offer of a scholarship which enabled me to take the PhD in the first place as well as providing the funding for me to present my work at several conferences.

Finally, I wish to thank eCOST for funding that enabled me to spend two months working in Finland and the Aalto Nanospin group members for working with me whilst I was there.

Publications and Conferences

- A.Gee, A.H. Jaafar, I. Šalitroš, N.T. Kemp, "**Multilevel Resistance Switching in Spin Crossover Nanogap Devices**", . Phys. Chem. C, 121, 24, (2020), DOI: 10.1021/acs.jpcc.0c03824

- A.Gee, A.H. Jaafar, N.T. Kemp, "**Bilayer Nanoimprint Lithography and Feedback Controlled Electromigration for Molecular Electronics**", Nanotechnology, 31, 15, (2020), DOI: 10.1088/1361-6528/ab6473

- H. Jaafar, A. Gee, N.T. Kemp, "**Nanorods vs Nanoparticles: A Comparison Study of Au/ZnO-PMMA/Au Non-volatile Memory Devices showing the importance of Nanostructure Geometry on Conduction Mechanisms and Switching Properties**", IEEE Transactions on Nanotechnology, 19, (2019), DOI:10.1109/TNANO.2019.2949759

- N.H. Jabarullah, E. Verrelli, A. Gee, C. Mauldin, L.A. Navarro, J.H. Golden and N.T. Kemp, "**Large Dopant Dependence of the Current Limiting Properties of Intrinsic Conducting Polymer Surge Protection Devices**", RSC Advances, 6, (2016), DOI:10.1039/C6RA18549E

- Poster presentation, "**Multi-level Electronic Switching in a Two-Molecule Spin Crossover Device"**, SpintechX, Chicago, IL, USA, 24th – 27th June 2019.

- Talk "**Fabrication of Nanojunction Devices using Nanoimprint Lithography**", EsMolNa Madrid, Spain, 7^{th} – 12^{th} May 2017.

- Summer School "**Molecular Switches at the Nanoscale**", Mittelwihr, France, 4^{th}–9^{th} September 2016.

Abstract

Spin crossover is an effect shown in some transition metal complexes where the spin state of the molecule undergoes a transition from a low spin to a high spin state via the application of light, pressure or a change in temperature. This behaviour makes these complexes an attractive candidate to form electronic molecular-scale switches as the electrical resistance of the compound differs between the two spin states. Although the spin crossover effect is commonly studied in its bulk form, the integration of a single molecule into a solid-state device while maintaining the magnetic bi-stability is highly desirable, but remains challenging. This is not only due to difficulties in capturing a single molecule between electrodes and making electrical connections but it is also due to the strong coupling effects imparted on the molecule by the high-density metallic states of the electrodes that can prevent the spin transition from occurring.

In recent years there have been many attempts at studying spin crossover complexes at a single molecule level. Many of these have used scanning tunneling microscopy or break junction techniques. While these studies have highlighted the unique and promising electronic properties of these compounds, these techniques are unsuitable for real world devices. This thesis demonstrates a means to make electrical contact to single or small numbers of molecules between gold electrodes fabricated using a bilayer nanoimprint lithography and a feedback controlled electromigration method. This method, enabling high throughput and low-cost fabrication is potentially suitable for scaling to large area planar devices and as such may be used for commercially producing molecular devices.

To validate the quality of the nanogaps, devices containing self-assembled monolayers of benzenethiol were first studied. The shape and magnitude of I-V curves measured on nanogap devices containing the benzenethiol monolayers are in good agreement with previously published work using similar molecules in mechanically controlled break junctions. The resulting I-V characteristics were analyzed using the single level resonant tunneling model as well as transition voltage spectroscopy and are consistent with transport through molecular junctions in which the benzenethiol molecules are π-stacked. These highly conducting molecular junctions may have potential uses for "soft" coupling to sensitive target molecules.

Following validation of the molecular nanojunction fabrication and measurement process, the experimental work shifted to studying electronic transport through spin crossover complexes with a focus on Schiff-base compounds that are specifically tailored for surface deposition. In the case of measurements made on the bulk compound, a sharp spin transition centered at a temperature around 80 K was observed, while a shift to lower temperatures was found for thin films of the complex. In contrast, nanojunction devices containing single molecules displayed very different behaviour, with distinct and reproducible telegraphic-like switching between two resistance states when cooled below 160 K. These two states are attributed to the two different spin states of the complex. The presence of these two resistive states indicates that the spin crossover is preserved at the single molecule level and that a spin-state dependent tunneling process is taking place. Interestingly, in some cases a multi-level switching behaviour is detected with four possible conductance states. This behaviour is attributed to the presence of two spin crossover molecules in the nanogap.

Contents

Introduction

1.1 Background

Chapter 1

Spin crossover (SCO) compounds are a class of metal-ligand complexes that have promising applications in a number of technologies. They display bistable spin state switching between high spin (HS) and low spin (LS) states which is commonly brought about by a change in temperature.[1] The change in spin state is accompanied by a change in the compounds magnetic, optical and mechanical properties.[2]

Due to this ability to switch between two states with very different properties SCO compounds have been the subject of a great deal of research, not only because of a fundamental interest in this unique behaviour but also because these compounds show promise as the building blocks from which to construct devices with a range of possible functionalities.[3] In addition to the magnetic, optical and structural changes that occur in a compound undergoing SCO, in recent years, the electrical properties of these compounds have started to be investigated at both a macroscopic and single molecule level.

Molecular electronics is a flourishing interdisciplinary field combining aspects of chemical design and synthesis, low noise electronic measurement, vacuum and surface science as well as top-down nanofabrication techniques. Molecular electronics is defined as the field of science concerned with the study of electronic transport in circuits that incorporate single or small collections of molecules as the active functional component. In this way it is distinct from organic electronics which focusses on the macroscopic electrical behaviour and applications of thin organic films.

With the end of Moore's law in sight for traditional microelectronics [4][5] but with the continued drive for smaller component sizes, molecular electronics is envisioned as one route to continue this trend.[6] Molecules are the smallest possible building block and represent the ultimate in miniaturisation.

The versatility that molecules offer adds additional motivation to this field. The vast array of chemical groups offers multi-functionality, that is, the ability of these compounds to respond to many different stimuli such as light, pressure, electrical field, electric current, temperature, etc. and in combination with this, bottom-up fabrication techniques such as self-assembly makes the use of molecules an attractive basis around which to produce new electronic devices. Already this field has attracted widespread interest both from the research community and industry due to the wide-ranging potential applications (see for example recent work by IBM Zurich [7]).

The first mention of the term molecular electronics can be traced to a collaborative effort between the company Westinghouse and the United States Air Force in the late 1950's.[8] This work aimed to find alternatives to the newly emerging field of semiconductor electronics. While successful in developing new fabrication techniques, this work was ultimately superseded by the rapid progress being made in silicon integrated circuit manufacturing. In the 1970's work at the University of Göttingen succeeded in producing molecular thickness films and also the incorporation of these films into devices with top and bottom electrodes. Around the same time, Avi Aviram and Mark Ratner in the US began exploring ideas of using molecules as electronic components, drawing parallels between the p-n structure of a standard semiconductor diode and charge transfer salts - molecules containing regions rich and poor in electrons.

These ideas were later confirmed experimentally by measurements made on γ-hexadecyl-quinolinium tricyanoquinomethanide monolayers.

Since the 1980's the field has grown significantly owing mainly to the experimentally accessible methods of imaging, contacting and manipulating single molecules on surfaces using scanning tunnelling microscopy and atomic force microscopy. These versatile techniques allow for fast and detailed characterisation of molecular behaviour but still very much remain laboratory-based techniques, unsuitable for producing devices or complex circuits in a commercially viable manner.

Molecular devices have been shown to replicate classic nanoscale effects such as Coulomb blockade and behave as single electron transistors (SET). Molecular switches based on single rotaxane molecular layers have been shown to replicate switching behaviour such as that necessary to form the basic building blocks of a logic circuit or memory element but with an ultra-high storage density (6.4 Gbits cm^{-2}).[9] Further developments in this field have led to graphene-based single molecule devices incorporating diarylethenes as the active switching component as demonstrated by Guo *et al.* displaying remarkable stability (over 1 year) for a device of this size.[10] Moreover these devices are photo-switchable, opening doors to applications in photonic computing and optical signalling. High-speed operation has recently been demonstrated for a molecular rectifier based on ferrocenyl undecanethiol.[11]

Spintronics or spin transfer electronics is the field responsible for many recent technological advances, namely the massive increase in storage capacities of hard disk technology as a result of miniaturised magnetic field sensors. It is also the origin of new types of memory such as magnetoresistive random-access memory (MRAM) and emerging next generation technologies such as spin-transfer torque (STT) memory

thermal-assisted switching (TAS) memory and racetrack memory. Spintronics differs from traditional electronics in that it addresses an additional degree of freedom, namely the electron spin, in addition to electron charge to produce new device functionalities.

The archetypal spintronic device is the spin-valve, consisting of two magnetic electrodes separated by a non-magnetic spacer or barrier material. In this device the resistance state can be modulated by the presence of an external magnetic field. The relative orientation of the spin polarized currents in addition to the spin dependent scattering or tunnelling mechanism at work within the device determine both the sign and magnitude of the resistance change. These resistance changes can take the form of giant magnetoresistance (GMR) or tunnel magnetoresistance (TMR) depending upon device type.

The independent discovery of GMR by Fert and Grünberg in 1988[12][13] led to rapid commercialisation of ultra-small GMR based magnetic field sensors beginning in 1997. This discovery enabled a significant increase in magnetic hard disk storage capacity from around 1 Gbit/in^2 to over 600 Gbit/in^2 in 2008[14] and was recognised by Fert and Grünberg being awarded the 2007 Nobel Prize in Physics.

Molecular spintronics represents a further extension of the concepts relevant in both traditional spintronics and molecular electronics and is concerned with the spintronic behaviour of a magnetic device when the dimensions are reduced down to the atomic scale. Over the past several years there has been considerable effort in producing molecular based spin-valves. Most notable is a form of molecular spin-valve recently demonstrated using single TbPc (Pc = phthalocyanine) complexes arranged onto a single walled carbon nanotube (SWCNT).[15][16][17] This work represents a significant accomplishment in producing a molecular spintronic device, showing reproducibility as

well as a high magnetoresistance of 300%. However, quantum tunnelling of the magnetisation, which at room temperatures presents itself as a very rapid fluctuation of magnetisation direction of the TbPc molecule, limits the operation of these types of devices to only very low temperatures.[15]

Rather than using the direction of the spin quantisation in molecules positioned between electrodes, it has been suggested that a more successful approach is to use the total spin magnitude of a molecule as a means to change the resistance state of the device, with a switch from high to low spin having a corresponding switch in the resistance state of the device. Suitable molecular candidates for this role are the spin crossover compounds.[18][19]

1.2 Thesis Objectives and Structure

This thesis will outline the methodology behind making electrical measurements at a single molecule level using electromigrated nanogap devices fabricated using nanoimprint lithography and feedback controlled electromigration.

A high throughput and low-cost method of producing large numbers of nanojunction devices is presented that uses a unique bilayer nanoimprint technique. It expands upon conventional nanoimprint lithography processes to enables a clean, tear-free, lift-off in the fabrication of devices on oxidised silicon substrates with nanoscale sized features.

To make nanogap devices with gap sizes ≤ 2nm, very small conducting channels were first made using the nanoimprint lithography technique. Electromigration was then used to move atoms away from the central region of the conducting channel to form the nanogap. An in-house built electromigration system was made specially for this purpose.

Initial work focussed on producing nanoscale gaps in Permalloy nanojunctions that were fabricated using a more conventional single step nanoimprint process. The resulting nanogaps were then characterised using a combination of scanning electron microscopy (SEM) and electrical measurements to confirm their quality. After this initial work, the fabrication process shifted to a bilayer nanoimprint technique, to improve the device yield and different materials (Au, Co) were experimented with for making nanogap electrodes.

To demonstrate the validity of our devices for measurements at a single molecule level, diphenyl disulphide molecules were used to form devices with integrated benzene dithiol (BT) molecules. The I-V properties of these molecular junctions were measured and comparisons were made between the traditional Simmons tunnelling model and the single level resonant tunnelling model. The transition voltage spectroscopy technique was also used to identify the onset of conduction in these BT devices.

After proving our methodology for producing molecular devices, the research then moved on to investigating SCO compounds deposited onto Au nanogap electrodes. In this research it was discovered that some devices showed a temperature dependent resistance bistability which is indicative of the preservation of the SCO phenomenon at a single molecule level. In addition, multi-level resistance behaviour was also observed, which we attribute to the presence of two switching molecules present within the nanogap.

Finally, in the last chapter of this thesis, the major conclusions of this work are summarised and a brief discussion on the future outlook of this work in regards to using SCO materials in electrical memory devices is made.

Chapter 2

Literature Review

The earliest ideas of incorporating and utilising molecules as the active electronic component within a device dates back to the work of Mark Ratner and Ari Aviram in the 1970's. They theoretically proposed using the charged features of certain molecules to form a molecular diode. Specifically, molecules displaying a $D-\sigma-A$ structure were proposed where D represents a donor unit with high electron density while A represents an acceptor unit with low electron density. The two units are both separated by a molecular bridging unit, σ. Many examples of devices based on these types of molecules exist[20][21][22] and the field has progressed to the point where molecular rectification has been demonstrated at frequencies of up to 17 GHz[11] and also high rectification ratios of over 200.[23]

The idea behind making an electrical measurement on a molecule is in principle straightforward. Simply put all that needs to be done is to place a single molecule or a small collection of molecules between two conductive electrodes and measure the I-V characteristics or expose the device to other stimuli for example, light irradiation or modification of the local chemical environment. However, in practice this is very challenging simply because of the extremely small size of a typical molecule. The necessity to provide an electronic link from these length scales to measurement equipment makes this a difficult undertaking and a great deal of effort and multitude of different experimental approaches are still being developed to carry out this task.

Recently there has been interest in the use of spin crossover materials as the active switching component of an electronic device. A brief background of the spin crossover phenomenon is covered before then reviewing the current progress that has been made

in incorporating SCO compounds in devices as both thin films, nanoparticles as well as at a single molecule level.

2.1 Electrically Contacting Single Molecules

2.1.1 Review of Current techniques

Contacting single molecules is not an easy task simply because of the dimensions of molecules in relation to the macroscopic world. The highest resolution obtainable using standard lithographic techniques (electron-beam writing or nanoimprint) is around 10 nm.[24][25] This is still more than one order of magnitude larger than the size of a typical molecule (1 nm and smaller) and so alternative methods must be used to fabricate electrodes.

Some of these methods include scanning tunnelling microscopy, contact mode atomic force microscope, mechanical break-junctions and electrochemical deposition techniques. These are briefly outlined below.

2.1.1.1 STM and C-AFM

The scanning tunnelling microscope (STM) is type of surface probe microscope combining an ultra-sharp metal tip with a high-resolution scanning mechanism usually based on a piezoelectric scanning stage, figure 2.1 a). Its development by Binnig and Rohrer while working at IBM Zurich earned them the Nobel prize in Physics in 1986.[26] Using this technique, an image of a conductive sample may be built up by scanning the surface while maintaining the tunnelling current between tip and surface at a fixed value using a feedback mechanism.

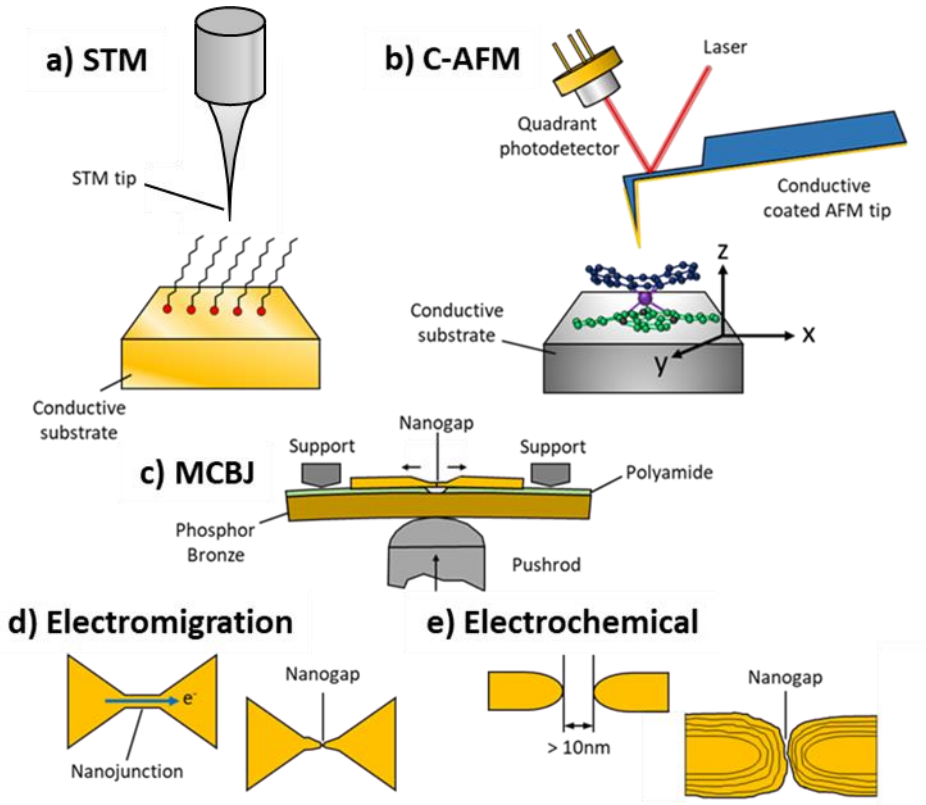

Figure 2.1 *- Techniques used to electrically contact single molecules a-b) Scanning probe techniques STM and C-AFM, c-e) planar device types including the MCBJ, electromigration and electrochemical techniques, respectively.*

By choosing a suitably flat and clean substrate, usually prepared *in-situ* by high temperature annealing and/or ion sputtering, a deposited molecule may be observed against the substrate surface. By placing the tip above a region of interest, for example a molecule, the I-V characteristic can be obtained by opening the feedback loop and sweeping the voltage applied to the tip.

A related technique is conductive-atomic force microscopy (C-AFM), figure 2.1 b) where a coated tip, usually made of Si, is used to both image and electrically contact molecules on a surface.[27] This technique shares many similarities including a high resolution piezoelectric scanning mechanism and feedback mechanism but relies on the interatomic repulsion/attraction that is present between tip and substrate and not a

tunnelling current. Most modern C-AFM systems sense the tip position using a laser feedback system.[28] This technique typically does not have the same level of resolution as STM and hence is more suited to imaging self-assembled monolayers on conductive substrates as well as samples which have both conductive and non-conductive regions of interest.

Because of the ability to image a molecule first before performing electrical measurements, STM is a very powerful tool for molecular electronics allowing detailed structural information about the adsorption and binding arrangement of molecules with surfaces to be gained while also simultaneously allowing for the electronic properties of molecules to be investigated. A great benefit is that many molecules can be identified on a surface, allowing for the repeated formation of a molecular junction, something which can be very time consuming if a single device is to be made for each measurement. However, the challenges associated with making these measurements, namely stability, cost and the complexity of operating these types of systems limits the availability of this technique.

2.1.1.2 Electrochemical Techniques

An alternative approach which has been used to make electronic measurements on single molecules utilises electrochemical deposition to produce a nanogap between two metallic conductors, figure 2.1 e).[29][30][31][32] In this technique a relatively large gap is first fabricated onto a substrate. The device is then immersed into an electrolyte solution containing metal ions and an electroplating process begins with the prepatterned metal forming the working electrode of an ultra-small electrochemical cell. Other electrodes are situated nearby which act as reference and counter electrodes.

These are either prepatterned onto the substrate near the working electrode or placed into the container with the electrolyte solution.

With a feedback mechanism the gap size can be controlled via successive plating and etching cycles. Typically, an Au working electrode is used and Ag is deposited from solution but this technique has been extended to include even the fabrication of ferromagnetic nanogaps.[33] One advantage of this method is that electrodes can be fabricated with dissimilar metals. Another is that electrochemical deposition technique can then be used to deposit molecules, *in situ,* directly within the formed nanogap. This technique even allows the possibility of synthesis of molecules locally within the nanogap.

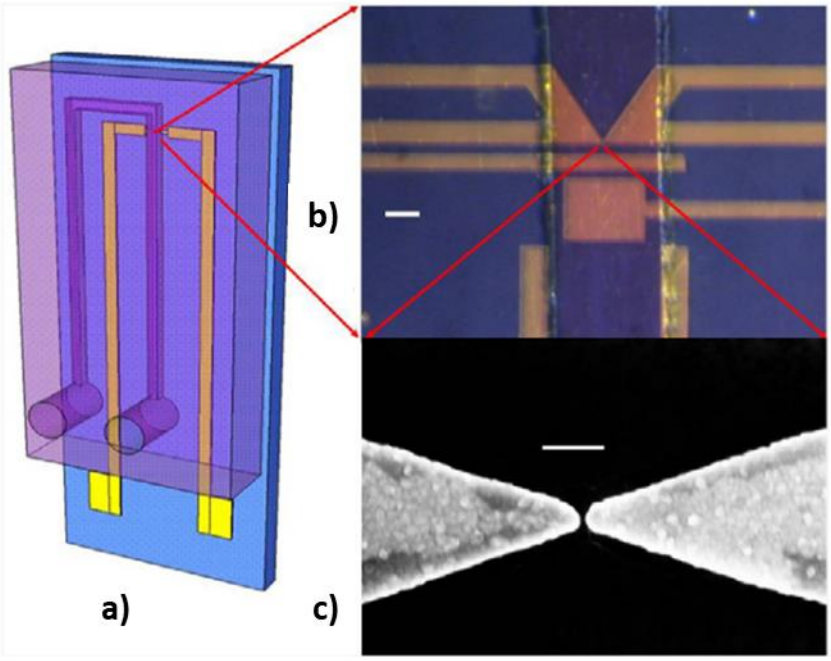

Figure 2.2 *- a) Silicon-PDMS microfluidic chip incorporating a b) miniature electrochemical cell, scale bar 5 µm and c) initial Au electrodes, scale bar 200 nm. Reproduced from* [29].

This method has had many successes. Xie *et al.* have demonstrated a gate controlled atomic-scale switch whereby the addition or removal of a single Ag atom using an

external electrochemical electrode modifies the conductivity of the device by one unit of the quantum conductance.[34]

This method also allows for the possibility of chemically modifying the electrodes as the device already exists in a wet chemical environment. This can be achieved, for example, by combining this technique with a microfluidic device as shown in figure 2.2 so that chemical groups can be attached to the newly formed nanogap electrode surfaces in a stepwise manner by first forming the nanogap electrodes through plating and then replacing the electrolyte with the required chemical solution allowing for successive chemical modification of the nanogap.[29] The disadvantages of this approach have led to it being dropped in favour of other techniques. These disadvantages generally relate to the poor mechanical stability of devices as well as the potential for contamination. Additionally, the device must be maintained in a liquid environment preventing measurements being made in vacuum or in cryogenic conditions.

2.1.1.3 Mechanically Controlled Break Junctions

One of the most successfully used techniques in molecular electronics is the mechanically controlled break junction (MCBJ) figure 2.1 c).[35][36][37] In this technique a thin wire is patterned on-top of a flexible support structure as shown in figure 2.3. This wire is made with a constriction of around 100 nm or less. The substrate is flexed until the wire breaks and produces a gap of around a few nanometres or less. The great advantage is that the width of the gap is fully controllable once it has formed. The gap size can be shortened by relaxing the support or lengthened by again flexing the substrate. Some of the setups used for this technique can be complex with the mechanism used to break and open the gaps provided by a very high-resolution piezo

stage. Due to the mechanical arrangement of the bending beam and supports a piezo push-rod with nanometre level resolution can translate into sub-angstrom control of the gap size.[35] In many systems the whole setup is housed in a cryostat capable of cooling to cryogenic temperatures so that highly stable or temperature dependent measurements can be performed.

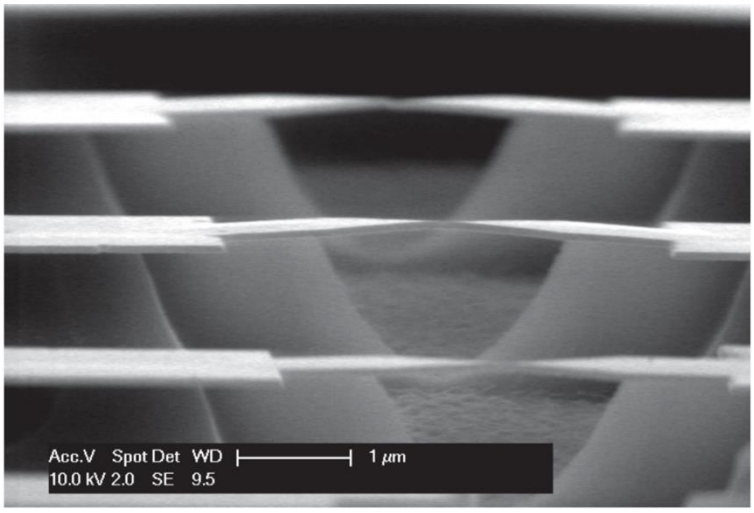

Figure 2.3 *- SEM image of a MCBJ device showing freestanding metallic nanojunction on a polyamide support structure. Image reproduced from* [37].

The great benefit of this technique is that many repeated openings and closings of the gap can be made allowing for length dependent effects to be studied and conductance histograms as a function of gap size to be built-up. These types of measurement can also reveal the signature of a molecule between the electrodes as the appearance of a plateau in the conductance vs gap size.[38] This is due to conduction occurring preferentially through a molecule as it binds to and bridges the electrodes, a behaviour that is easily discriminated from vacuum tunnelling which has an exponential dependence with the gap size.

This was the approach taken by Reed *et al.* in 1997 of the first reported electrical measurement of a single molecule in a planar type device. This point marks the birth of molecular electronic in a practical sense (excluding measurements made previously with STM). A single benzene-1,4-dithiol forms a molecular bridge between the two Au electrodes, figure 2.4 a). As shown in figure 2.4 b), the current flow through a device shows a notable current suppression at low bias, due to on- and off-resonant transport. This types of transport is described by the resonant tunnelling model (see 3.1.3).

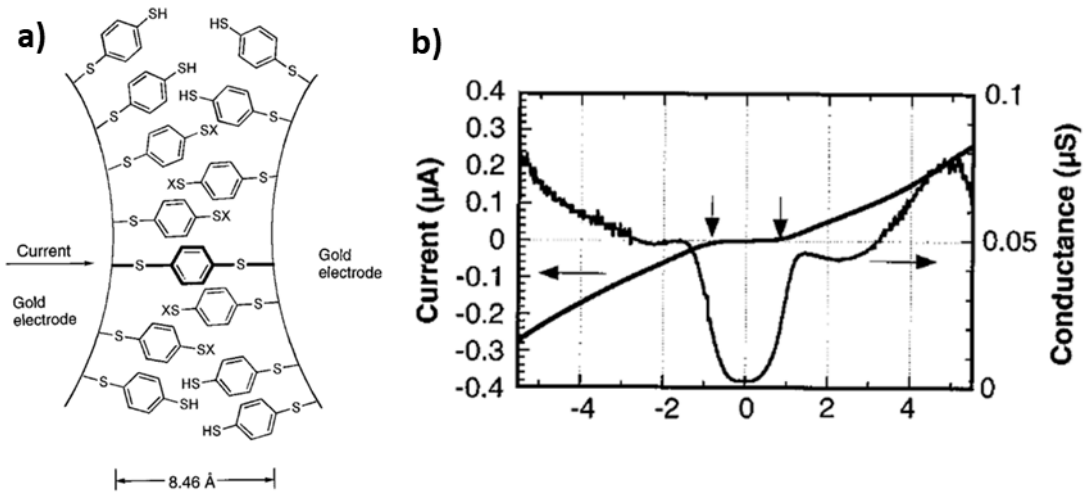

Figure 2.4 *- a) Proposed arrangement of a Au/benzene-1,4-dithiol/Au molecular junction as first investigated by Reed et al. b) I-V and dI/dV characteristics of a molecular device showing a voltage suppression (gap) of approximately 0.7 V. Reproduced from* [36].

At the time of this work, the theoretical behaviour of a single molecule device was still in its infancy and results are mixed in predicting the behaviour of these experiments with some predicting linear behaviour and others reproducing the current suppression at lower bias.[39] The benzene-1,4-dithiol has become a testbed system in molecular electronics and subsequent measurements have reported varying levels of conductivity from approximately 0.011 G_0 [40] at zero bias to conductance values as low as 5×10^{-5} G_0 [41]. Here G_0 corresponds to the conductance quantum and has a resistance value of

approximately 7.75×10^{-5} S or 12.9 kΩ. This discrepancy in experimental results can be attributed to different binding arrangements of benzene-1,4-dithiol to the Au electrodes [42][43] and with discrepancy between theoretical results now realised to be due to the different calculation methods available.[8]

2.1.1.4 Electromigrated Break Junctions

Owing to their mechanical stability and the possibility of incorporating a gate electrode with high molecular coupling, the electromigrated nanojunction, shown in figure 2.1 d), is a popular technique.[8] With this technique, a thin metal wire (nanojunction) is first fabricated on a rigid substrate. This is then connected to leads and contact pads so that electrical contact can be made using a probe station or using wire bonding.

As its name suggests, the process behind forming this kind of break-junction is based on the process of electromigration. This is the processes that occurs under a sufficiently high current density whereby the metal ions that make up the nanojunction can be forced out of their normal lattice positions. For gold this occurs once the current density flowing through the constriction surpasses the electromigration threshold (typically at a value of 10^8 Am^{-2} for gold).[8] As the voltage across a metallic wire is increased, the point at which electromigration begins is signalled by an irreversible increase in its resistance as the cross-sectional area narrows due to material transport. A thinning (or pinching) of the conduction channel in the lateral direction occurs usually at the midpoint of the channel where there is maximum heating or at desired position along the length of the channel, that can be determined by placing a notch. With continued application of a current, usually imparted via voltage pulses, the pinching effect occurs until at some point, a single atom is present. This is confirmed by the observation of

quantized steps in the conductance.[8] With time, and or more application of pulses, a gap typically forms, which generally consists of the formation of a sub-2 nm gap between the two electrodes.

The electromigration technique was first demonstrated by Park *et al*. as a means by which nanometre-separated electrodes can be produced for electrical measurements on single molecules.[44] The first approach was rather simple, increase the voltage applied to a metallic constriction and monitor the current. At a certain point the wire fails which is signified by a sudden drop in the current. After the bias is removed around 15% of devices showed a tunnelling current large enough to be measured. Later this electromigrated nanogap fabrication was improved using feedback techniques as well as multi-ramp processes.[45][46][47]

The electromigration technique has been shown to work well with noble metals, Au[47][46], Ag[48] and Pt[49][50] which are popular as they resist oxidation and allow for functionalisation with molecules containing thiol groups. Electromigration has also been used to form nanogaps in other metals such as Ni[8][51], Permalloy (Ni/Fe alloy)[52] and Co[51] by using a feedback or multi-ramp processes that gradually thins the conductor before carrying out the final breakage.

Typically, the nanojunction is fabricated using electron-beam lithography (EBL) using a lift-off or thin film etching technique. This can make the fabrication of a device a slow and costly process. Other techniques have been used that involve stencil lithography which avoids the need to use expensive EBL facilities but still requires the fabrication of a stencil and use of high precision deposition stage.[53][54] These are fragile, time consuming to use and have a limited lifetime before cleaning is required to remove the

build-up of deposited material. A comprehensive review of nanogap fabrication techniques using electromigration can be found by Hoffman-Vogel.[55]

2.1.2 Conductance Evolution of a Nanojunction During Electromigration

When a metallic conductor is thinned continuously from a macroscopic length-scale then the conductance will initially decrease in accordance with the following dependence:

$$G = \sigma \frac{A}{l} \tag{2.1}$$

where σ is the material specific conductivity, A is the cross sectional area and l is the length of the metallic conductor. With a continued reduction in the size the measured conductance departs from this relationship and conductance begins to evolve in a discontinuous manner. Jumps in conductance are related to the quantum wave-nature of electrons traversing the constriction as well as the atomistic make-up of the conductor.

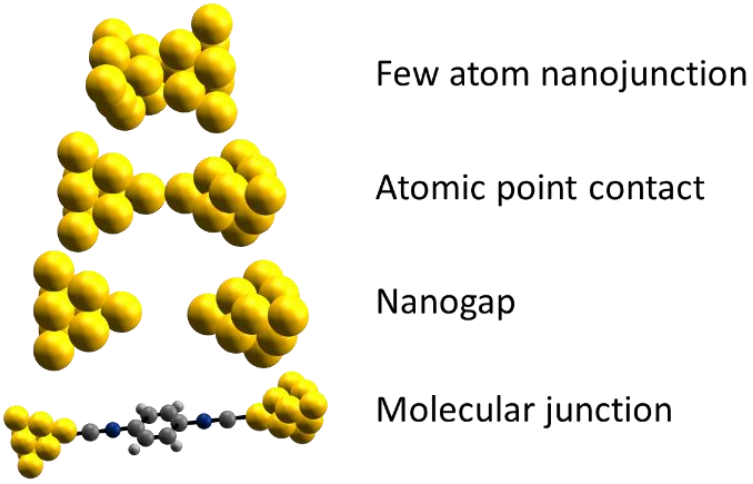

Figure 2.5 *- Final stages in the formation of a nanogap and molecular junction using electromigration as the fabrication technique.*

Nanojunctions broken using the electromigration technique often display this quantised conductance before final breakage. As the bias applied across a nanojunction is increased, the resistance will increase due to joule heating and as electromigration begins the resistance begins to increase at a faster rate as the cross-section reduces. A sudden transition can occur that signifies that the junction has thinned to such an extent that the dimensions are comparable to the electron scattering length.[56] This is a key signature that the electromigration process is being carried out smoothly and in a controlled manner. At this point the nanogap has not formed but is a few nanojunction as shown in figure 2.5.

Electron transport in this regime takes place through a quasi-ballistic process, electrons effectively traverse the nanojunction without encountering a scattering mechanism. As the nanojunction thins towards a few-atom contact, the conductance values begin to take on integer values of G_0 before the nanojunction eventually breaks to form a nanogap. The reduced dimensions of the conductor can be considered as a waveguide for the conduction electrons. The conductance now depends upon the number of current carrying modes available for conduction which is directly related to the few-atom make-up of the nanojunction as well as the specific material that it is made from.[57] This behaviour is summarised by the Landauer description of conduction (see section 3.1.2) where one expects that a perfect open conduction channel will contribute $G_0 = 2e^2/h$ (approximately 12.9 kΩ).

2.1.3 Electromigrated Molecular Junctions

TEM investigations of electromigrated junctions prepared using a feedback controlled process reveal many interesting phenomena including the formation of crystalline

electrode interfaces,[58] atom-by-atom surface diffusion,[59] reversible grain structure motion [60] as well as void and hillock formation.[61] Importantly, the narrowing and final breakage of the constriction has been shown to usually result in the final nanogap situated between electrodes with an extremely small radius of curvature. This is shown in figure 2.6. This electrode geometry makes it highly likely that only a single or a small number of molecules become electrically connected at a time when bound within the nanogap.

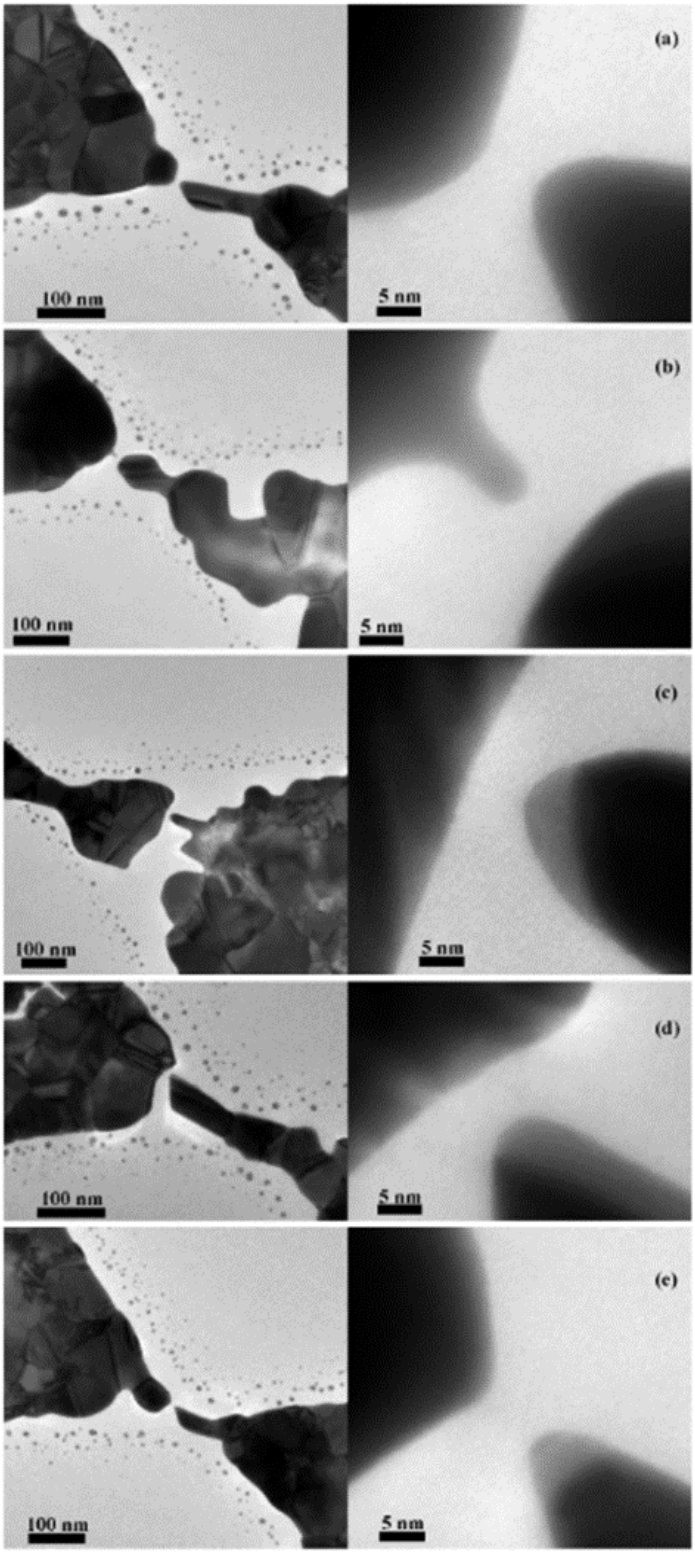

Figure 2.6 *- TEM images of nanogaps formed using feedback controlled electromigration of Au nanojunction on a SiN_x membrane. Adapted from* [62].

A disadvantage of the electromigration technique is that only a single molecular device can be formed at a time. This means that large numbers of devices must be made as measurements are at the mercy of the low probability of forming electrical contact with a single molecule or small number of molecules. The consequence is that many devices can be required which is in contrast with other techniques such as the MCBJ or STM where contacts can be repeatedly formed and broken allowing a single good device or tip to be used multiple times.

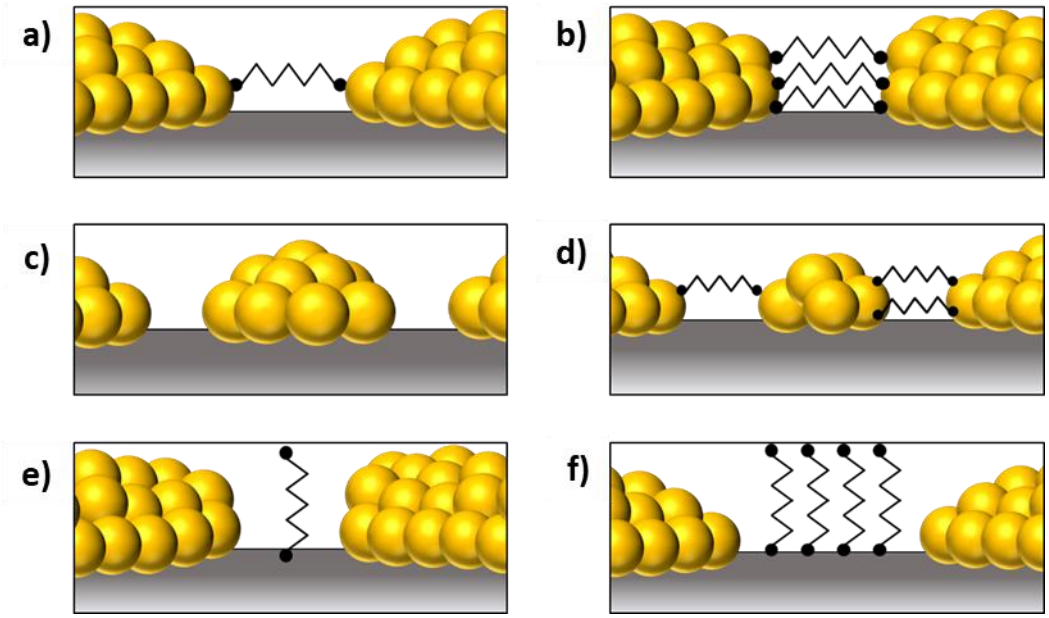

Figure 2.7 *- The many different types of electromigrated molecular device. a) single molecule bridge, b) few molecule bridge, c) metallic cluster, d) molecules bridging metallic clusters, e) single molecule and f) several molecules physisorbed to the substrate between electrodes.*

In addition to the problem of the electromigration technique requiring large numbers of devices, the process also initially suffered from the problem of metal particle formation during the breaking process, depicted in figure 2.7 c) and d). The inclusion of these metal clusters within the nanogap could replicate molecular characteristics (e.g. Coulomb diamonds in conductance vs gate voltage).[63] More recently the use of more

complicated electromigration techniques, such as feedback controlled electromigration[58] or by making use of the self-breaking phenomenon that occurs with certain metals,[64][50] allows the formation of these metal clusters to be avoided. However, it still remains that the actual configuration of the molecular contact cannot be determined using the electromigration technique and a range of possible arrangement is depicted in figure 2.7.

2.2 Electrical Properties of SCO Materials

2.2.1 Thin film SCO devices

Metal-organic materials can also be problematic from a device fabrication perspective. As with organic materials, they are susceptible to degradation due to environmental O_2, UV exposure and can experience structural changes with exposure to moisture and solvents.[65] The results of these factors combine to produce a high device failure rate, poor device longevity as well as large variations between devices.

Several different methods have been explored in order to electrically measure spin state switching in SCO compounds. However, a fundamental problem with these compounds is that they are in general very poor conductors. When faced with this problem there are generally three approaches: either scale the number of molecules down so that current flows through only a few molecules in a nanogap type geometry, increase the electrode area or produce a hybrid material such that the spin transition can be detected in an indirect way through the influence it has on a secondary material.[66]

Most analysis of SCO materials is performed on powder samples, probing the bulk behaviour of these materials. However, several techniques have been successfully used

to produce thin-films of SCO materials on substrates, with reports of thin films obtained using Langmuir-Blodgett deposition[67], molecular self-assembly[68], dip-coating and drop-casting.[69] Spin coating can be used but suffers from the drawback that most SCO compounds have very poor solubility.[69] These techniques are not always compatible with standard industrial fabrication methods which can limit commercialisation of these types of materials.

Using thermal deposition under high vacuum allows for precise thickness control and is a routinely used process in the electronics industry to form high quality multi-layered thin films of material. Due to poor stability at the temperatures required for deposition, only a minority of SCO compounds out of the hundreds synthesised so far have been shown to be stable enough for use with this technique. Because of the compatibility of thermal deposition with measurement techniques such as STM these compounds are generally very well studied.[70][71][70] The first reported thermal deposition of a SCO material is by Shi *et al.* with the $[Fe(phen)_2(NCS)_2]$ (where phen=1,10-phenanthroline) complex.[72] They were able to detect the magnetic properties of a thin-film of SCO molecules using superconducting quantum interreference device (SQUID) magnetometry, shown in figure 2.8. This revealed that the SCO phenomenon was present for a 280 nm thin film. Using temperature dependent optical absorption, it was found the SCO behaviour is preserved down to a film thickness of 10 nm, the limit of their equipment sensitivity. As we will discuss later in this chapter, the SCO behaviour of this this complex has been shown to be preserved even at single molecule level.

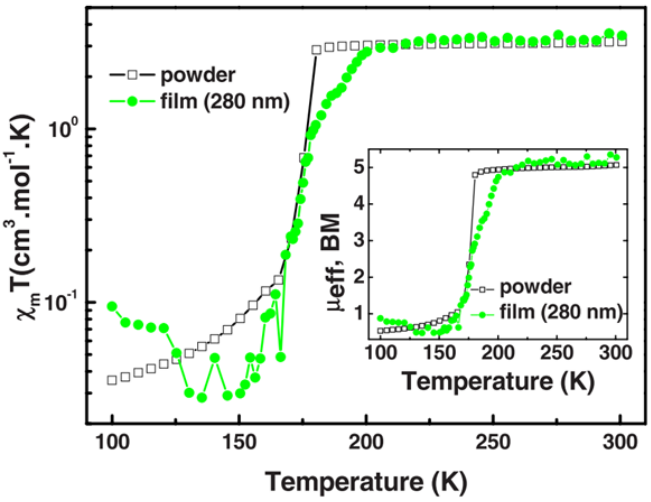

Figure 2.8 *- Temperature dependence of X_mT for a powder (black line) and thermally deposited thin film of [Fe(phen$_2$(NCS)$_2$] (green line) showing preservation of SCO. Reproduced from* [73].

A thin film of SCO/Au nanoparticles is presented by Devid *et al.* by using large micron sized electrodes in combination with gold nanoparticles coated with $[Fe(AcS\text{-}bpp)_2]\text{-}(ClO_4)_2$ where AcS = (S)-(4-((2,6-(dipyrazol-1-yl)pyrid-4-yl)ethynyl)phenyl)ethanethioate. This is a SCO compound with a $T_{1/2}$ (the temperature at which half of the SCO material is in a LS state) around room temperature.[74]

After first forming self-assembled monolayers of Au-SCO/octanethiol on a water-air interface, again using a microtransfer printing technique, they were then able to transfer this monolayer onto prefabricated 20 µm length x 100 nm gap Au nanotrench electrodes.

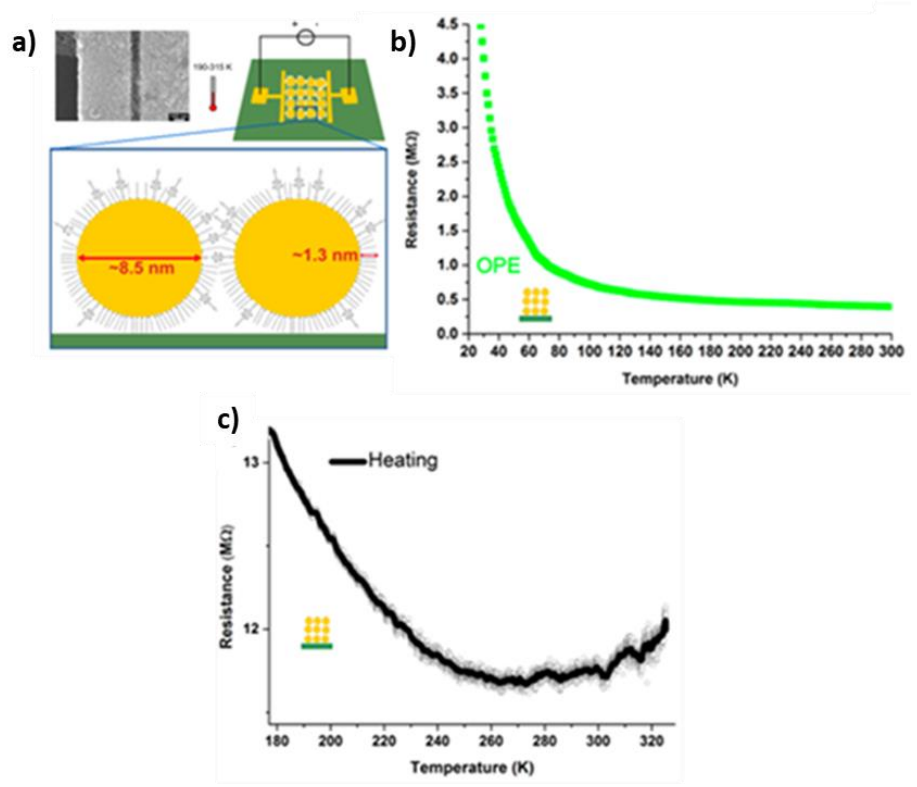

Figure 2.9 *- a) Device structure showing approximate coverage of SCO molecules on the Au nanoparticles and nanotrench electrodes. c) Resistance vs temperature for Au nanoparticles and octanethiol on nanotrench electrodes. d) Resistance measured as a function of temperature showing change of spin state as evidenced by a resistance increase. Adapted from* [74].

The SCO compound used here is rod-like in shape with sulphur anchoring groups at both ends. When mixed with Au nanoparticles it forms a network of interlinked particles with the SCO molecules and octanethiol molecules acting as spacers, figure 2.9 a). In this way conduction occurs through many parallel pathways through SCO molecules circumventing the problem of poor conductivity albeit at increased complexity of the system. The authors went on to perform temperature dependent conductivity measurements and showed that there is indeed a temperature dependence that can be attributed to the spin transition, shown in figure 2.9 c). This was proven by carefully performing control experiments on Au-octanethiol devices, figure 2.9 b) alone and with

theoretical work which combined DFT calculations with a model incorporating the behaviour of the many Au nanoparticles and the behaviour of the octanethiol spacers.

A hybrid type device has been demonstrated by Dugay *et al.*. Here the authors were able to detect the spin transition of a $[Fe(Htrz)_2(trz)](BF_4)]$ (where Htrz = 1H-1,2,4-triazole) nanoparticle thin film. This was achieved by forming a compact nanoparticle film on a liquid interface and then transferring this to a single layer graphene substrate again using microcontact printing.[75] This is shown in figure 2.10 b).

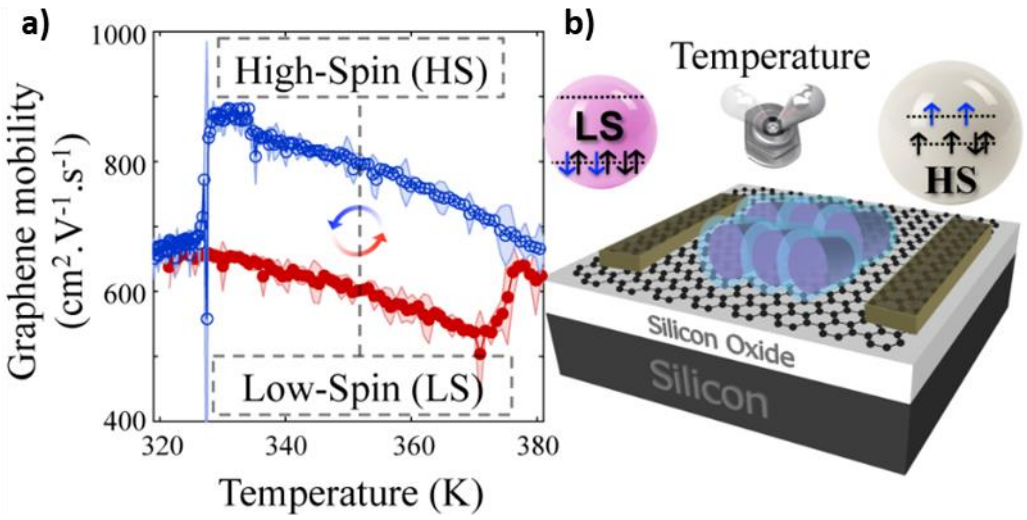

Figure 2.10 *- a) Temperature dependence of the device with a micro-contact printed* $[Fe(Htrz)_2(trz)](BF_4)]$ *nanoparticle thin film in heating (red) and cooling (blue) b) Schematic of a hybrid graphene-SCO nanoparticle device. Reproduced from* [75].

The unique properties of graphene make it a highly sensitive sensor for many physical phenomena.[76][77][78] The use of graphene (and also graphene oxide) for non-covalent attachment of SCO nanoparticles has been studied several times[79][80] with a particular interest in the way that surface proximity effect alters the spin transition behaviour of attached complexes. In addition, understanding the role of spin-phonon

coupling in graphene sheets decorated with single molecule magnets (SMMs) has been at the forefront of carbon based spintronic devices.[81]

Dugay *et al.* make use of a property whereby the remote interfacial phonon scattering rate and the conductivity of the graphene layer is modified by the spin transition in the SCO nanoparticles. This type of device has been shown to be a highly reproducible electrical probe of the spin state of the assembled SCO nanoparticles, figure 2.10 a) while also circumventing the challenge that most SCO compounds are poorly conducting by having the spin transition affect another physical process which in turn affects the overall conductivity of the device.

An example of a more direct electrical measurement on these compounds is the work carried out by Poggini *et al*.[82] They applied a technique of using a liquid metal top electrode, in this case a eutectic GaIn alloy, onto an ultra-thin film of SCO molecules arranged on a conductive Au substrate which also served as the bottom electrode. This is shown in figure 2.11 a).

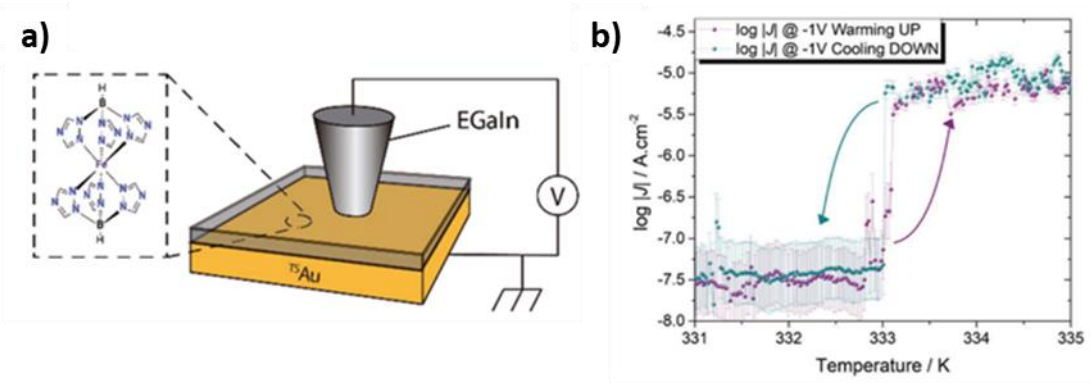

Figure 2.11 *- a) Arrangement of liquid metal top electrode with template stripped gold bottom electrode used to measure the electronic properties of a SCO molecule. b) Current density measured above and below the SCO transition temperature showing resistance switching associated with the spin transition. Adapted from* [82].

Use of this technique is limited in application as the molecular film must be extremely thin, just a few molecular layers thick, as well as being pinhole free over the entire electrode area to prevent electrical short circuits. This can be very difficult to achieve as the liquid droplet can be several mm^2 in area. The technique is also limited to temperatures above the melting point of the electrode material and so when applied to SCO materials it necessitates a complex with a high transition temperature around room temperature. A suitable candidate compound which these authors use is [Fe(tris(1H-1,2,4-triazol-1-yl)borohydride)$_2$]. Reproducible and abrupt SCO has been observed in this compound at 333 K as shown in figure 2.11 b). In addition this SCO compound displays remarkable stability at elevated temperatures allowing it to be thermally deposited under high vacuum from a quartz crucible to form high quality ultra-thin films while retaining the SCO behaviour.[65][83]

2.2.2 Spin Crossover Molecules in Nanogap Electrodes

Investigations in which SCO molecules have been studied at a single molecule level have mainly taken place using STM at low temperatures. These have chiefly investigated SCO compounds capable of being thermally deposited onto surfaces *in situ*. However, a few examples exist of these compounds being studied using break junction techniques. This section will first discuss two notable STM studies as, although an STM experiment is far removed from any form of practical device, it provides a proof of concept that the SCO phenomenon can act as a conduction switching mechanism for an electronic device. Finally, some of the recent work on break junction techniques will be presented.

It has been clearly shown in an STM study by Miyamachi *et al.* that the properties of bulk (or thick films of) SCO compounds differ greatly when compared to single molecules on

a surface.[84] In this work, isolated molecules of $[Fe(phen)_2(NCS)_2]$, figure 2.12 a) were deposited onto a clean copper surface under cryogenic ultra-high vacuum conditions. The deposited molecules were imaged at low bias using a custom built STM with very high resolution as shown in figure 2.12 b).

Two noticeably different forms of the complex existed, one which gave a smooth current trace when scanned across and a second form displaying a central current spike located approximately at the location of the central Fe ion in the complex as shown in figure 2.12 c) and d).

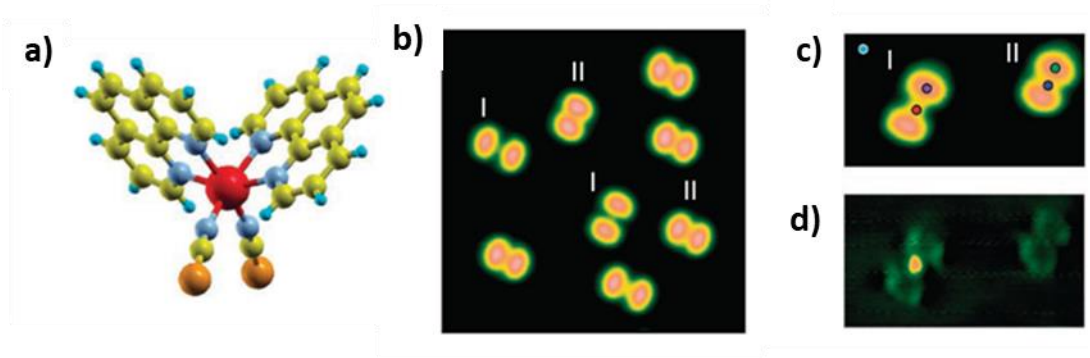

Figure 2.12 - a) Structure of the Fe(1,10-phenanthroline)$_2$(NCS)$_2$ molecule b) STM image of the molecules deposited on the Cu surface. The double lobed image shows that it is likely that the NCS groups have bonded with the substrate as expected c) A pair of SCO molecules showing HS state I and LS state II and d) dI/dV map of the current showing the presence of the Kondo peak. Adapted from [84].

The latter feature was attributed to a Kondo resonance which is a signature of unpaired electron spins allowing the group to determine that these molecules were in a HS state while the featureless form not displaying this feature was presumed to be the complex in a LS state. The Fe-phen molecules were shown to be locked into one spin state and were not reported to be switchable between spin states by the application of a voltage

pulse from the STM tip. This is likely due to the two NCS (isothiocyanate) groups being strongly coupled to the Cu substrate, preventing the necessary structural changes from occurring when charge is injected.

Reducing the molecule-substrate interaction by growing a thin insulating CuN layer on the Cu surface before depositing the SCO molecules has been explored as a way of preserving the SCO behaviour of Fe-phen molecules. In STM studies, the apparent size and shape of the SCO complex gives an indication of the level of molecule-substrate coupling with a smaller apparent size of the complex an indicator of reduced coupling. By injecting current, using the STM tip positioned close above each molecule and performing cyclic I-V sweeps, it was demonstrated that the Fe-phen complexes can abruptly switch conductivity in a similar manner to a memristor devices. The authors are able to demonstrate repeatable switching using set and reset pulses of +1.5V and -1.2V respectively to switch the isolated molecules between HS and LS states.

Recently Burzurí *et al.* have measured the temperature dependent conductivity of electroburnt graphene nanogaps containing $[Fe(L')_2](BF_4)_2$ CH_3CN H_2O where L' = 4-(2,6-di(1H-pyrazol- 1-yl)pyridin-4-yl)benzyl-4-(pyren-1-yl)butanoate, as shown in figure 2.13 a). This compound studied here is similar to that measured by Devid *et al*. in Au nanoparticle arrays but with the addition of two pyrene end groups, the idea being that these additions are expected to decouple the interaction of the graphene electrode via π-π stacking between the pyrene end groups. The aim being to preserve the spin-crossover effect when molecules are deposited onto a surface.

They did this by first patterning graphene flakes produced via chemical vapour deposition into nanojunctions using electron-beam lithography and O_2 plasma etching. The devices were then electroburnt, a process similar to electromigration but occurring

in the present of O_2[85], so that graphene nanogaps with 1 - 2 nm separation are formed. The SCO molecules were deposited from solution onto the nanogaps and dried before performing electrical characterisation. The devices show a bistability in the current as a function of time.

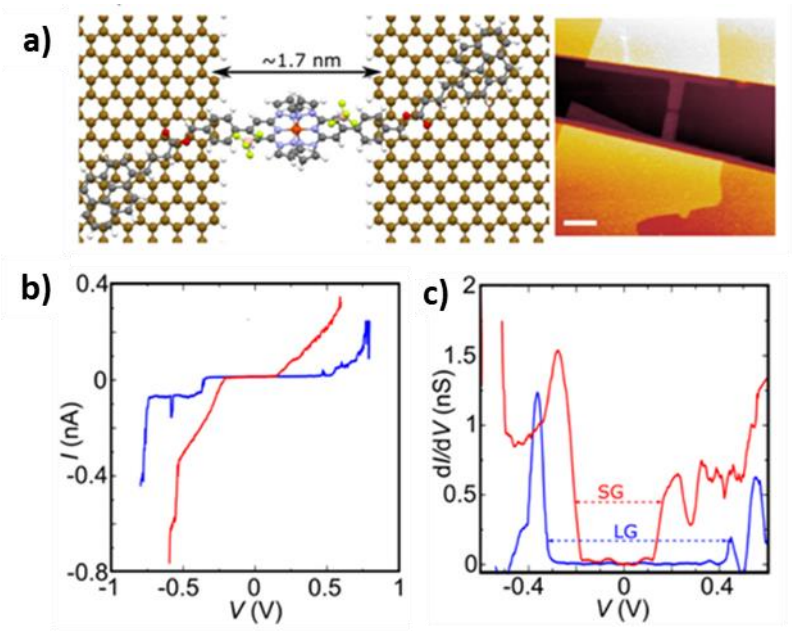

Figure 2.13 *- A SCO molecule in an electroburnt nanogap displaying conductance switching a) proposed geometry of graphene – SCO molecule junction b) I – V and c) dI/dV showing two distinct behaviours attributed to high spin (red) and low spin (blue) states of the complex.Adapted from* [86].

By making repeated I-V curves the authors were able to explore the characteristics of these two states. Both states showed a current suppression, a clear signature of off-resonance transport though a molecular junction with one state showing a wider current suppression than the other. As shown in figure 2.13 b) and c), these two states are given the name LG and SG for large gap and small gap respectively.

This bistability was independent of temperature and occurred from room temperature down to 2 K as is shown in figure 2.14. With the aid of DFT calculations incorporating the

SCO molecule bridging the graphene nanogap the origin of these two conductance states could be attributed to spin crossover in the molecule.

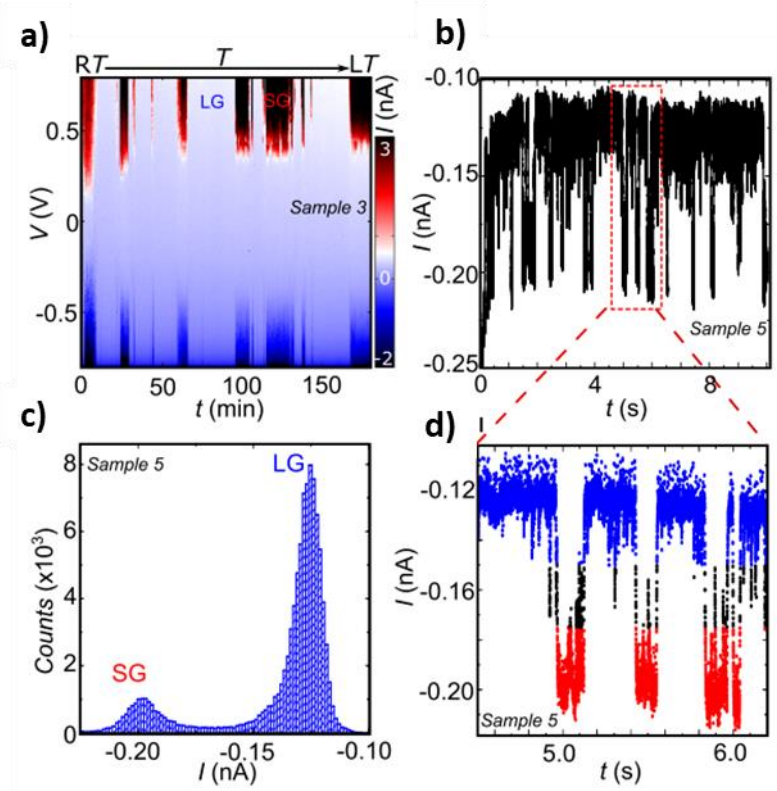

Figure 2.14 *- a) I-V recorded during cooling of the SCO nanogap device and showing temperature independent switching behaviour. b) Current trace at a bias of -0.6V at low temperature. c) histogram of recorded current values from b). d) reduced time trace from b) showing switching between two states highlighted red and blue. Adapted from* [86].

2.2.3 Induced Switching of SCO complexes

STM based work exploring the role of the tip-molecule interaction in mechanically inducing the spin transition on SCO complexes has been shown to be possible.[87] Reversible spin transitions from LS to HS with the application of bias, such as via the electric field from the electrodes or from a third gate electrode situated in close proximity to the SCO complex would be a highly desirable functionality of a SCO based

memory device. A voltage induced switching mimics the action of resistive random-access (ReRAM) type memory currently in commercial production while a gate-controlled switching mimics the behaviour of traditional field-effect transistor.

In low temperature experiments, this has already been demonstrated by Meded *et al.* in molecular transistors containing $[Fe-(L)_2]^{2+}$] where L = 4'−(4'''−pyridyl)−1,2':6'1''-bis-(pyrazolyl)pyridine (figure 2.15 a)) via a ligand charging process with support from theoretical calculations.[88]

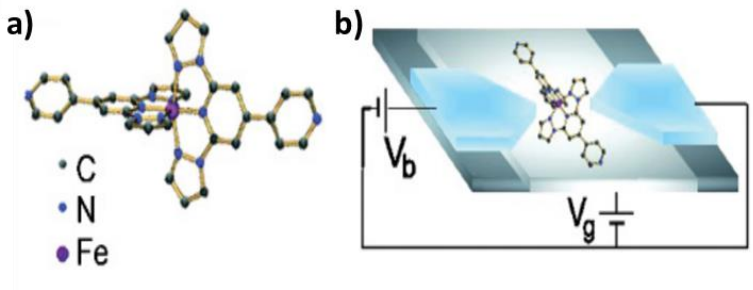

Figure 2.15 *a) $[Fe-(L)_2]^{2+}$] SCO complex with linker units. b) Three-terminal molecular transistor. Adapted from* [88].

These devices consist of Au source and drain electrodes, connected to the spin crossover complex via thiol linking groups which anchor the complex within the device (figure 2.15 b)). A third gate electrode electrostatically couples to the molecule. These devices are created by patterning a metal nanojunction on top of a partially oxidised Al gate electrode. The nanogap is formed using the electromigration technique at ambient conductions. Molecules are deposited by transferring the device into a dilute solution of the SCO complexes and following this electronic characterisation is performed after cooling the device to 1.5 K.

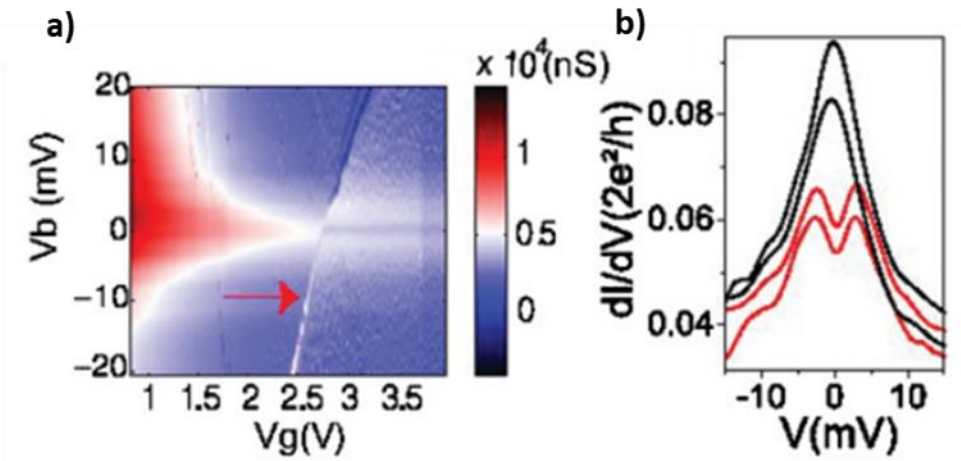

Figure 2.16 *Differential conductance vs gate voltage plot, red arrow indicates position of diagonal line corresponding to an electrostatic shift caused by the ligand charging induced spin transition. b) Differential conductance traces at gate voltage of 2.0, 2.4, 2.9 and 3.3 V showing emergence of split Kondo peak. Black traces correspond to lines on the left and red to the right of the diagonal line in a). Adapted from* [88].

The measured transport features are characteristic of electronic transport through a molecular transistor and most importantly, electrical control of the spin transition via applied gate voltage. The manifestation of the HS or LS state is revealed by the presence of a diagonal line in the differential conductance vs gate voltage plots, as shown in figure 2.16 a), as well as the presence (or absence) of a split zero bias anomaly (figure 2.16 a)) which is a characteristic of unpaired spins in a nanoscale system.

Such a voltage induced switching has also been observed in several studies using STM of SCO molecules which have been self-assembled or drop cast onto surfaces where the application of a tip bias was seen to change the spin state from LS to HS.[89] Additionally, it has been seen that electric field can cause this crossover.[90] Work by Miyamachi *et al.* (figure 2.17) as well as Gopakumar et al. have reported voltage induced spin state switching at a single molecule level. However, the mechanism for these types of

transitions is currently poorly understood and several explanations have been proposed.[91]

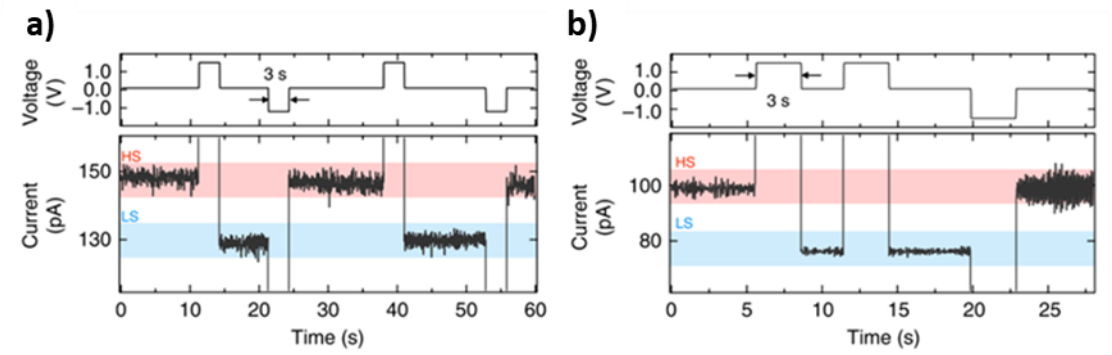

Figure 2.17 *- a) [Fe(phen)$_2$(NCS)$_2$] molecule on CuN surface demonstrating deterministic switching between HS (150 pA) and LS (130 pA) states via voltage pulses of +1.5 V and -1.2 V. b) The first pulse (+1.5 V) switches the molecules into the LS state. A second positive pulse does not result in a change of spin state. Finally, a third pulse (-1.2 V) results in a change of state to the HS state. Adapted from* [84].

Voltage induced spin-crossover has also been observed in break junction devices of heteroleptic SCO complexes whereby the molecule bridges a MCBJ device with two bidning ligands, while a second pair are free.[92] Here the conductance of a device is seen to abruptly switch between two states which has been attributed using statistical analysis of multiple devices to the spin-transition caused by a voltage triggered distortion of the free ligands.

To the best of our knowledge no surface probe study has investigated using temperature as a way to induce SCO. Likely this is due to stability of the system, with a large temperature sweep not practical as this would induce large amounts of thermal drift as well as possible movement of the molecules under study. Furthermore, the Kondo effect

which is commonly presented as a method of detecting a high/low spin complex is only present at low temperatures.

2.2.4 Deposition of Molecules into Nanogap Devices

For STM and AFM studies the quality of the deposited molecules (and substrate) is very important and a great deal of technology is applied to depositing compounds in either monolayer or sub-monolayer form. Effusion cells under UHV, transfer from a Langmuir-Blodgett trough, electrospray deposition or exfoliation techniques are examples of the techniques used in these surface probe measurement.[93][94]

In a break junction device the nanogap is lateral. This means there is less consideration needed towards the quality of the deposited film as long as a molecule of interest is placed within the nanogap. Often the gap is broken in air and the substrate is immersed in a solution allowing for adsorption or self-assembly of the molecules into the nanogap. The reverse of this technique can also be used where molecules are first assembled or deposited onto the nanojunction and then the junction is broken. The hope is that a molecule will diffuse into the newly formed gap for measurement.

In the case of electromigrated devices, the latter technique is often favoured as the elevated temperature present as the junction is heated during electromigration results in an increase in the surface mobility and gives a good chance that a molecule will be found across or within the gap for measurement. Additionally, this allows immediate measurement of the device without removal from the measurement setup, avoiding the risk of contaminating the freshly formed nanogap surfaces. A disadvantage is that the empty gap cannot be first characterised as the molecules will “short” the gap as soon as it is formed.

Theory

3.1 Electron Transport in Metal-Molecule-Metal Devices

Chapter 3

3.1.1 Simmons Tunnelling Model

If we consider two electrodes separated by a thin oxide or insulating layer, we can expect that electrical conduction will be blocked for any reasonable applied voltage below the breakdown voltage of the barrier material. However, if the insulating layer is very thin, for example below a thickness of 20 nm, then we may observe significant conduction as a result of electron tunnelling. This process takes place due to the evanescent electron wavefunction extending into the barrier and if this barrier is thin enough, the wavefunction can have a non-zero value within the other electrode. The result is that there will be a probability of finding the electron on the other side of the barrier.

This tunnelling process occurs whenever an electron encounters a barrier regardless of thickness but the rapid decay of the wavefunction means that for most thicknesses above only a few nanometres there will be a very small probability of this process occurring.

The tunnel effect has been studied since the early 1930's by Bethe and Sommerfeld and later by Holm and Kirschstein.[95] Improving upon the earlier work, Simmons proposed a model in 1963 which has been applied with success to a many types of metal-insulator-metal systems.[96]

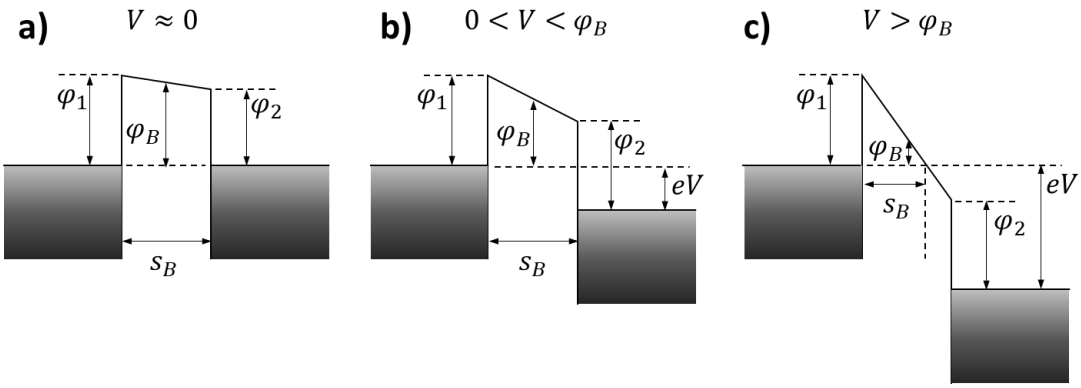

Figure 3.1 *- Electron tunnelling through a potential barrier of thickness s_B and height φ_B between electrodes with work functions φ_1 and φ_2. at a) low voltage b) and intermediate and c) high voltage regimes.*

Using the WKB approximation, Simmons arrived at a general model that incorporates electron tunnelling across any arbitrarily shaped potential barrier. As a simplification in the barrier can be approximated as a rectangular barrier giving the Simmons tunnelling equation as:

$$J = J_0\{\varphi_B \exp[-A\sqrt{\varphi_B}] - (\varphi_B + eV)\exp[-A\sqrt{\varphi_B + eV}]\} \tag{3.1}$$

where φ_B is the average barrier height relative to the negative electrode and:

$$J_0 = \frac{e}{2\pi h\alpha^2 s_B^2} \text{ and } A = \frac{2\alpha s_B}{\hbar}\sqrt{2m}$$

α is a constant of order unity and s_B is the width of the barrier. When $0 < V < \varphi_B$ the tunnel barrier is still approximately rectangular (figure 3.1 b). Multiplying the current density by A, the electrode area, equation 3.1 can be expressed in practical units for the intermediate voltage regime as:

$$I(V) = A\frac{6.2\text{x}10^{10}}{s_B^2}(\varphi_0 - {}^{V}/_{2})\exp\left[-1.025s(\varphi_0 - {}^{V}/_{2})^{1/2}\right] -$$

$$(\varphi_0 + {}^{V}/_{2})\exp\left[-1.025s(\varphi_0 + {}^{V}/_{2})^{1/2}\right] \quad (3.2)$$

At $V > \varphi_B$ the barrier becomes triangular (figure 3.1 c)). This has the effect that the barrier thickness now takes on a voltage dependence with higher voltages reducing the barrier thickness. The result is that now the tunnelling current in this regime has an exponential dependence with voltage. Electrons from the right electrode cannot tunnel into the left electrode due to a lack of empty states. The reverse condition exists for electrons tunnelling from left electrode into the right electrode with completely unoccupied states. This regime is known as Fowler-Nordheim tunnelling or field emission.

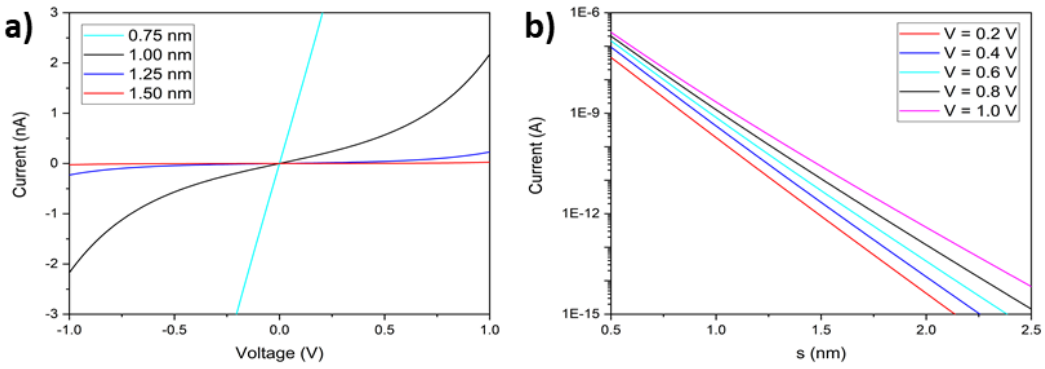

Figure 3.2 *- a) Plots of equation 3.2 at several electrode spacings. b) Plot of equation 3.2 showing tunnelling current as a function of at several voltages. Both cases demonstrate the very high sensitivity to electrode separation that the tunnelling current has. The junction area A is set at 1 nm^2 and φ = 1 eV for both plots.*

A plot of equation 3.2 for various gap sizes (figure 3.2 a)) and voltages (figure 3.2b)) which illustrate the sensitivity of the tunnel current on the distance s. What is not included in this model is the effect that image forces have on reducing the barrier height

and rounding the shape of the potential. Neither is the effect of thermal broadening of the fermi functions of the electrodes on conduction and the effect that temperature has on the tunnelling current. However, these effects have a relatively small contribution to the transport characteristics.

3.1.2 Landauer Scattering Theory

The fundamental origin of conduction in nanoscale systems can be explained by considering conduction as transmission and reflection of electrons by a scatterer separating two electrodes. This is the approach taken by Landauer in the 1950's where conduction through a 1D conductor is treated as a scattering problem.[8] If we take a channel of length L with transmission function $T(k)$ and with $f_L(k)$ and $f_R(k)$ being the Fermi functions of the left and right electrodes we can write the current density as:

$$J_{L-R} = \frac{e}{L}\sum_k v(k)T(k)f_L(k)[1 - f_R(k)] \tag{3.3}$$

Identifying $^1/_L \sum_k g(k) = {}^1/_{2\pi} \int g(k)dk$ we can write:

$$J_{L-R} = \frac{e}{2\pi}\int dk\, v(k)T(k)f_L(k)[1 - f_R(k)] \tag{3.4}$$

We can make a change of variables from k to E by identifying $\frac{dk}{dE} = \frac{m}{\hbar^2 k}$ since $E = \hbar^2 k^2/2m$ we can write:

$$J_{L-R} = \frac{e}{h}\int dE\, T(E)f_L[1 - f_R(E)] \tag{3.5}$$

The current traversing from the right electrode to the left, J_{R-L}, has a similar form (if we take the same transmission probability). Since this is the current density in 1D, we can express the total current as $I(V) = J_{L-R} - J_{R-L}$. Including spin degeneracy, we get:

$$I(V) = \frac{2e}{h}\int_{-\infty}^{\infty} dE\, T(E)[f_L(E) - f_R(E)] \tag{3.6}$$

where $f_L(E)$ and $f_R(E)$ are step functions at zero temperature (and broadened at finite temperature) having the value 1 at $E_F \pm \frac{eV}{2}$ and 0 above this energy. In the low voltage regime, the right of the above expression reduces to the familiar form of the Landauer equation:

$$I = VG \tag{3.7}$$

where

$$G = \frac{2e^2}{h}\sum_{n=1}^{N} T_N \tag{3.8}$$

Here T_N is the number of conducting modes available in the conductor. From equation 3.7 and 3.8 we can see that a device with one perfectly contributing mode has a resistance value of approximately 12.9 kΩ. In the case of an atomic point contact the number of modes per atom can be directly measured by shot noise measurements or by superconducting measurements.[8][97] For these systems the origin of the number of modes available is related to the valency of the material.

This type of behaviour is particularly well demonstrated at low temperature for example in a GaAs/AlGaAs heterostructure where the width of a 2-dimensional electron gas (2DEG) sheet is modulated by a gate electrode as shown in figure 3.3 b). This behaviour is also observed in the final breaking of nanowires using STM indentation experiments[57] (figure 3.3 a)) as well as in MCBJ stretching[98] and electromigration[56][47] experiments.

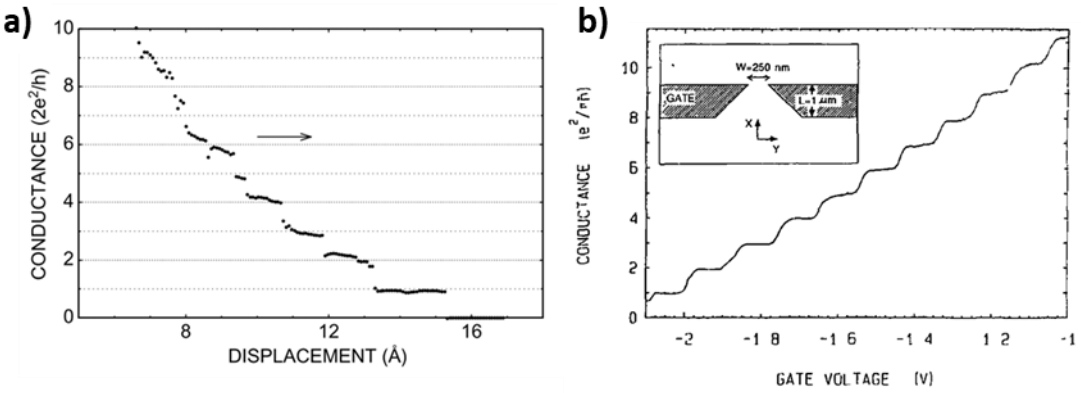

Figure 3.3 *- a) Current as a function of displacement measured during an STM indentation experiment. A tungsten tip is brought into contact with a gold electrode at room temperature and in UHV conditions. The conductance is measured as the tip is removed, as shown by the direction of the arrow. A 10 - 20 Å long nanowire is formed as the tip is retracted from the gold surface which is gradually thinned as the wire is elongated. Quantised conductance is observed in units of* $2e^2/h$*. Figure adapted from* [99]*. b) Gate control of quantised conductance using a 2DEG approach and top gate. The voltage applied to the gate controls the width of the conducting channel in a GaAs-AlGaAs heterostructure. Insert shows the top gate contact with the 2DEG structure beneath. Figure adapted from* [100].

3.1.3 Conduction in Molecular Junctions

Introducing a molecule between metal electrodes and forming a molecular junction adds complexity to the simple system described by the Simmons model. With a molecule present, the potential barrier can no longer be treated as a featureless barrier and the I-V characteristics of a molecular junction are dependent upon the energy level structure of the molecule and the ways that the energy levels interact with the continuous metallic states of the electrodes.

Several ideas have built upon the tunnelling model that incorporate the behaviour of molecules electrically coupled to electrodes. The simplest of these models is known as

the single level resonant tunnelling model.[8] In this model, a molecule sits between two metallic electrodes with a connection to each made via tunnel barriers. The molecule is represented by a series of energy levels that are broadened due to hybridization with the metallic electrode states.

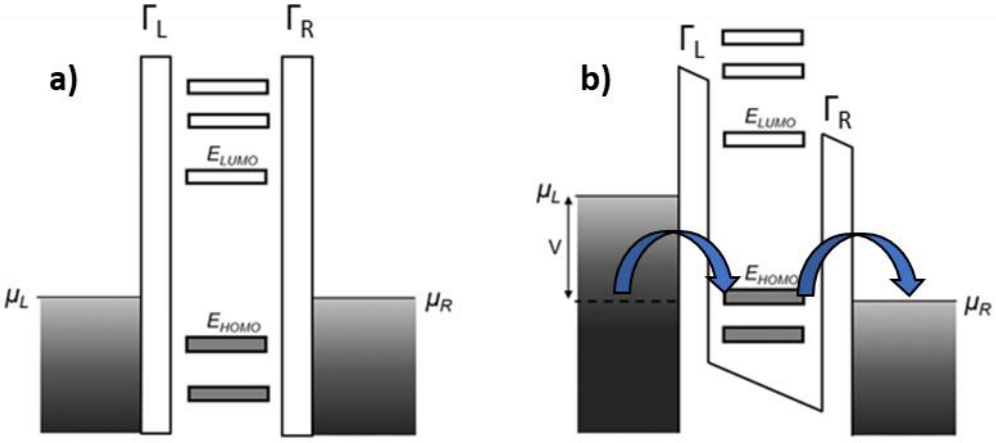

Figure 3.4 *- Chemical potential landscape of a molecular junction in the intermediate coupling regime at a) zero-bias off resonance condition in which the fermi levels of the electrodes align with a gap in molecular levels. b) applying a bias V brings a molecular level into resonance with the electrodes resulting in increased conduction (blue arrows).*

A molecule situated in a junction couples to the two metal electrodes via tunnel barriers as shown in figure 3.4, where Γ_L and Γ_R are the electron transfer/coupling terms representing the rate at which electrons are transferred from the left electrode (source) to the right electrode (drain). These terms are determined by the wavefunction overlap of the orbitals of the molecule and those of the electrodes. The combination of these two terms ($\Gamma = \Gamma_L + \Gamma_R$) determines the degree of level broadening that is present and is a measure of orbital hybridization between molecule and electrodes.[101] Three distinct coupling regimes can be considered for molecular junctions where the degree of coupling is small, intermediate and large. These are in relation to the thermal energy,

k_BT and also the electron confinement energy, Δ_C, determined by the physical charging energy of the system given by $E_C = e^2/C$ where C is the capacitance of the molecule with respect to the environment.

In the first case, a molecule is weakly coupled and $\Gamma < \Delta_C, E_C, k_BT$. This can occur for example via the physisorption of the molecule onto the electrode surfaces. In this case the levels of the molecule will remain fairly unchanged and broadening can be neglected. The molecular orbitals can be treated as Dirac delta functions.[8] Charge transport is incoherent in this regime meaning that the phase information of the electrons is not retained due to the long residence times on the molecule with the energy – time uncertainty principle being responsible for this increased residency time. Charge transport is characterised by a two-step, first order process where the occupancy of each of the molecular states is determined via a set of rate equations. Behaviours such as Coulomb blockade are prevalent in this coupling regime.

The other extreme is when $\Gamma, k_BT > \Delta_C, E_C$. This is the strong coupling regime where a large hybridization of the molecule and electrode orbitals takes place resulting in a strong broadening of the molecular levels, with the levels taking on a semi-continuous, multipeaked nature.[16] Transport effects become undetectable due to quantum fluctuations of the current flow and the device exhibits a featureless transport characteristic.

The intermediate regime where $\Gamma, k_BT \lesssim \Delta_C, E_C$ is the regime characterising most devices incorporating covalently bonded molecules. Here level broadening must be considered and transport is coherent.

If the broadening is still smaller than the level spacing, as is generally the case in the intermediate regime, then conduction takes place through one level at a time. For a molecule where the chemical potential of the electrodes is situated between the HOMO-LUMO of the molecule, the signature of this type of transport is a current suppression at low bias or "gap" with a sudden onset of conduction as the voltage applied to the molecular junction is increased. Conduction at low bias is through a direct tunnelling process with the molecule simply acting as a barrier, as no states are located on the molecule within the bias window available for conduction. This situation exists until the applied bias distorts the energy level structure enough to bring one of the molecular levels into alignment with that of conduction band of the electrode. It now becomes possible for electrons to tunnel through these states and lift the current suppression.

Equation 3.9 is obtained by solving the Landauer equation (equation 3.7) analytically for a one-level system in the low temperature limit. Here we have assumed that the electrode states are not energy or voltage dependent. This is valid for electrode materials such as Au that have a flat DOS at the fermi-level.[8][38]

$$I(V) = \frac{4G_0}{e}\frac{\Gamma_S\Gamma_D}{\Gamma_S+\Gamma_D}\left[\arctan\left[\frac{\varepsilon_0+{}^{eV}/_2}{\Gamma_S+\Gamma_D}\right] - \arctan\left[\frac{\varepsilon_0-{}^{eV}/_2}{\Gamma_S+\Gamma_D}\right]\right] \quad (3.9)$$

where $G_0 = \frac{2e^2}{h}$, ε_0 represents the level position relative to the fermi level of the electrodes, $\Gamma_{S,D}$ are the coupling parameters of the molecule to the electrodes and are set so that $\Gamma_S = \Gamma_D$. [38] Plots of equation 3.9 where the value of ε_0 is varied are shown in figure 3.5 a). Figure 3.5 b) shows several plots where the coupling parameter, $\Gamma_{S,D}$, is varied. Taken together, this illustrates the role of level position and coupling of the

molecule to the electrodes in determining the current level and shape of the I-V characteristics for a molecular junction.

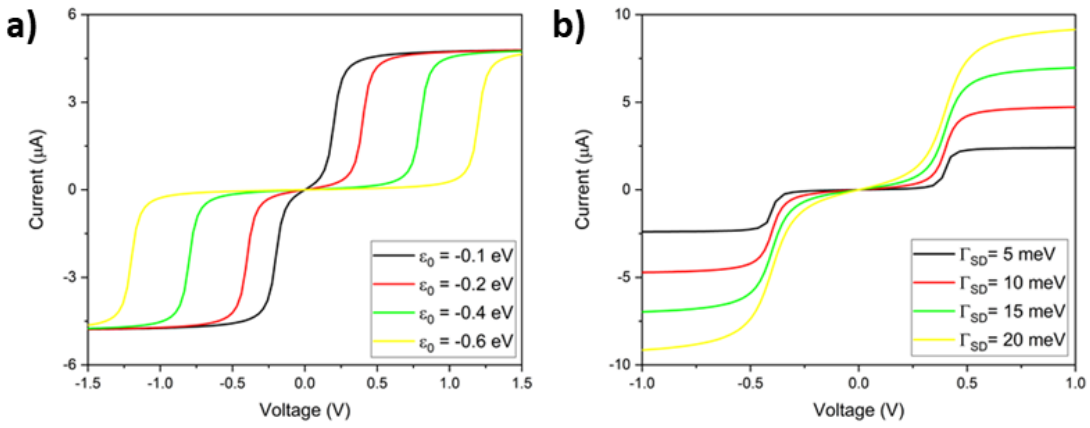

Figure 3.5 *- a) Plot of equation 3.9 with different values of* ε_0 *while keeping* $\Gamma_{S,D}$ *fixed at 10 meV b) different values of* $\Gamma_{S,D}$ *with fixed* ε_0 *at 0.2 eV.*

Presented here is an overview of the conduction mechanisms prevalent in molecular electronics. Determining the actual chemical potential landscape of a molecule is complicated due to the interactions a molecule has with the electrodes and the way its specific states hybridize with those of the electrodes. In combination, image-charge effects also act to modify the systems behaviour from that of the molecule when in its isolated gas phase.[8]

From a theoretical perspective, density functional theory (DFT) and non-equilibrium greens function (NEGF) techniques can be used to determine the transmission function and hence the I-V characteristics of these systems. A discussion of these techniques is given in relation to the conduction through SCO complexes in section 3.3.6 but a full description of these techniques is beyond the scope of this work. However, an excellent introduction is given by Cuevas and Sheer.[8]

3.2 Theory of Electromigration

As discussed in section 2.1.1.4, electromigration has been used to form nanogap electrodes. The following section will give a theoretical understanding of forces driving the electromigration process at a microscopic level.

The origin of electrical resistance in macroscopic conductors is in part due to electron scattering with impurities, grain boundaries, dislocations as well as with the metal ions displaced from their equilibrium positions due to thermal motion. When an electron scatters off, some of its momentum is transferred to the scatterer and a force is exerted. This is referred to as the electron "wind" force. Under ordinary circumstances these collisions between electrons and ions do not result in migration of the metal ions owing to the large mass difference and strong interatomic bonding between ions within the lattice of the metal. However, if the rate of these electron-ion collisions occurs beyond a certain threshold then the momentum transferred to the ion is great enough that a displacement will occur. These displacements occur with greater frequency as both the current density and temperature are increased.

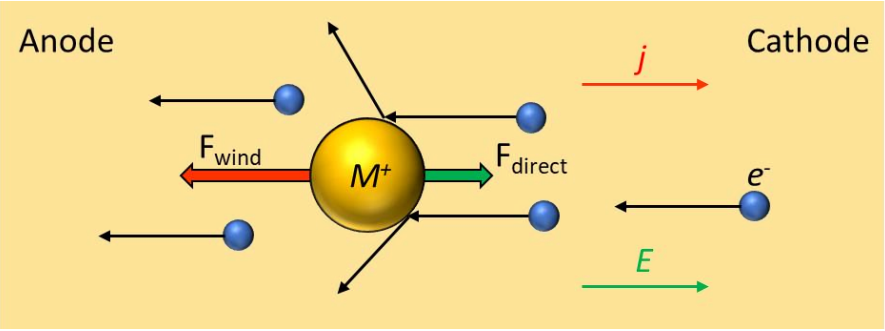

Figure 3.6 *- Two competing forces act on a migrating atom, one due to the electric field as a result of the applied voltage on the conductor and the second, a momentum transfer process as a result of electron collisions.*

The electromigration process is often described as resulting from two processes acting upon a scatterer which are depicted in figure 3.6. The first of these processes is known as the electron "wind" force. The origin of this force is as a result of electron-ion collisions and will drive material transport in the direction of electron flow.

A simple model of the electromigration wind force can be found in the work of Fiks.[102] Under an applied electric field, E, electrons in the conductor will gain momentum:

$$\Delta p = -\tau e E \tag{3.10}$$

where τ is the average time before each electron undergoes a scattering event. These collisions take place with a scattering atom over a given area, represented in this model by a scattering cross section term σ_x as shown in figure 3.7. Since electrons within only a certain distance are able to reach a scatterer in time τ. We can therefore write:

$$l = v_F \tau \tag{3.11}$$

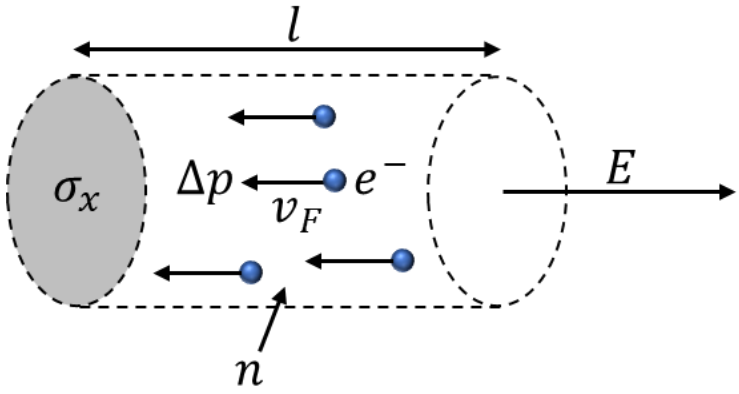

Figure 3.7 *- The "wind" force acting on a migrating atom can be determined by considering the volume of material with electron density n. This area is determined by the scattering cross section σ_x and length l. Within this volume, electrons gain momentum Δp under application of an electric field E in a time τ.*

Summing the number of momentum transfer events occurring in a time τ gives the force acting on a scattering atom if we take into account the electron density n of the material and therefore have $nl\sigma_x$ electrons taking part in the scattering process:

$$F_W = \frac{1}{\tau}\sum \Delta p = -nl\sigma_x eE = -Z_w eE \tag{3.12}$$

The calculation of the direct force acting upon a charged impurity is generally more complex, with the initial belief that $F_D = ZeE$. It was later realised that this simple equation 3.12 does not incorporate charge screening effects and other non-equilibrium behaviour that occurs around the scatterer. An equation incorporating these effects was proposed by Landauer in 1977 as:

$$F_D = \frac{ZeE}{1+(1/3)\beta \Delta n/n_0} = Z_D eE \tag{3.13}$$

where Z_D is the effective charge of the scatterer, β is a constant of order unity, Δn is the localised increase in electron density as a result of the scatterer and n_0 is the average electron density in the material. Combining these two mechanisms gives an expression for the total force acting on a scatterer as:

$$F = F_W - F_D = -(Z_W + Z_D)eE \tag{3.14}$$

To calculate all of the forces acting within a material, the forces for all the different types of defects, their occurrence and their structure has to be taken into account as the electromigration forces differ when the impurity is located at a grain boundary, a surface or within the bulk of the material.[103] For the commonly used materials Al, Au and Cu, the screened ions have a positive overall charge and the two forces act in opposition. However, the wind force is the dominant driving mechanism for electromigration in these metals.[55]

3.2.1 Effect of Microstructure on Electromigration

The electromigration process is generally greatest at the grain boundaries in a metallic conductor. The greatest amount of momentum transfer occurs here due to the large disruption in the crystalline structure and also because the metal ions are weakly bound at the grain interface. From a microscopic viewpoint, electromigration induced thinning and the eventual breakage of a conductor occurs when there is a discontinuity in material flow. Above a certain current threshold, these forces acting upon the impurities within the conductor will result in a material flux. A uniform flux of material does not result in breakage. However, if the material entering a given region is not the same as that exiting, then the geometry will change leading to void formation and eventually a breakage of the conductor.

In particular, there is a large discontinuity present at a triple connection point between three grain boundaries. At these locations the flux of material incoming into the point cannot be met by the flux leaving leading to electromigrated thinning. The size of the grain structure also impacts the electromigration process. A conductor which does not possess these triple points is said to have a “bamboo” like structure and grain boundary are orientated almost perpendicular to the current flow. A conductor with this type of structure displays the counterintuitive behaviour of having an extremely small cross section while possessing a greater resilience to electromigration when compared to a wire of the same material but with slightly greater cross-sectional area.[104] This is shown in figure 3.8.

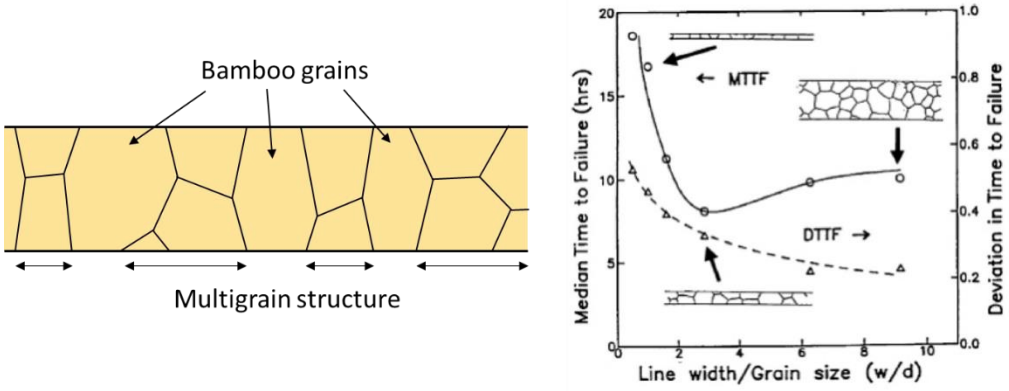

Figure 3.8 *- Different types of grain structure in a thin metal conductor and the influence on MTTF. A minimum in MTTF does not occur for the smallest cross-section wire. Adapted from* [105].

The electromigration process is well studied not only because of its use in molecular electronics, as a mean by which to form molecular contacts, but also because it is one of the main mechanisms of failure in integrated circuits. The drive for smaller integrated circuit components has the consequence that the interconnects between them are also reduced in size. Without careful consideration of the layout and design of these interconnects, current flow through an interconnect could exceed the critical current density leading to electromigration effects and failure of the integrated circuit.

Because of the importance of electromigration induced failure in integrated circuit design, in 1967 [106][107] Black developed a phenomenological equation that predicts the mean time to failure of an integrated circuit as a result of electromigration. This equation is now known as Black's equation:

$$MTTF = \frac{A}{J^2} e^{-E_A/k_B T} \tag{3.15}$$

here A is a material specific constant, J is the current density, E_A is the activation energy of the process. The electromigation process is temperature dependent due to an increase in the material mobility as well as an increase in phonon scattering.

3.3 Spin Crossover

Certain transition metal complexes exhibit an effect known as spin crossover where the spin state of the complex can be modified by the application of an external stimulus. The external stimulus can be a change in temperature, applying pressure to the compound, irradiation with selected wavelengths of light or subjecting the compound to a strong magnetic field.

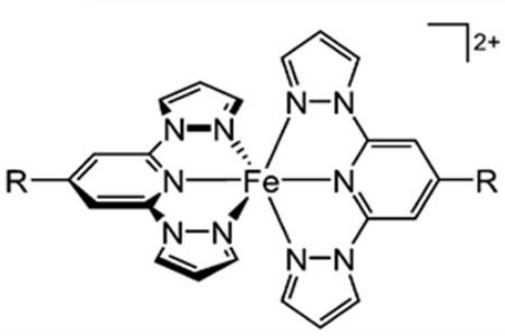

Figure 3.9 *- An example of the typical structure of a SCO compound, in this case the* $[Fe(bpp)_2]^{2+}$ *where bpp = 2,6 – biz(pyrazol-3-yl)pyridine) family of SCO compounds. Adapted from* [108].

In general, SCO compounds all share a similar molecular structure consisting of a transition metal core, referred to as the coordination centre, which is bound to ligands. A typical structure is shown for the $[Fe(bpp)2]^{2+}$ compound in figure 3.9. The binding around the coordination centre has an octahedral symmetry. The most commonly investigated SCO molecules are of the d^6 configuration and incorporate Fe as the

transition metal core. SCO has also been observed in d^4, d^5 and d^7 configurations for all of the first series of transition metals complexes.[1]

Compounds synthesised using Fe are most frequently encountered owing to the rich variety of coordination compounds possible with this element and temperature is by far the most common stimulus used to induce the spin transition. The point at which there is a 1:1 coexistence of the HS and LS states is defined as the spin transition temperature, written $T_{1/2}$ and several different forms of spin transition curves are shown in figure 3.10.[109]

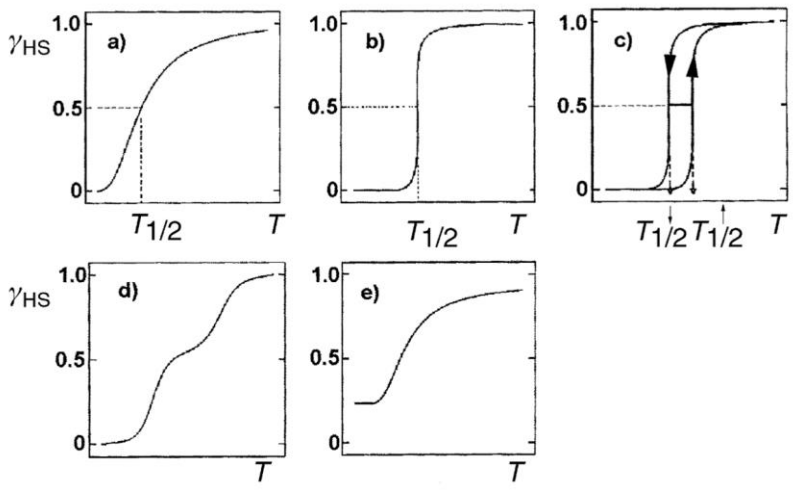

Figure 3.10 *- Plots of the high spin molar fraction (γ_{HS}) as a function of temperature showing different types of thermally induced spin transition behaviour: a) gradual, b) abrupt, c) hysteretic, d) multi-stepped and e) incomplete. Reproduced from* [110].

3.3.1 Ligand field theory

The SCO phenomenon was first described in 1931 by Cambri *et al*. but it was several decades before the effect was fully understood as a spin dependent effect with the development of ligand field theory.[111] If we consider an isolated transition metal ion, the energy levels of the d-electron orbitals are degenerate. However, if we introduce

this ion into an environment surrounded with point charges in an octahedral geometry, as is the case when the ion is coordinated to ligands in these SCO complexes, we lift this degeneracy.

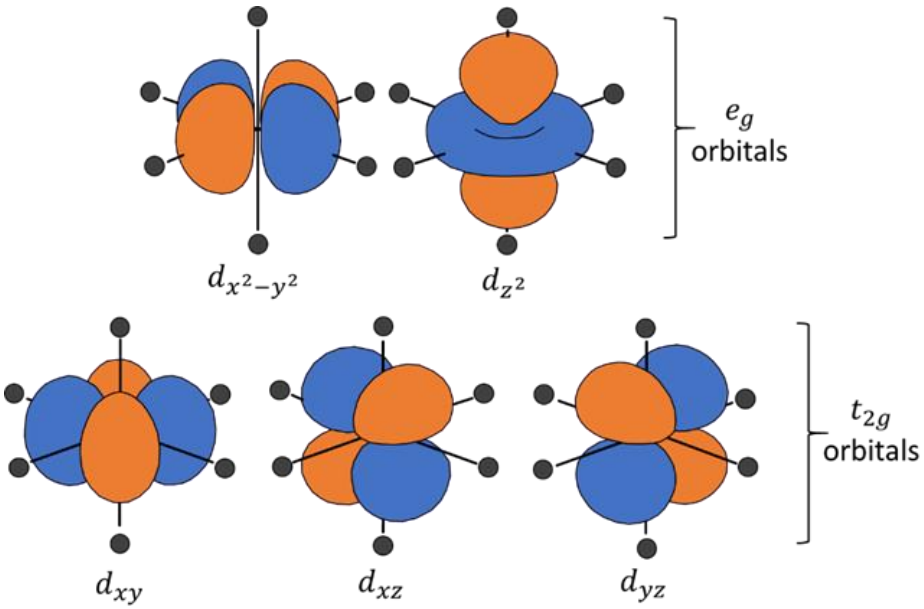

Figure 3.11 *– Depiction of the d-electron orbitals. For a metal ion placed in an octahedral ligand field (black spheres). The e_g orbitals increase in energy while the t_{2g} orbitals decrease in energy when compared to a metal ion surrounded by a spherically distributed charge.*

As is shown in figure 3.11, the d_{xz}, d_{yz} and d_{xy} (t_{2g}) orbitals are orientated between the bond axis while the d_z^2 and $d_{x^2-y^2}$ (e_g) orbitals lie on the axis. The orbitals that lie on axes, d_z^2 and $d_{x^2-y^2}$, experience a greater interaction with these point charges. The result of this is there are now two sets of energy levels, t_{2g} and e_g, separated by a splitting energy, Δ_O , with the lower energy levels corresponding to the orbitals that are positioned away from the point charges (d_{xz} , d_{yz} and d_{xy}) and the higher energy levels corresponding to the orbitals aligned with the point charges of the ligands (d_z^2 and $d_{x^2-y^2}$). The strength of Δ_O depends upon the central metal ion and the type of ligands. The ligand-metal interaction arranged by increasing strength follows the spectrochemical series: $I^- < Br^- < SCN^- < Cl^- < F^- < OH^- < H_2O < NCS^- < NO_2^- < CN^- < CO$.

A metal complex possessing more than three d electrons may be high spin (HS) or low spin (LS) depending upon the occupancy of the e_g and t_{2g} orbitals. Hund's first principle states that it is energetically unfavourable for electrons to doubly occupy the same orbital. The origin of this repulsion between electrons is fundamentally due to the exchange interaction and Coulombic repulsion. This repulsion takes the form of an energy barrier, Δ_{EP} , and for a HS complex the value of Δ_O must be less than Δ_{EP}. If Δ_O is greater than Δ_{EP}, then the complex will be LS as electrons doubly occupy the lower energy t_{2g} orbitals as shown in figure 3.12.

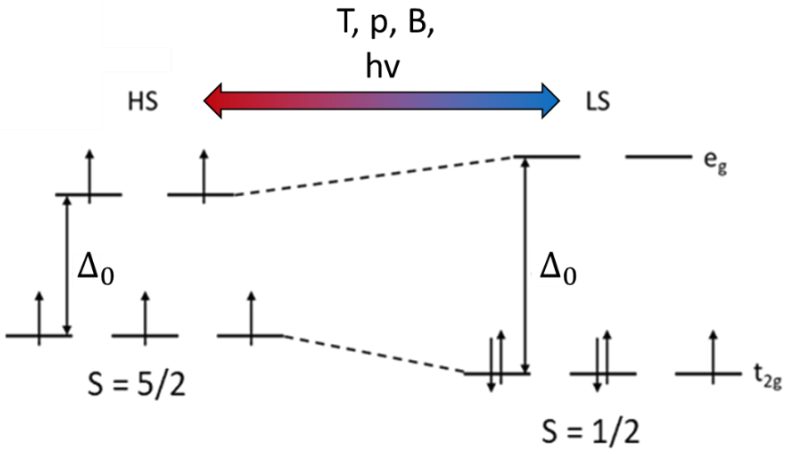

Figure 3.12 *- Resulting energy level splitting by Δ_O and the ability to transition between these two spin states via selected photon irradiation, temperature changes, pressure or strong magnetic field.*

SCO occurs in complexes which have very similar splitting and pairing energies. If we consider the case of temperature being the driving stimulus for the spin transition then this process can be understood as follows. Thermal expansion of the complex results in variation in the metal – ligand bond distance, r, with the interaction strength between metal and ligands following an r^{-5} dependence. A larger Δ_O at low temperatures results in LS state whilst increasing the temperature results in a gradual reduction in Δ_O.

Increasing the temperature results in a point at which the complex will transition to a HS state once Δ_O becomes less than Δ_{EP}. Although there are many transition metal compounds with an octahedral structure it is only a select few which display spin crossover due to the necessary fine balance between Δ_O and Δ_{EP}.

3.3.2 Detection of SCO

The bulk properties of a material in a LS or a HS state can be drastically different allowing the transition to be detected by a number of different techniques. Most commonly the bulk magnetic susceptibility as a function of temperature is measured. Other techniques exist such as Mössbauer spectroscopy,[112] measurements of heat capacity,[79] x-ray absorption spectroscopy and methods which detect the change in the optical properties of the material, for example using UV-vis spectroscopy,[113] Fourier transform infrared spectroscopy (FTIR)[114][113] and Raman spectroscopy.[74][115]

The temperature induced spin transition curves between different SCO compounds can take several forms but the spin transition temperature of a given compound is very well defined, being determined fundamentally by the interaction strength Δ_O. Between different compounds however, the temperature can vary greatly with reported transition temperatures ranging from above room temperature[116] to 100 K and lower,[117] depending upon the structure of the SCO molecule.

In addition to the magnetic properties of SCO compounds, the electron repopulation from the t_{2g} to the e_g anti-bonding orbitals results in a change in the metal-ligand bond distance which in turn can result in an overall change in the volume of the material. [1][118] These changes in bond lengths can be measured exactly using temperature

dependent x-ray crystallography and typically increase by around 10% during the transition from the LS to the HS state.[119][109]

3.3.3 Light Induced Spin Crossover

Finally, it is worth briefly discussing an effect that SCO compounds exhibit known as light-induced excited spin state trapping (LIESST).[120] This is a method of inducing the spin transition of these metal complexes at a temperature different from that of the normal spin transition temperature. The LIESST effect was first reported by McGarvey *et al.* in 1982 in $Fe(biz)_2^{2+}$, $Fe(ppa)_3^{2+}$ and $Fe(pyimH)_3^{2+}$ compounds in solution.

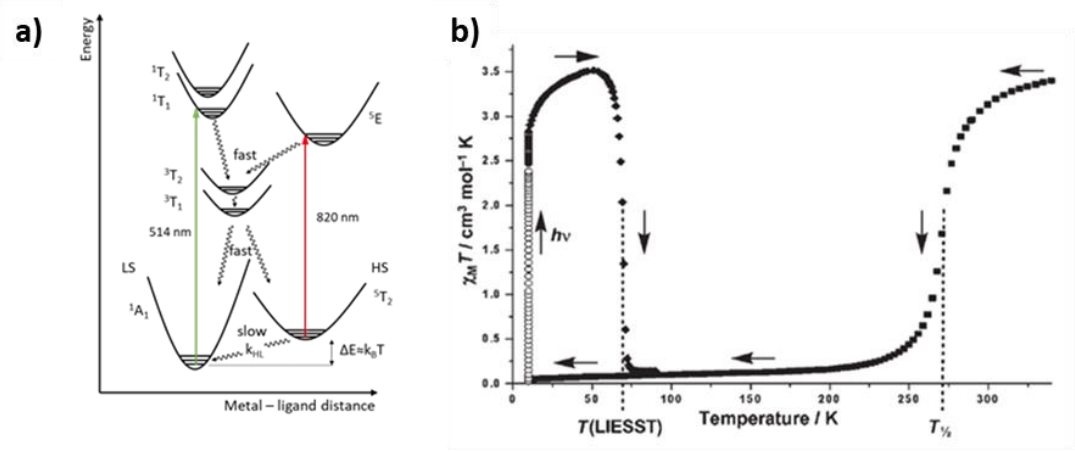

Figure 3.13 *- Energy level diagram showing the electronic transitions that take place during the LIESST and inverse-LIESST effect, figure adapted from* [110] *and* [2]*. b) SQUID magnetometry data of a sample showing ordinary SCO behaviour during cooling (■). The sample is irradiated with laser light at 10K until the magnetisation reaches a value similar to the high spin value (○) recorded at high temperature. The sample is warmed to show the thermal relaxation of the spin state (◆). Adapted from* [121]*.*

The energy level transitions involved in this process are outlined in figure 3.13 a). A complex initially in a LS state at low temperature can be optically excited into a HS triplet state with laser irradiation. Experimental data for this is shown in figure 3.13 b) by the

magnetisation increase at low temperature. Irradiation using a green light (514 nm) promotes electrons into a trapped state whereby their decay must take the form of a forbidden transition from a triplet to a singlet state. Only quantum tunnelling can revert the spin state back from HS to LS resulting in a long-lived HS state.[121] Irradiation with infrared light (820 nm) induces a transition back to the LS state and is termed the inverse-LIESST effect.

This photo-induced excitation is an extremely fast process at the molecular level, with sub-picosecond switching times measured using high speed transient absorption measurements on several different SCO complexes.[122] The decay to the LS state after excitation with light can be very slow, with a relaxation timescale from several hours to even days or weeks when performed at liquid helium temperatures. However, at room temperature the lifetime is on the order of μs or ns.[112][123]

3.3.4 Electronic Properties of SCO Compounds

The motivations behind using SCO compounds in electronic devices is the potential for the spin transition to be used as a switch or for the hysteresis exhibited by some SCO compounds to be used as the active component of an electronic memory.[124] A type of memory could be envisioned which is similar in operation to that of phase-change random access memory (PRAM) which is currently at the stage of being widely commercialised.[125] With this type of memory a layer of chalcogenide alloy, most commonly $Ge_2Sb_2Te_5$ (GST), can be made to switch between an amorphous and crystalline phase by applying current to the material directly or to a heating element located in close proximity.[126] These two states differ in conductivity by several orders of magnitude allowing data to be represented by the high or low resistance state.

Additionally an incomplete phase-change of the material can produce intermediate values to be written allowing for the possibility of analogue data storage and applications in neural networks and artificial intelligence.[127] In the case of a SCO based device, it can be envisioned that the localised heating by a microfabricated heating element[128] results in a switch in spin state of the SCO complex which can be read by measuring the resistance of the device. Already a crossbar array based on this idea has been used as a means of producing a display device utilising the thermochromic properties of certain SCO complexes.[129][3]

3.3.5 Bulk Insulator Conduction Mechanisms

SCO compounds are generally very highly insulating dielectric materials. For example, a conductivity of between 10^{-8} and 10^{-10} S/cm has been measured for $Fe(Htrz)_2(trz)](BF_4)$.[130] Several conduction mechanisms are at work in these materials namely hopping type conduction, Pool-Frenkel emission and space charge limited conduction.[73]

3.3.5.1 Hopping Conduction

Hopping type conduction between shallow trap states occurs in many disordered systems including oxide thin films and polymeric materials.[131] Charge carriers hop with two distinct hopping process: nearest neighbour hopping (NNH) and variable range hopping (VRH), figure 3.14.[132]

Hopping conduction, or phonon assisted tunnelling, is the dominant charge transport mechanisms that takes place in SCO thin film materials. Due to the dependence on the phonon spectrum modulating the hopping rate, the spin transition can be detected as a

changing in conductivity as a result of the change in vibrational frequencies that occur during SCO. Literature reports on bulk measurements of SCO materials generally take place at room temperature, where thermally assisted processes increase the conductivity to measurable levels.[133][130]

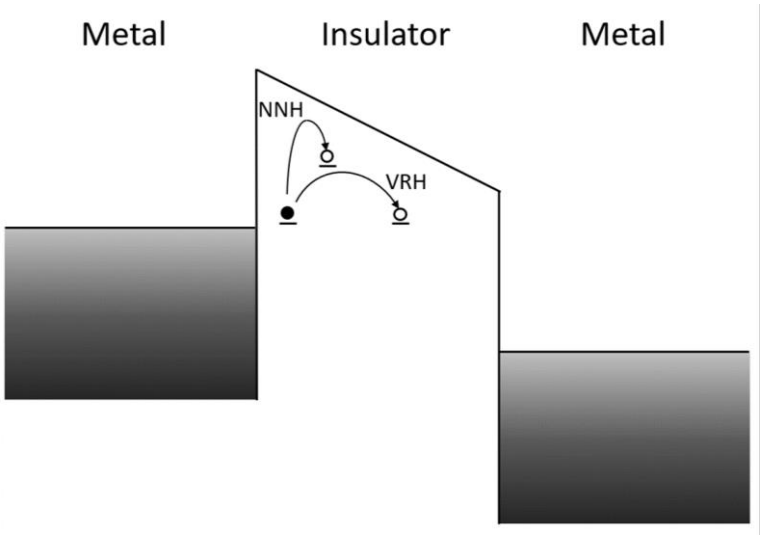

Figure 3.14 *- Schematic of two hopping conduction processes, VHR and NNH. Charge transport occurs via successive hops between states.*

VRH is a process whereby charge carriers hop with a preference for states of similar energy and hence may not be located spatially close together. The rate at which this process occurs is dependent upon three factors:

- the energy difference between the two states,
- the wavefunction overlap of the two states
- the phonon spectrum of the material.

The VRH mechanism was realised by Mott and is sometimes referred to as Mott variable range hopping. It takes the following temperature dependence:

$$\sigma(T) = \sigma_0 \exp\left(-\frac{T_0}{T}\right)^{\frac{1}{(d+1)}} \tag{3.16}$$

where σ_0 is the conductivity of the material at 0 K and d is the dimensionality of the system. For bulk materials the equation becomes:

$$\sigma(T) = \sigma_0 \exp\left(-\frac{T_0}{T}\right)^{1/4} \tag{3.17}$$

The hopping mechanism present in a material can be determined by plotting the temperature dependence of the conductivity $\ln[\sigma(T)]$ vs. $1/T$.

If the states are highly localised (Anderson localization) and the wavefunction overlap of the two states is extremely small, then NNH takes place with the conductivity having the following temperature dependence:

$$\sigma(T) = \sigma_0 \exp\left(-\frac{T_0}{T}\right) \tag{3.18}$$

To distinguish between different hopping mechanism, a plot of $\ln[\sigma(T)]$ vs. $1/T^{1/4}$ reveals a linear fit for VRH while a plot of $\ln[\sigma(T)]$ vs. $1/T$ reveals a linear fit for NNH.

3.3.5.2 Poole-Frenkel Emission

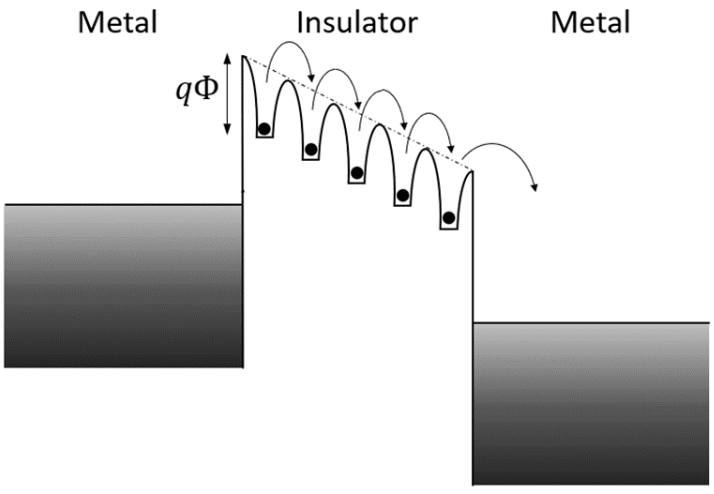

Figure 3.15 *- Schematic of Poole-Frenkel emission. An applied field reduces the energy barrier allowing charge transport to occur via thermal excitation.*

Another method by which insulators conduct is via Poole-Frenkel emission, figure 3.15. Here electrons move through a material as a result of thermal fluctuations between localised states. These states have been reduced in energy by an amount $q\Phi$ allowing for an increased rate of conduction through the material. The temperature dependent of Poole-Frenkel emission is given by:

$$\sigma(T) = \sigma_0 \exp\left(\frac{\beta_{PF} E^{1/2}}{2k_B T}\right) \tag{3.19}$$

where β_{PF} is a material constant, E is the applied electric field and:

$$\sigma_0 = C \exp\left(-\frac{q\Phi}{2k_B T}\right) \tag{3.20}$$

A plot of $\ln[\sigma(T)]$ vs $E^{1/2}/2k_B T$ yields a linear slop with gradient β_{PF}.

3.3.5.3 Space charge limited conduction

Space charge limited conduction (SCLC) is a conduction regime whereby the inbuilt electric field produced by injected charge carriers within a material limits further charge injection. The behaviour is described by the Mott-Gurney law:

$$J = \frac{9}{8}\varepsilon\mu\frac{V^2}{d^3} \tag{3.21}$$

Where V is the voltage applied to the material, ε is the permittivity, μ is the carrier mobility and d is the thickness of the material (film).[134] The onset of SCLC can be identified as a change in the gradient of and I-V plot as shown in figure 3.16 for a SCO thin film.

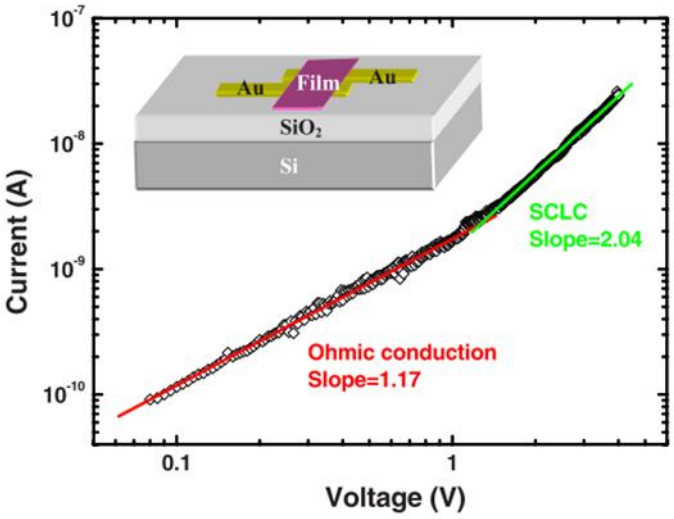

Figure 3.16 *- Transition from Ohmic conduction to SCLC in a 240 nm thick thermally deposited $Fe(phen)_2(NCS)_2$ thin film between Au electrodes with a channel area of 2 x 100 μm^2. Reproduced from* [73].

3.3.6 Studies of SCO Devices using Density Functional Theory

Density functional theory (DFT) is a computational tool used to calculate and predict physical, chemical and material properties of nanoscale system.[8] It does this by providing an approximate solution to the Schrödinger equation for these many-body systems by considering only the spatial-electron density.[135]

Using DFT, many groups have attempted to address the question as to what effect, if any, the spin transition has on the conductivity of a SCO complex when coupled to electrodes at a single molecule level. Results are fairly diverse, in part due to the rich variety of different SCO compounds but also due to the complexity of the calculations with results being sensitive to the exact binding arrangement that the molecule has with the metallic electrodes.[39] In general, DFT predicts that the spin transition is

accompanied by a change in conductance with the HS stage usually possessing higher conductivity.[84][136]

In work studying triazol based SCO complexes, Aravena *et al*. have determined very large differences in the spin resolved density of states (SR-DOS) for the complex in the LS and HS states. The calculated SR-DOS for the simulated device is shown in figure 3.17 c) for the LS and figure 3.17 d) for the HS state.[137][138] The electronic transport properties and the overall conductivity of a molecule between electrodes is dominated by the orbitals lying close in energy to the fermi level. For this particular system, depicted in figure 3.17 a), they have determined these energy levels are those associated with the t_{2g} orbitals, located predominantly on the central Fe ion of the complex, while the ligand orbitals lie higher in energy and have little contribution to the transport properties.

Figure 3.17 b) shows the calculated I-V characteristics of the molecule in both spin states, showing the large variation in conductance level, with the HS state being around five times more conductive than the LS state. DFT calculations by Burzurí *et al.* for the $[Fe(L')_2](BF_4)_2$ CH_3CN H_2O complex in contact with graphene electrodes also result in similar conclusions.[139]

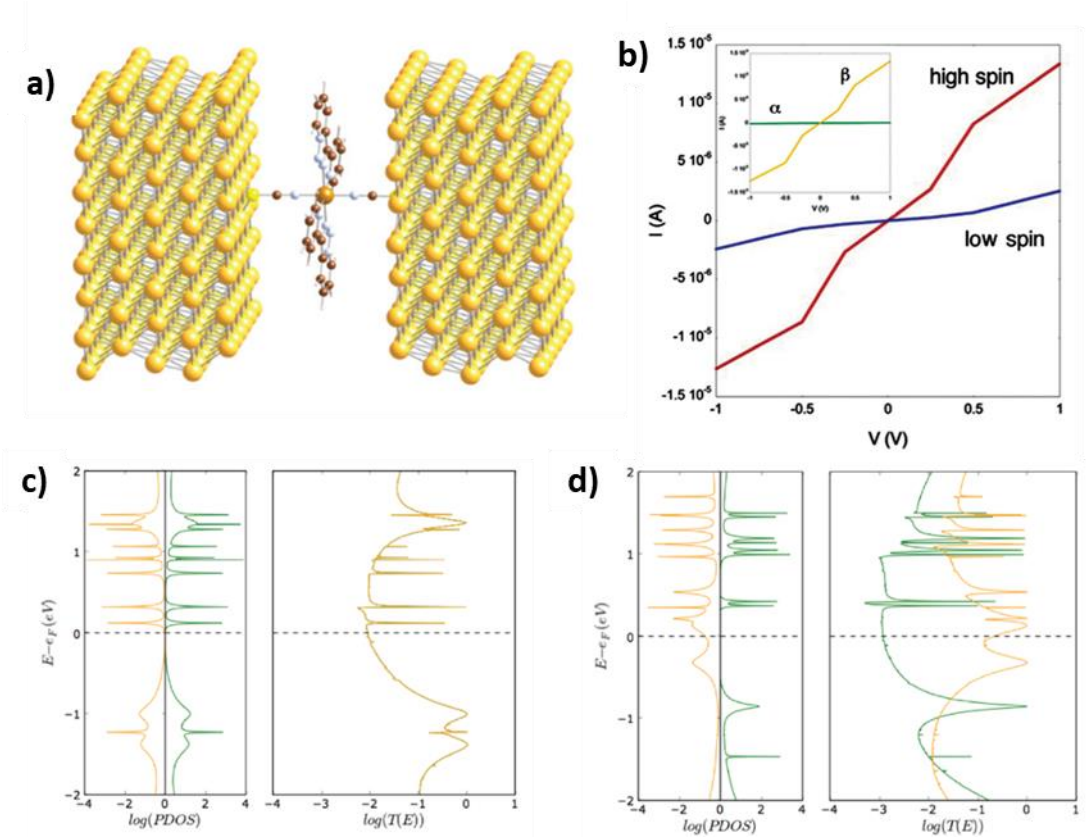

Figure 3.17 *– a) Molecular arrangement used in DFT calculation of a triazol SCO molecular junction. b) Calculated I-V characteristics in high and low spin states. c) Spin-resolved density of states (left) and transmission function (right) for the molecule in low spin state and d) Spin-resolved density of states (left) and transmission function (right) for the molecule in high spin state. Insert shows the contribution from high spin and low spin electrons to the high spin state revealing the spin-filtering behaviour of this device (note: yellow and green traces correspond to spin up and down electrons respectively). Reproduced from* [138].

Baadji *et al.* have also determined a resistance decrease for a [Fe(2,2':6,2''-terpyridine)$_2$]$^{2+}$ complex bound to Au electrodes and also report similar behaviour for a second compound, [Fe(2,6-bis(pyrazol-1-yl))]$^{2+}$.[18] The group predicts that the conductance change is highly bias dependent, at low bias the HS state is more conducting while at finite bias the difference in conductivity has the potential to be very large with calculated I-V characteristics suggesting a difference of up to 3 orders of

magnitude in the conductivity between the HS and LS states.[140] This arises from a significant lowering of the HOMO-LUMO gap as the terpyridine complex transitions from the LS to a HS state. This is shown in figure 3.18.

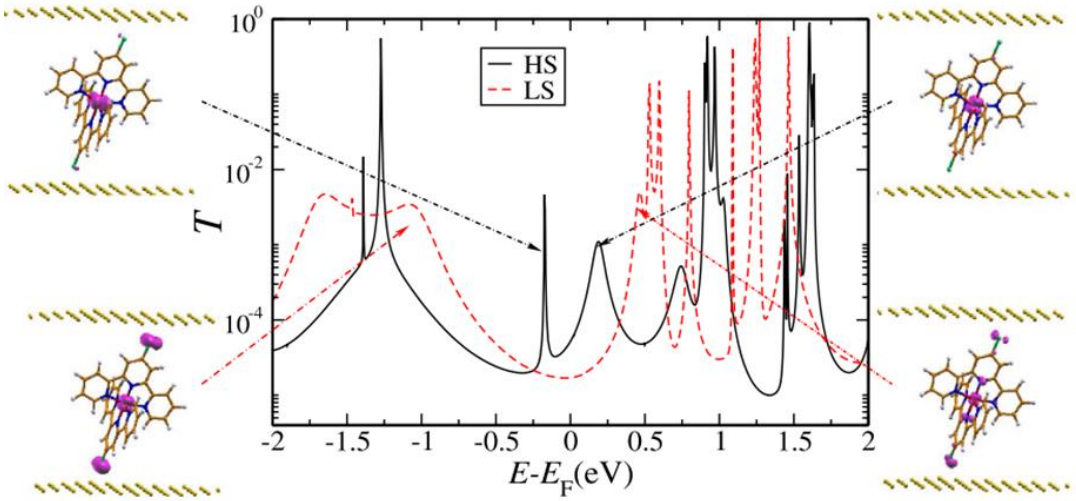

Figure 3.18 *- Transmission coefficient for a [Fe(2,2':6,2''-terpyridine)$_2$]$^{2+}$ complex showing differences in the HOMO-LUMO gap size in two different spin states. Reproduced from* [18].

An interesting observation made by Aravena, Huang[19] and later by Burzurí is the ability of these complexes to act as a spin filter. This is due to the large differences between the transmission functions for spin up and down electrons. In the HS state, current flow out of the molecule is highly spin polarized giving such a device geometry promising application in molecular spintronics.

4.1 Nanoimprint Lithography

Nanoimprint Lithography (NIL) is a nanofabrication technique able to pattern materials with nanometre resolution at both high throughput and low cost. It is seeing increasing use in both scientific and industrial applications due to the advantages it has over traditional techniques such as EBL and UV lithography, being fast, high resolution and suitable for volume roll-to-roll substrate patterning processes. In addition it offers the unique ability to produce 3-dimensioanl patterns allowing for a reduction in processing steps as multiple layers can be fabricated with a single lithography step. NIL can be divided into two main classes; thermal-NIL and UV-NIL.

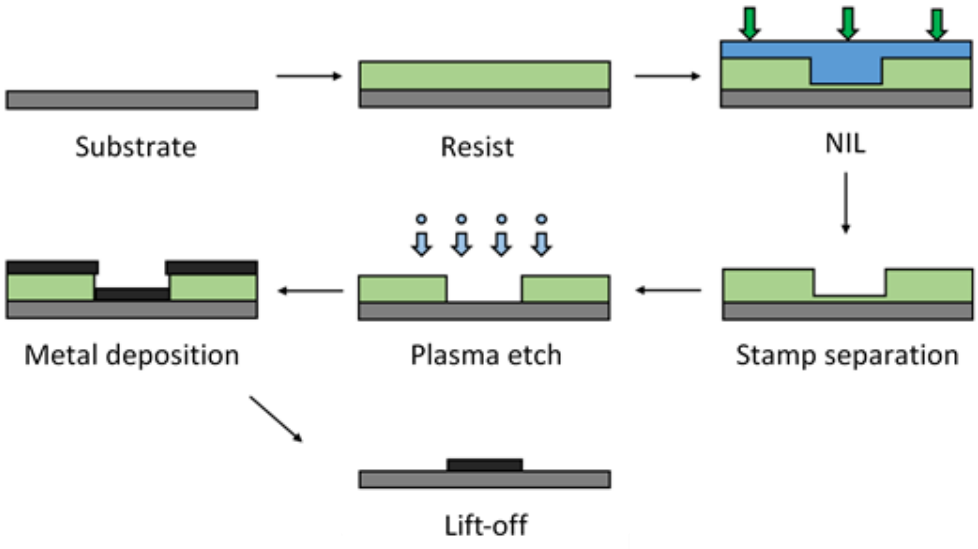

Figure 4.1 *- An example of the NIL process used to pattern a substrate using a lift-off process. The NIL step could be a thermal imprinting process and/or include a step where resist is UV cured.*

In thermal-NIL a stamp is first prepared with the features that are to be imprinted. A silicon wafer is almost always used as the substrate to make the stamp on as it is both strong, low cost and flat while also being compatible with other nanofabrication processes. The process used to produce the features on the is a series of EBL and/or photolithography steps followed by reactive ion etching so that the windows opened into the resist can then be used to transfer the features into the silicon wafer.

To carry out an imprint, a substrate is coated with a uniform layer of thermoplastic resist usually by spin coating and then a stack is made with the stamp. By applying heat and pressure to the stack, the pattern is transferred in to the resist layer and after separating it from the stamp this patterned resist can be used as a mask for deposition of metal, as shown in figure 4.1, or for other processes such as pattern transfer through etching.

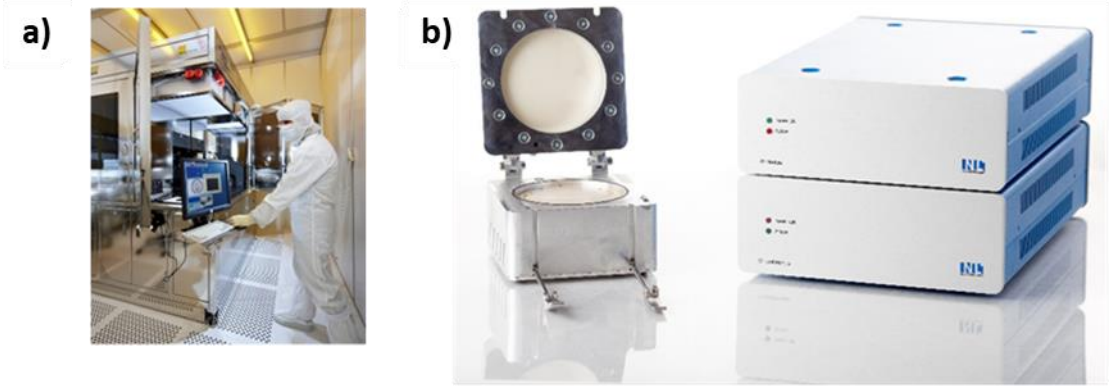

Figure 4.2 *- The equipment used in NIL can vary significantly, here we show a) a state of the art step and flash imprinter used for pattering 200 mm wafers with high resolution stepping and alignment (SET SAS NSP300) and b) the CNI (Compact NanoImprint) tool used in this work consisting of a chamber with pressure bladder, ceramic heater and controllers (NIL Technology).*

The process of NIL is very similar to hot embossing and these terms are sometimes used interchangeably. However, hot embossing refers to processes which transfer a pattern

into a material which is typically much thicker than the features being imprinted such as a polymer sheet.

The residual layer thickness, h_r, can be determined by considering the imprinted depth, d, and the overall protrusion coverage, PC, of the stamp. Equation 4.1 is obtained by considering the conservation of volume when resist is displaced during an imprint as:

$$h_r = h_0 - (1 - PC)d \tag{4.1}$$

The velocity of the imprinting process can be determined by solving the Stokes equation for imprinting a protrusion of width, W, under an imprint pressure, p, into a resist with viscosity, η, and with a thickness, h, to give:

$$v_{imprint} = \frac{2}{3}\frac{h^3 p}{\eta W^2} \tag{4.2}$$

Equation 4.2 reveals several important parameters about the imprint speed at any given moment in time. Firstly, that the speed of the imprint is inversely proportional to the viscosity. It is obvious therefore that choosing a resist with a low viscosity will result in an imprint to a given depth much faster than for a resist with a high viscosity. Because viscosity is heavily temperature dependent and typically decreases around an order of magnitude for every 10°C rise in temperature (once heated above T_g), it may be favourable to choose a specific resist and modify its viscosity by heating 10 – 20 °C higher rather than choosing a completely new resist polymer. The viscosity of some common polymer resist materials is shown in figure 4.3.

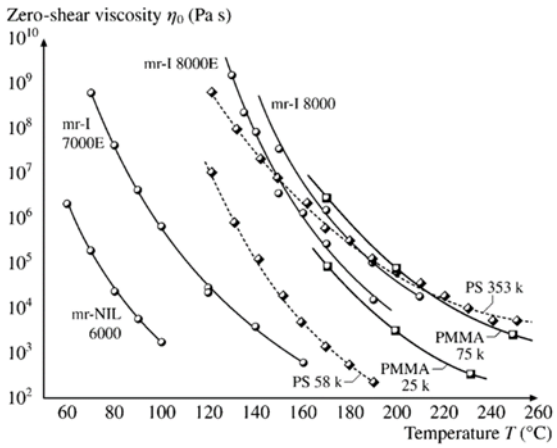

Figure 4.3 *- A selection of commonly used imprint resist in NIL showing their zero-shear viscosities (η_0). Reproduced from* [141].

Secondly, it can be seen that as the imprint progresses and the protrusion begins to thin out the remaining resist that the velocity slows. For a finite duration imprint there will always be a residual layer of resist remaining after the imprint stops. This will need to be removed by some means if NIL is to be used as a direct mask for metallization or lift-off.

Finally, the imprint speed depends linearly on the imprint pressure. If the stamp geometry contains protrusions which vary in area then, for a hydrostatic press, there will be a local variation in the imprint speed. This leads to stamp bending. A solution to this problem is to imprint for a far longer time than would ordinarily be necessary. This will give time for the larger features to "catch up" with the much faster smaller features.

Although this discussion and the work here focuses on thermal-NIL, it is worth briefly discussing UV-NIL and the advantages it may have in imprinting the features used in this work. These two NIL processes differ in that thermal-NIL uses far higher temperatures, typically 130 - 190°C, and relies on the heating and cooling of the polymer resist above and below its glass transition temperature, T_g, to retain to the shape of the imprinted

features. UV-NIL on the other hand uses a UV flood exposure once the stamp has imprinted that cross-links the polymer and maintain the shape of the imprinted features once the stamp is removed. Because the rigidity of the polymer is produced through a chemical change, and not simply by cooling the polymer below T_g, the polymer can be made to have a very low viscosity and a very fast imprint can be achieved with small residual layer thickness. An additional benefit of UV-NIL is that it also offers the possibility of alignment of the imprinted features with already fabricated features if the stamp or substrate is made of a UV transparent material. This is possible with UV-NIL as the pressures involved are far reduced leading to a minimal shifting of the stamp and substrate during imprinting as well as the possibility of having a UV and optically transparent stamp/substrate allowing for viewing of alignment markers.

4.1.1 Defect Control

The imprint process is usually performed in vacuum so that the resist undergoes a degassing step for several minutes before pressure is applied. This allows any remaining gas or solvent to be removed from the resist film which can otherwise lead to trapped gas between the stamp and film. These are detrimental to the imprint as they present themselves as bubbles near the imprinted features.

A main issue encountered with NIL is dust and particulates between the stamp and substrate. NIL is very sensitive to these since the stamp protrusion height and resist film thickness is in the range of 50 to 300 nm and a dust particle may have a size of several micrometres. A dust particle can easily prevent imprinting of the pattern due to the vastly different size difference. Fortunately, the stamp is not a perfectly rigid structure and there is a certain degree of flexibility. The result is that if a particle is present, it is

only the area surrounding the particle which does not become imprinted. By making a stamp/device design which can tolerate a certain amount of contamination, NIL can still be used successfully.

A mentioned previously, with NIL it is desirable to increase temperature as high as possible as this will increase the imprint speed and, given sufficient time, will allow all features to be imprinted to the same depth regardless of their area. However, this is not without problems. Firstly, a higher temperature imposes greater stress on the tool and stamps. With an increased thermal cycling there is a greater stress on both the stamp and anti-stick coating as well as the imprinting tool giving a shorter lifetime before cleaning and recoating or maintenance of the equipment is necessary. Secondly, a higher temperature promotes the formation of flow defects in the resist. These are defects caused by electrostatically driven capillary forces which act between the resist surface and stamp and cause unintentional and detrimental flow to occur.[142][143] Such flow takes the form of bridging between the incoming stamp and resist surface as shown in figure 4.4 and is exaggerated at higher temperature due to reduced viscosity.

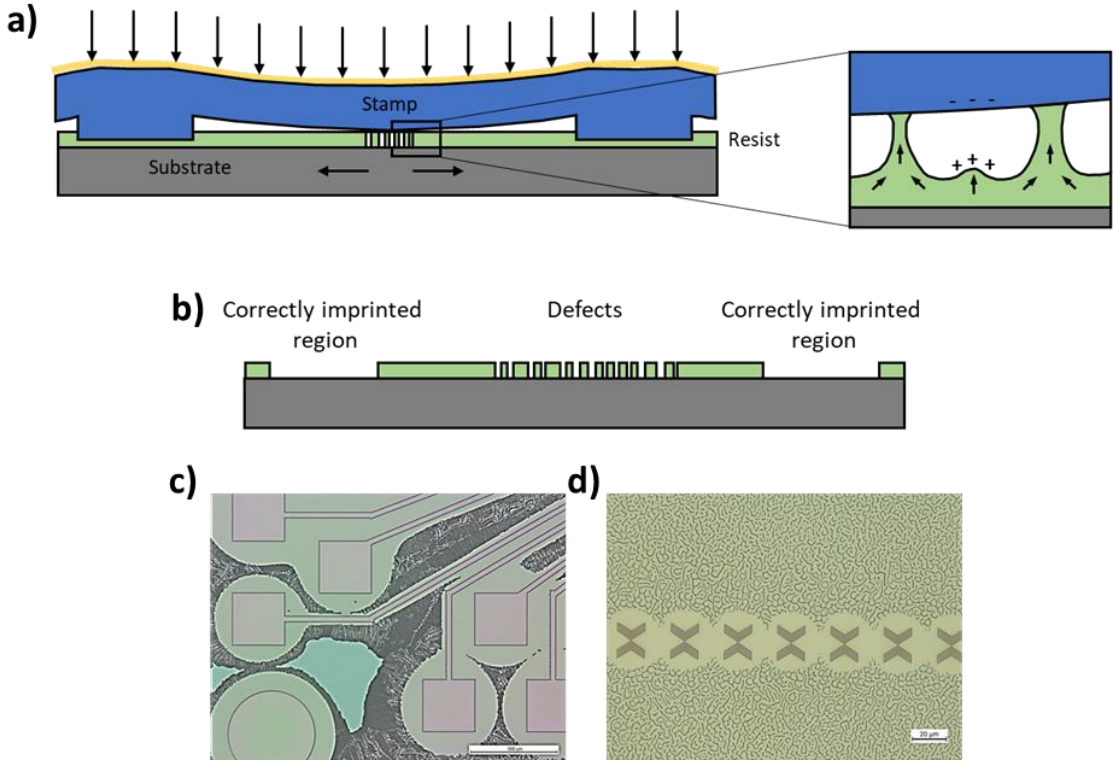

Figure 4.4 *- a) Bending of the NIL stamp can result in the occurrence of resist bridges around stamp protrusions (or particles) b) resultant patterned resist contains many voids which can be transferred to the substrate in a patterning process. Microscope images of flow defects in c) mrI-8000 and d) PMMA 15k polymer resists 150 nm thickness.*

Bending of the stamp around particles or between stamp protrusions often results in the appearance of these defects.[144] Almost always, this type of polymer flow exposes regions of the substrate that are especially detrimental to the lift-off process, resulting in areas of the substrate that will unintentionally become patterned during metallization. If the entire stamp makes contact with the resist surface uniformly then these types of defects are avoided. Most likely this is due to the avoidance of localised charge non-uniformity as occurs when the stamp makes contact due to bending.

Temperature plays a very critical role in reducing the occurrence of these types of defects and obtaining a successful imprint. In this work it was found that there exists a "temperature window" above and below which these defects occur. At high

temperature, the resist viscosity is very low and an upward flow of resist that bridges with the stamp easily occurs. Increasing the resist thickness to a value greater than that given by equation 4.1 is a successful strategy to avoid these defects. This is because this equation assumes a complete imprint whereby the stamp protrusions “bottom-out” and come into contact with the substrate surface. In reality this never happens as the localised resist viscosity underneath a stamp protrusion dramatically increases as the polymer chains of the resist become confined between the stamp and substrate, effectively preventing the imprint from completing in any reasonable time.[145][143] Depending upon the exact geometry of the stamp, the stamp may begin to bend rather than imprint further and once the stamp comes into close proximity with the low viscosity resist surface, bridging defects will then occur. Increasing the thickness of the resist avoids this situation but has the disadvantage that a longer residual layer removal step may be necessary. Similarly, these defects occur if the imprint is carried out at a low temperature and thus high viscosity (but still above the glass transition temperature of the resist).

At low temperatures a large amount of stamp bending is present from the beginning of the imprint since none of the features can imprint into the high viscosity resist. The result is that there exists an optimised point in temperature (for a fixed imprint pressure) above and below which flow defect appear on the imprinted resist due the resist viscosity being sufficiently reduced so the imprinting will occur uniformly but not reduced to such an extent that polymer brining can easily form. The importance of temperature on the NIL process is highlighted in figure 4.5 where a stamp was imprinted at three different temperature showing the occurrence of flow defects at 190 °C and 150 °C while at an optimised temperature of 180 °C no defects were present.

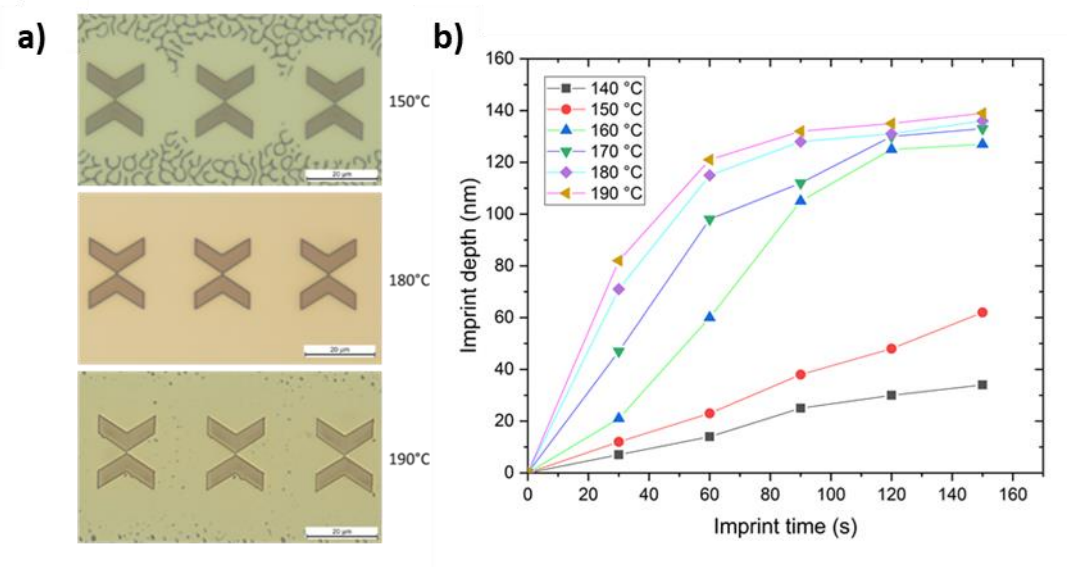

Figure 4.5 *- a) Imprinting of the nanojunction (Master) stamp into bilayer resist at increasing temperatures leads to the appearance of flow defects. Areas immediately surrounding the imprinted features appear well imprinted due to a squeeze flow of resist at 150°C while at 190°C voids appear. 180°C gives optimum imprinting behaviour. b) Imprinting depth measured at increasing temperature into 150 nm thick, 15k PMMA resist with constant applied pressure 2 bar. The CNI imprinter was rapidly cooled to a temperature below 110°C in order to halt the imprinting process, however it is likely that some small amount of imprinting depth will occur during cooling.*

4.2 Single-Step Device Fabrication

4.2.1 Stamp design

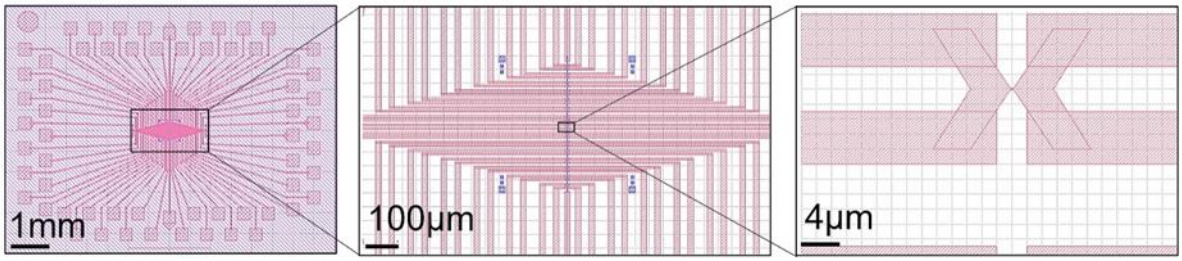

Figure 4.6 *- The stamp design used for fabrication of nanogap electrodes shown in the program GDSII design software Klayout.*

Considering the above, this discussion will now focus on the design of the stamp that we used to imprint a complete nanojunction device. A number of design criteria must be met when designing this stamp:

- It must contain a large number of devices to account for failures during metallization, lift-off, electromigration and molecule incorporation.
- Each junction must be connected to four leads which each terminate at a contact pad. This will enable us to eliminate lead and contact resistance using a four-point measurement technique that is discussed later.
- Contact pads must be as large as possible so that they can be contacted with probes easily but small so that imprint speed is as fast as possible.
- The conducting channel (or junction) must be as small as possible so that a high enough current density can be reached for electromigration, but large enough so that the stamp is mechanically stable and will be able to withstand many imprinting cycles.

The design of this stamp is shown in figure 4.6 with the stamp fabrication being carried out by NIL Technology, Denmark. A single 100mm diameter Si wafer is used and contains 12 copies of this single design.

4.2.2 Single Step Devices

To imprint the stamp containing the complete device in a single step, the imprint polymer mr-I 8030E (Mirco Resist Technology) is spin coated onto a silicon wafer with 1 µm of thermally grown oxide (SVM Microelectronics). The resist thickness is 200 nm and 1 µm of oxide is used as this provides a good a non-conductive substrate for the devices. The substrate is cleaned and dehydrated before coating so that the adhesion of the resist with the oxide surface is maximised. This reduces the likelihood that any resist will delaminate and contaminate the stamp when it is separated after the imprint. By systematically imprinting with increasing temperature as well as also varying the applied pressure and duration, an imprint temperature of 190°C, pressure of 5 bar and a time of 60 mins is found to be sufficient for imprinting the features of the stamp while minimizing the occurrence of defects and giving a minimal residual layer for this particular stamp geometry.

After NIL, the stamp can be separated from the resist/substrate using a scalpel blade. To remove the residual layer from the bottom of the imprinted features an O_2 plasma asher/cleaner (Diener Electronic GmbH) is used. This system uses an inductively coupled plasma in a cylindrical quartz chamber rather than a directional parallel plate type etcher that was used for reactive ion etching. As such the etch is more isotropic and will result in a broadening of the features and so the etch time is limited. Because this length of time is dependent upon the residual layer thickness, decreasing the residual layer

thickness is one of the parameters which is tailored when finding the correct imprint parameters. A great deal of time was spent determining and improving the uniformity of the etch etching within this type of plasma asher. It was found that towards the walls of the vessel the etch rate was much greater than towards the centre and so care was taken to place samples in the same position during the etching process. A custom-made substrate holder was used to improve etch uniformity across the wafer by rotating the substrate at around 2 rpm using a small motor and gearbox during the etching. During the plasma etching the chamber pressure is maintained at 0.35 mbar and the power level is maintained at 50 W. The residual layer is removed after 12 minutes of etching.

The removal of the residual layer is confirmed by stylus profilometry (Bruker DektakXT) or tapping mode AFM (Bruker Dimension Edge). Using profilometry the complete removal of this layer can be determined by placing a scratch nearby to an imprinted feature. Surface profilometry can then compare the depth difference between the bottom of the scratch (the substrate surface) and the depth of the imprinted feature. In this method it is assumed that the substrate is flat across the several millimetres between the scratch and imprint which is valid for a silicon wafer but may not work well for substrates such as float glass. Another method used is AFM to image the bottom of imprinted features after incremental cycles of plasma etching. There is a distinct difference between residual polymer and substrate seen in the phase channel of the acquired data. This is likely due to the different mechanical properties of the polymer resist when compared to the hard SiO_2 surface of the substrate.

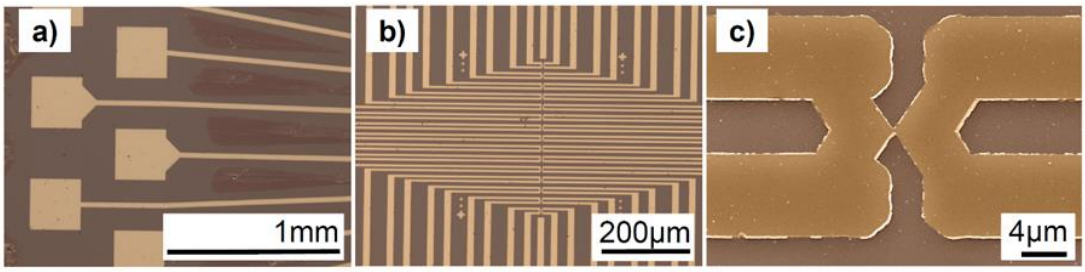

Figure 4.7 *- Optical a - b) and c) SEM images of nanojunction electrodes fabricated using single step NIL.*

The imprinted and etched wafers are then loaded into an electron beam evaporator with a base pressure of 2×10^{-7} mbar and 20 nm of Permalloy ($Ni_{81}Fe_{19}$ (WT%)) is evaporated at a rate of 0.01 nm/s with the substrate rotating at 0.5 rev/s. The composition of the evaporated films is checked with EDX performed on a thick test sample and is in good agreement with the source material. Lift-off is accomplished by immersing the substrate into acetone with sonication and takes approximately 10 minutes. A completed device is shown in figure 4.7. Because of build-up of metal during deposition "ears" are formed on the edges of the features on devices. A brief etch in 10% HCl solution for the Permalloy devices removes this material. A comparison of a junction before and after this etch is shown in figure 4.8.

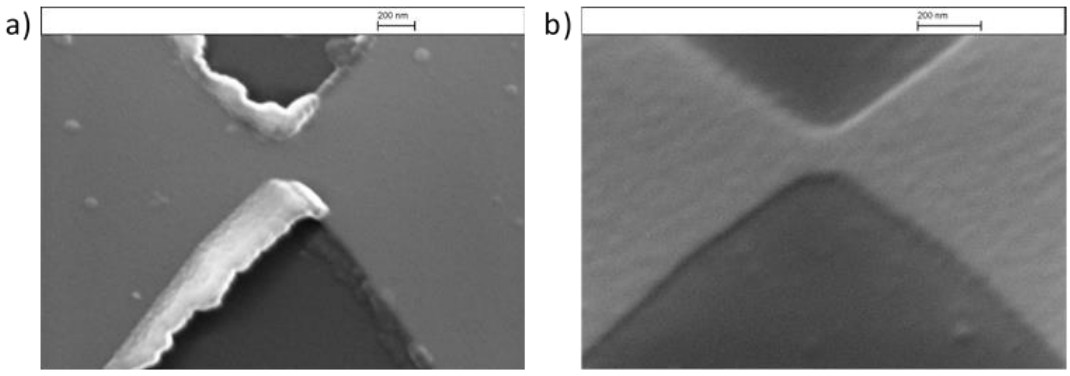

Figure 4.8 - *Representative SEM images of nanojunctions on two devices a) no etching and b) after etching for 45s in 10% HCl : DI water solution at room-temperature with agitation.*

Overall the devices produced using this method were not very reliable. Out of 15 junctions per device, approximately 50% suffered from short circuits (resistance was far lower than that of the junction alone) or showed an open circuit. The single step process meant that large contact pads needed to be imprinted so that electrical contact can be made to the device. Because of the large amount of resist that must to be displaced to imprint these pads, a large pressure must be applied to increase the speed of the imprint and a large number of flow defects were present on the devices. This resulted in electrical short circuits and although electromigration of some of these junctions is shown to be possible, the next sections will discuss the work done to improve device reliability, namely a two-step lithography process in which a bilayer resist was used for NIL.

4.3 Bilayer Nanoimprint Lithography

One of the inherent flaws using NIL is that it is very difficult to develop a lift-off process. The resist sidewalls are at best vertical with respect to the substrate surface. While a single step imprint process has been demonstrated to work, as shown in the previous section, the edge quality of the patterned features remains poor and it was only possible to produce working devices using metals which have good substrate adhesion such as Permalloy. When attempting lift-off with Au it was found that the layer did not remain attached to the substrate.

For good lift-off and edge quality of the features, and to allow a wider choice of metals for the nanojunctions, it is necessary to produce an undercut in the patterned resist. This profile prevents metal depositing on the sidewalls and forming interconnects

between metal deposited on the substrate and metal deposited on the sacrificial resist surface.

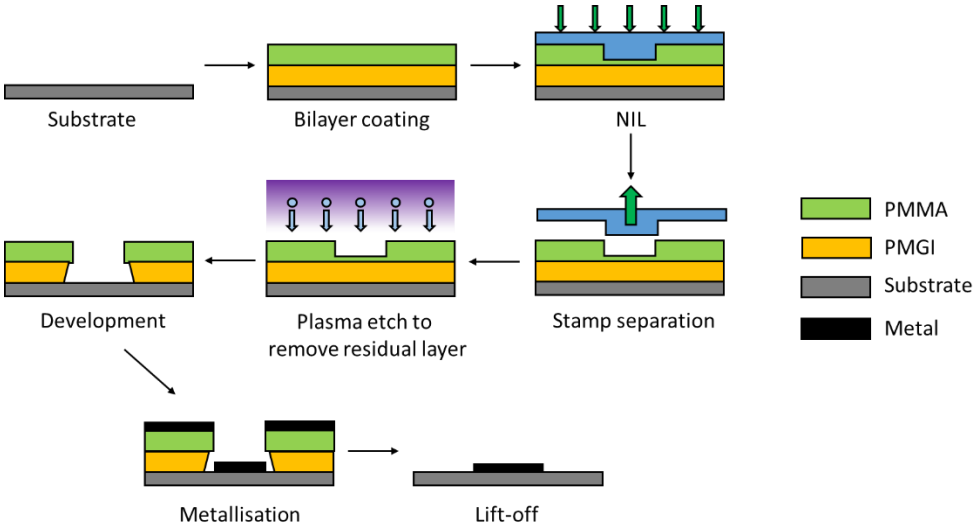

Figure 4.9 *- The process used for bilayer NIL.*

To obtain this type of resist profile using NIL the work of Carlberg *et al.* was used as a starting point.[146] In this work a bilayer resist is used and an undercut into the bottom layer is achieved by selectively removing it in a solvent. A careful choice of polymer resists as well as the solvent used for development is needed for this technique to work. A polymethylglutarimide (PMGI) resist is chosen for a lift off layer that remains highly viscous at the imprint temperature used and so does not flow which would result in a disturbance of the bilayer structure. The bilayer imprint process is depicted in figure 4.9.

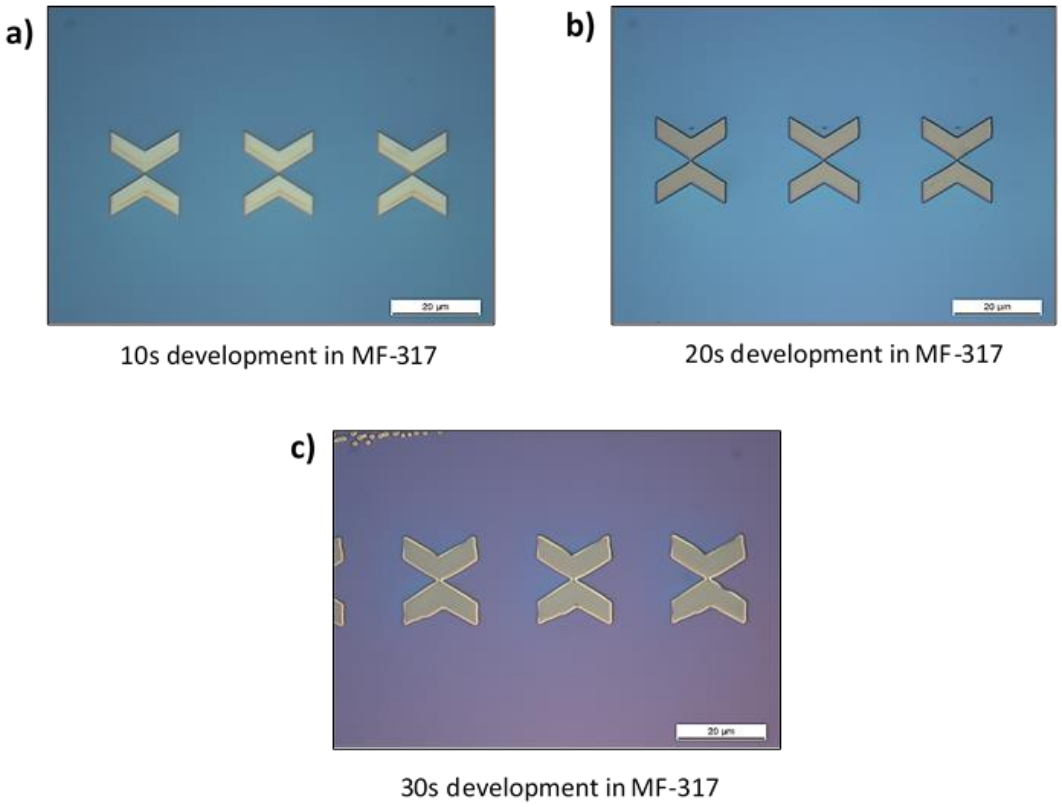

Figure 4.10 *- Optical images of the development process. a) the imprinted features after PMMA residual layer removal b) shows greater contrast on the profile edges indicative of an undercut formation and c) an over-developed structure with a collapsed and distorted pattern.*

First a layer of PMGI SF5 (MicroChem) is spin coated at 3000 rpm to obtain a 150 nm thick film and baked at 190°C for 2 minutes. This baking step set the development time and is chosen to be the same as that of the imprint temperature. Following this PMMA 15k M_w is dissolved in chlorobenzene and filtered to remove undissolved particulates. This is spin coated on top of the PMGI to a thickness of 200 nm and baked at 170°C for a further 2 minutes. This bilayer is then imprinted using a stamp with 150 nm protrusions. When the stamp is separated, the residual PMMA layer is removed using an O_2 plasma etch for 6 minutes to expose the lower PMGI resist. An undercut can then be formed by selectively dissolving the PMGI layer using MF-319 developer (Shipley) with the development time being used to determine by optical microscopy, figure 4.10. SEM is

also used to precisely characterised the plasma etching of the top PMMA residual layer and the degree of undercutting of the layer during development. An example of an SEM image of this undercut bilayer structure is shown in the figure 4.11. Metal is deposited using the same methods as for the single layer imprint except 15 nm of Co or Au is used. Lift-off is achieved by first removing the PMMA layer with acetone and then the PMGI is removed with a soak in 1-methyl-2-pyrrolidone.

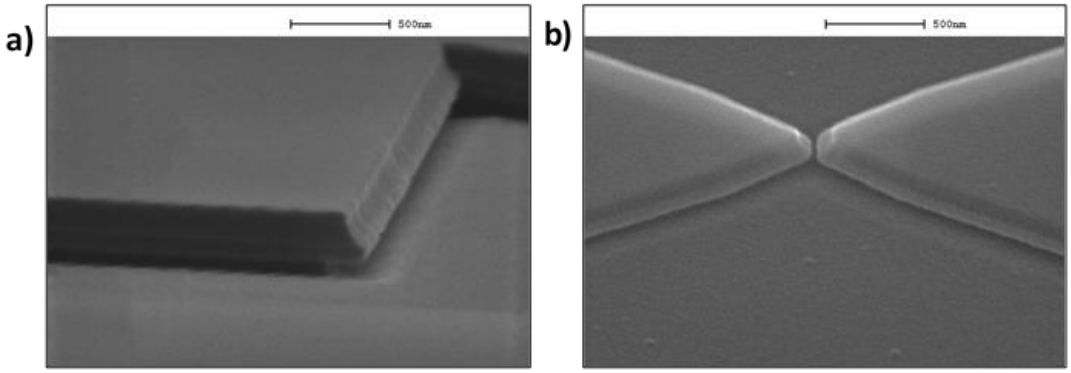

Figure 4.11 *- SEM image of an a) edge profile of the imprinted bilayer resist and b) nanogap region of the resist used to form the narrow conducting channel of the device.*

In addition to using NIL with a bilayer resist, we used a two-step lithography process whereby the large contact pads and leads are patterned separately from the junctions. This has the benefit that it removes the need to imprint the large features resulting in a faster imprint and a reduced and uniform residual resist layer across the entire imprinted substrate.

4.3.1 Stamp Fabrication

The stamp used in this two-step process was fabricated at the Micronova cleanroom at Aalto University, Finland. The method used to fabricate the stamps involves using EBL

to pattern a resist layer that acts as a mask for protecting the silicon substrate during a reactive ion etching procedure. This process is outlined in figure 4.12.

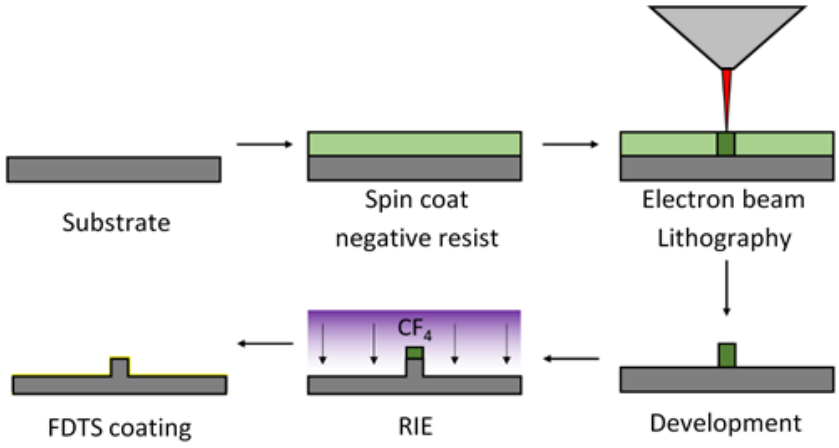

Figure 4.12 *- The steps used in fabricating a NIL stamp on a Si wafer using a series of EBL and reactive ion etching.*

A Vistec 5000 EBL system was used to pattern the resist. This system has a beam spot size of 2.2 nm and can reliably pattern resist with features around 10 nm. This system is also able to pattern 100 mm diameter wafers and produce 56 copies of the design shown in figure 4.13 for a total of 780 total nanojunctions on one wafer during a single run.

This is achieved by first spin coating AR-N 7520 resist (Allresist GmbH) to a thickness of 300 nm. The thickness is determined by the polymer etch resistance with respect to the Si substrate and the etch depth. The Si substrate used is a n-type degenerately doped Si wafer. This reduces the possibility of charge build up on the substrate which could negatively affect the resolution of the EBL process. The beam current and dose were optimised by running test arrays onto silicon wafer offcuts coated with the same resist and thickness but with different beam parameters (current and dose). The resulting features were developed and inspected with SEM to determine the optimum

parameters. It is important that the EBL process is optimized so that the developed features have sharp edges and be a uniform height. Also, it is important that there is little residual resist in areas that have not been patterned. This is achieved predominantly by optimising the development time but also adjusting the beam parameters. This is vital as residual resist will produce a non-uniform etching depth around features into the underlying silicon wafer when it comes to transfer this pattern using etching. These unwanted features will then be transferred to the final design when this is used as a stamp in nanoimprint lithography. A dose of 700 µC/cm^2 and 8 nA beam current is found to give satisfactory results with a development time of 70 s using AR 300-47 (4:1 in DI water).

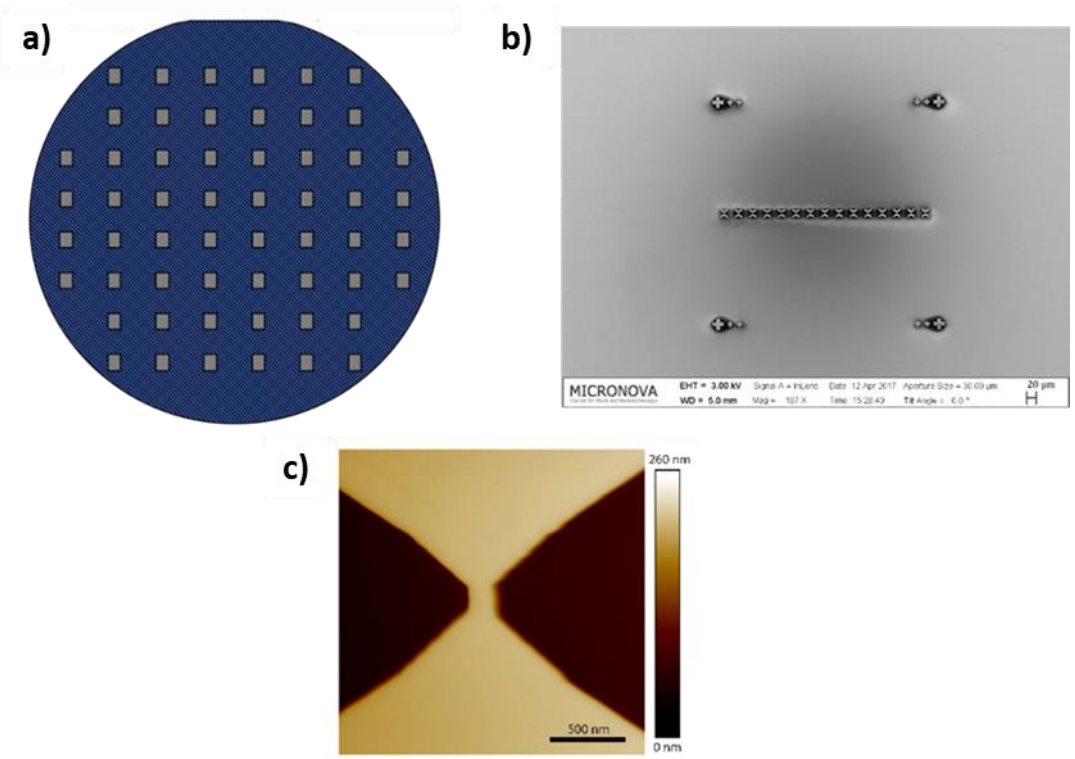

Figure 4.13 *- a) Stamp design consisting of 56 groups of 15 nanojunction (crosses) on a 100 mm diameter Si wafer fabricated using EBL and reactive ion etching. b) SEM image of one group of 15 nanojunction showing marks for photolithography alignment. c) AFM height map of the stamp and showing the channel region (yellow) that is at the centre of a single cross and used to make a nanojunction by electromigration.*

After development, the wafer is etched to a depth of 150 nm using $CF_4 + O_2$ reactive ion etching (Oxford Plasmalab 80) and then cleaned of resist with a second high-power pure O_2 plasma. An anti-stick coating of perfluorooctyltrichlorosilane (FDTS) is applied by placing the stamp in a vacuum chamber along with a droplet of FDTS.

4.4 UV Lithography

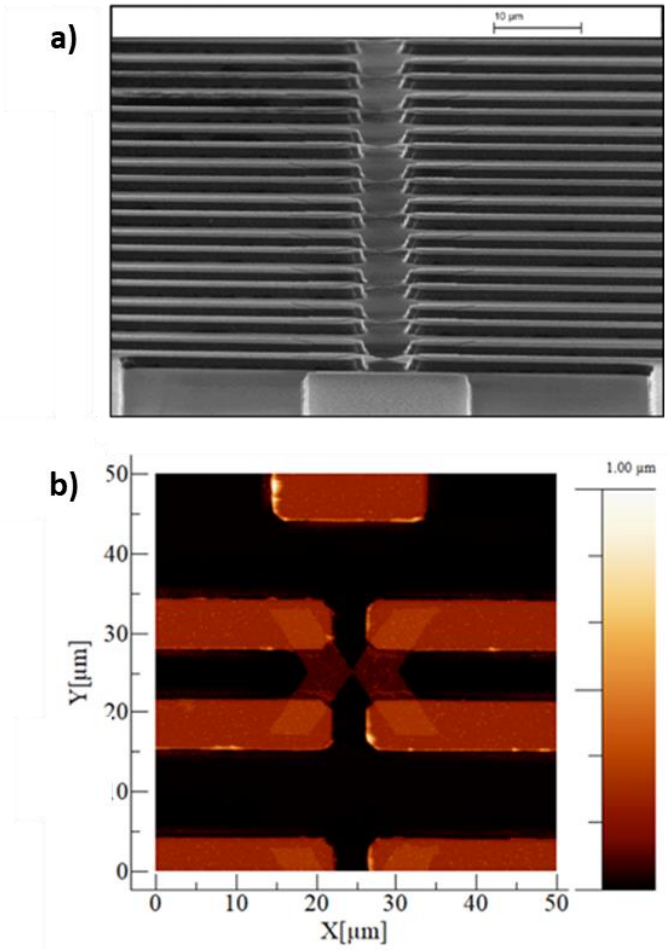

Figure 4.14 *- a) AFM scan of a completed nanojunction with interconnects b) Image of a completed device using the two-step lithography process (NIL and UV lithography) after 200 nm of Al is deposited.*

UV lithography is used to connect the nanojunctions to contact pads. AZ5214E resist is used for this purpose as it is very well suited for lift off processes. By using this resist in

the image reversal mode, it is possible to produce a significant undercut of the resist sidewalls which allows fast and easy lift off even for the thick Al films necessary for wire bonding.

To electrically connect the nanojunctions 200 – 400 nm of Al was deposited to form the wire bonding pads and connections from these to the features made by NIL. Images showing this structure are shown in figure 4.14. In many cases the nanoimprinted and photolithography features were electrically isolated after a device was completed. Heating the devices to 300°C for around 1 hr was found to close some of the connections but the failure rate was still high. By close examination of SEM images it was eventually realised that a residual layer of resist was present after the lithography steps which separated the imprinted features from the metal being deposited and prevented connection. Heating the devices may have caused some inter-diffusion of the metal through the residual layer and allow for an electrical connection. To eliminate this residue from preventing connection the photolithography process was modified to include a plasma “de-scum” step before and after the photolithography. The etch time was chosen so that 50 nm of photoresist was removed. After implementing this step in the device fabrication process, a success rate above 90% was achieved.

4.5 Temperature Dependent Electrical Resistance Measurements

After the devices are diced to the required size, they are mounted onto a chip carrier using GE varnish (Oxford Cryospares). After curing, the devices are wire bonded using a thermo-sonic ball bonder (K&S 4522). The order of this process is crucial to avoid destroying the nanojunctions through accidental static discharges. First all of the leads of the chip carrier are bonded together and grounded to the work holder of the machine.

Then a bond is made from one pad on the carrier PCB to a pad on the device. This is repeated for all connections on the device. A completed device is shown in figure 4.15.

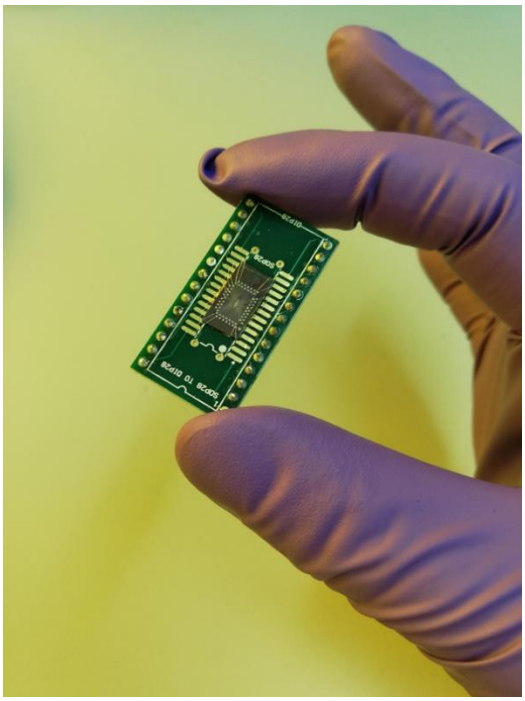

Figure 4.15 *- A completed nanojunction device wire-bonded to carrier PCB.*

When the device is mounted in the cryostat the shorting wires between the carrier legs can then be removed. Within the cryostat the device is shielded from most sources of electrical noise, however, it was discovered that the devices are very sensitive to static discharges and care is needed to shield them when transporting them from the cleanroom to the lab where they are measured. Proper ESD practises are needed when handling the devices (e.g. static bracelet, conductive mat and correct tools). Most important is the need to properly ground the chip carrier before starting the wire bonding process. Wedge bonding may be a better method of connecting devices as this avoids the use of a high voltage spark to melt the wire and form a ball.

The sample is mounted in a custom-made device holder which fits within a continuous flow cryostat (Oxford Instruments). The holder consists of a copper block with

dimensions chosen so that it makes tight contact with the walls of the cryostat and heat exchanger via a spring-loaded band. A copper stub protrudes to make thermal contact with the sample placed in the holder. The holder allows for 28 electrical connections to be made via BNC connections at the top of the removable cryostat insert. A PID temperature controller (Oxford ITC4) along with a program written in LabView is used to carry out cooling and heating cycles and also allows the sample temperature to be controlled at a fixed point in the range from 300 K down to a minimum of 64 K using liquid nitrogen. The temperature is measured using a calibrated Pt-100 resistance sensor placed in close proximity to the sample with a secondary sensor located on the heat exchanger section of the cryostat. A diagram of the cryostat setup is shown in figure 4.16.

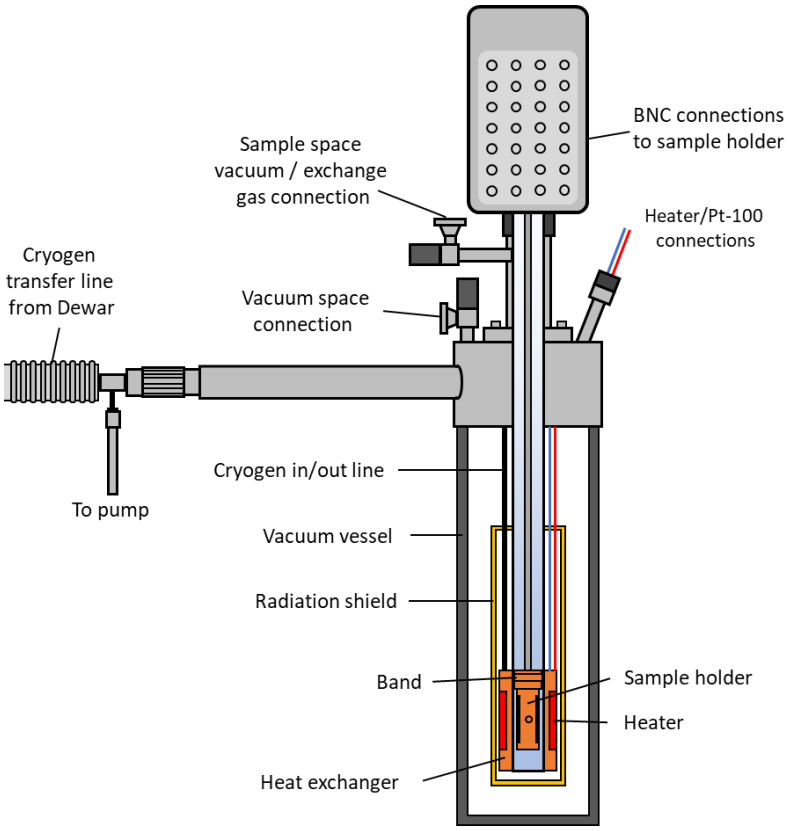

Figure 4.16 *- Schematic of the cryostat used to perform temperature dependent measurements.*

When mounting a device in the cryostat for measurement the device is mounted on the insert which is then placed into the cryostat. The sample space is evacuated using a turbomolecular pump to a pressure of less than 1×10^{-7} mbar. High purity helium gas is then introduced into the sample space to a pressure around 1 – 2 mbar to form an inert thermal link between the heat exchanger and sample. To cool the sample, a pump is used to draw LN_2 up a capillary tube from a Dewar and into a reservoir within the cryostat. By applying a vacuum to this reservoir and throttling the flow of LN_2, temperatures below 77K can be achieved. Temperature control is obtained by using a heater in thermal contact with the sample.

4.6 Electromigration Setup

Electromigration is used to break metallic nanojunctions to produce nanometre separated electrodes suitable for the incorporation of single molecules. In the process used here, voltage pulses are applied to the device while continually monitoring the junction resistance. The electromigration technique used is automated using a computer program written in LabWindows and a program continually records the resistance of the junction using a lock-in technique and increases the pulse bias at predetermined rate of approximately 150 μVs^{-1}. The bias is removed if the resistance value exceeds a certain pre-set value. The pulse length can be set between 1 - 100 ms with a frequency of between 5 - 30 Hz which is provided by a BNC-2120 board (National Instruments) connected to the PC.

The resistance of a nanojunction undergoing electromigration can vary from as low as 10 Ω to values in excess of 20 kΩ. A lock-in technique is used to track the progress of electromigration in real time. An SR830 lock-in amplifier (Stanford Research) applies a

small 4 - 8 mV AC signal to the device using a summing amplifier. By measuring the voltage drop across a low-noise wire wound resistor placed between the device and the ground connection, so that the progress of electromigration can be monitored. This voltage drop is amplified using an SR560 low-noise pre-amplifier. This pre-amplifier serves a number of purposes:

- Firstly, the signal is amplified so that it can be measured by the lock-in amplifier.
- Secondly, it allows an internal 3 Hz – 10 kHz band-pass filter to be applied to the signal. This removes high frequency components of the signals but most importantly it removes the large DC voltage that is present on this signal when the pulses are on and would otherwise overload the lock-in amplifier.
- Finally, it provides a low noise DC voltage source that powers much of the instrumentation in the setup.

After the preamplifier the voltage is returned to the lock-in amplifier which measures the component of the signal at the reference frequency. The lock-in communicates with the PC running the electromigration program providing it with a voltage value which can then be converted into a junction resistance value, R_J, using equation:

$$R_J = \frac{V_{lock-in} R_S}{(V_A - V_B)} \times G_{pre-amplifier} \tag{4.3}$$

where $V_{lock\text{-}in}$ is the AC oscillation output from the lock-in amplifier, $R_s = 10\ \Omega$, $V_A - V_B$ is the voltage measured by the preamplifier and $G_{pre\text{-}amplifier}$ is the gain setting of the SR560 pre-amplifier.

The chosen lock-in excitation frequency is important as it must be a sufficiently high frequency so that our signal of interest is placed out of the 1/f noise but not too high or distortion may be introduced into the lock-in oscillation by the potentiostat or feedback

voltage source. The result will be an incorrect measurement of the junction resistance. The chosen lock-in frequency must also not sit at a harmonic of the square wave which is used to drive the EM process otherwise this will also give an incorrect resistance value. To check a suitable lock in frequency, a fast Fourier transform (FFT) is applied to the output signal of the feedback voltage source and the peak of the lock-in excitation is adjusted so that it sits between harmonics. Typically, a frequency of around 1 kHz is used. The experimental setup is shown in figure 4.17.

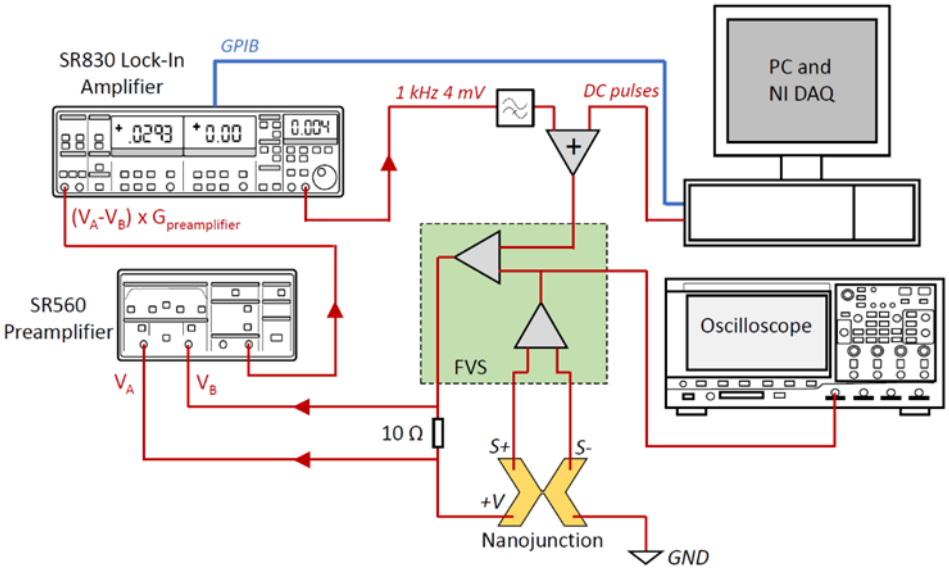

Figure 4.17 *Experimental setup for performing feedback controlled electromigration. The feedback voltage source labelled here as FVS (green square) is either the potentiostat or custom-built circuit.*

4.6.1 Feedback Voltage Source

Thermal runaway is a problem inherent with electromigrated break junctions.[45][147] This occurs because the nanojunction resistance increases as electromigration begins and the power being dissipated by the junction, in the form of heat, also increases. The rate of electromigration is increased with elevated temperature and a thermal runaway

will most likely occur in the absence of any form of limiting mechanism.[148][149] Nanojunctions broken as a result of thermal runaway tend to have large gaps.[46] With our technique, a voltage source with a feedback mechanism reduces the power being dissipated at the nanojunction as resistance increases by maintaining the voltage across the junction constant as the resistance changes. Combined with a fast feedback loop, this technique can prevent a thermal runaway from occurring and very small gaps can be created in a nanojunction.

A commercially available piece of equipment that fulfils this feedback mechanism is a four electrode potentiostat. Specifically, a 273A potentiostat (EG&G) with external electrometer is used. This instrument can take an external voltage signal and maintain this potential across two leads (WE and CE) using feedback provided by two leads (SE and RE). However, this equipment was later substituted with a feedback voltage source as it was found that large voltage transients were present when enabling the electrometer and the instrument introduced a large amount of noise (up to 200mV_{pk-pk}) making high resistance measurements challenging as it necessitated unacceptably slow measurements due to large lock-in time constants. Furthermore, it was not possible to control the compliance voltage that the system could provide which meant that a faulty feedback connection on a device could result in a very large voltage being applied. In some cases, this could be enough to cause a breakdown of the silicon oxide and completely destroy a device. Despite these problems it was still possible to successfully produce electromigrated Permalloy nanogaps, produced using the single step imprinting process and this setup served as an initial inroad into forming electromigrated nanogaps with other materials.

A custom-made feedback voltage source was later used which gave use greater control over the compliance voltage and also avoids voltage transients and large signal noise present with the potentiostat setup. This circuit is a low noise, high precision op-amp based and is designed to respond very quickly to changes in the feedback inputs while also remaining stable against oscillation under most conditions likely to be encountered in these measurements. The circuit diagram of the feedback voltage source is shown in figure 4.18.

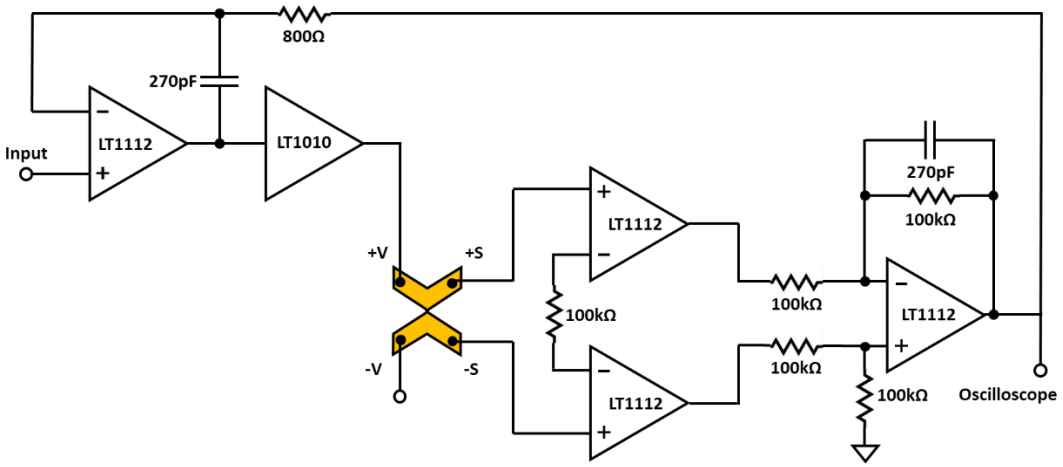

Figure 4.18 *- Schematic of the custom build feedback voltage source showing connections to the nanojunction shown in gold.*

In the feedback voltage source, the voltage drop across the junction is measured by an additional pair of leads which connect to an instrumentation amplifier, the output of which is fed into the non-inverting input of the feedback op-amp. The circuit is stabilised by tuning the capacitance and resistance in the feedback stage such that an adequately fast response is obtained whilst preventing overshoot and oscillation. This was achieved by applying voltage pulses to a dummy resistance load while monitoring the circuit behaviour on an oscilloscope. It was found that adding capacitance across the feedback

path of the instrumentation amplifier was also needed in order to provide a stable feedback mechanism without excessive overshoots and oscillation.

4.6.2 Deposition of Molecules in Nanogap Electrodes

Several techniques exist to trap small numbers of molecules between few-nanometre separated electrodes. Perhaps the most basic technique is to coat the device prior to forming the nanogap. The localised heating that occurs during the electromigration process is expected to enhance the surface diffusion of any molecules giving the possibility of finding the molecules within the nanogap. A dilute solution of molecules is chosen, with a typical concentration of approximately 0.01 mM. These solutions are prepared immediately prior to carrying out measurements in order to avoid possible degradation of compounds while in storage.

Another commonly used method is to first form the nanogap and then to deposit the molecule into the gap. This has the benefit of being able to characterise the formed empty nanogap prior to incorporating molecules but carries with it the risk of contaminating the device during transfer between measurement setup and deposition. In addition, in our system it was not possible to easily remove the device from the cryostat setup once it had been connected to the feedback voltage source, and to also avoid ESD damage or contamination. Therefore, all compounds were deposited prior to breaking the nanojunction when used within the cryostat system.

4.7 Thin Film Deposition

Thin films of metals were used for forming the electromigrated junctions, the interconnects and bonding pads. This was accomplished using physical vapour

deposition (PVD), specifically thermal evaporation under high vacuum. Directional material deposition is required so that problems with the lift-off process are avoided which excludes processes such as magnetron sputtering.

Two systems were used in this work. The first, system is an Auto 500 coating system (HHV). This was used to produce very high-quality films with high purity, well controlled thicknesses and low surface roughness. The system is equipped with an electron beam physical vapour deposition (EB-PVD) source allowing for very good control of the entire deposition process. With this technique, pellets of the evaporation material are contained with a graphite or refractory metal crucible which is bombarded by a high-power electron beam. This occurs under high vacuum conditions (1×10^{-7} mbar is typical for this system) and the material is deposited onto the substrate placed above.

The second system, an Edwards E306A coating unit, is used for evaporating thick aluminium films suitable for wire bonding where thickness control and surface quality are less important. This system uses a W coil or boat to heat pellets of Al to the evaporation point and again form films on the pre-patterned substrate. This system has a base pressure of 2×10^{-6} mbar.

With both deposition techniques, the film thickness is measured using a quartz crystal microbalance (QCM) which is calibrated for the specific material being deposited and also for the relative position of the sample within the vacuum chamber.

4.8 Microscopy

AFM and SEM were vital to carry out the experimental techniques presented here and it is worth briefly describing their two different modes of operation.

4.8.1 Atomic Force Microscopy

Atomic Force Microscopy (AFM), is a surface probe technique which produces an image by scanning a sample with a very sharp tip using a piezoelectric scanning stage. The tips are usually fabricated from Si using an etching process. The shape and sharpness (or radius of curvature) of the tip determines the resolution. Commercially available tips have a radius of curvature typically below 20 nm. A Dimension Edge AFM (Bruker) was used exclusively for this work, using TESPA V2 tips, also manufactured by Bruker.

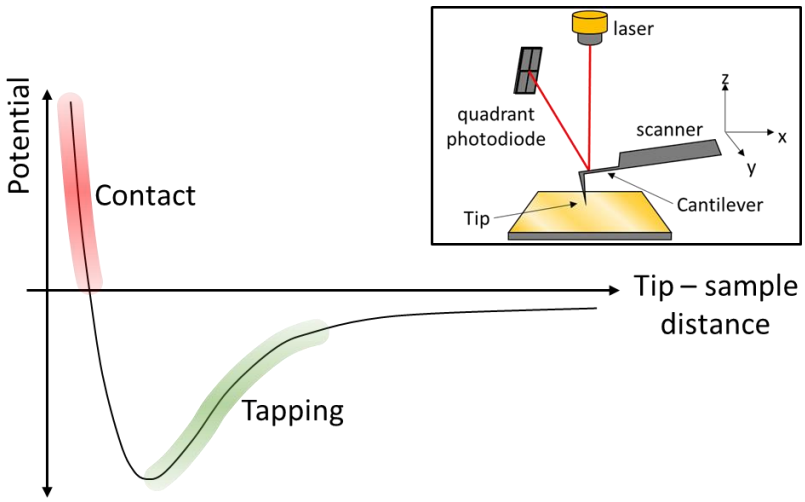

Figure 4.19 *- Leonard-Jones type interaction potential between AFM tip and sample and the regions at which contact and tapping mode operate. Insert shows a schematic of an AFM including tip, laser and detector arrangement.*

Two modes of operation are commonly used, contact and tapping mode. Contact mode works similarly to a surface profilometer with the tip being scanned across the sample surface whilst recoding the deflection. In an AFM this is achieved using a laser and quadrant photodetector. This deflection signal is maintained constant by a PID control loop and is used with the scan position to form an image. In tapping mode, the tip is made to oscillate at its resonant frequency. As the tip is lowered the sample-tip interaction causes a decrease in amplitude. This shift in amplitude due to the sample is used as feedback and the system tracks this signal to give topography information.

The interaction between the surface of the sample and the AFM tip is a Leonard-Jones type potential and the different AFM modes, contact and tapping, operate in different regions of this potential as shown in figure 4.19. Contact mode, as its name suggests operates with the tip in close proximity to the sample surface. At this close proximity the tip experiences a large repulsive force. The origin is due to the overlap of atomic orbitals between atoms in the tip and sample. High vertical resolution is possible because large changes in force occur with small changes of separation in this region of the potential. Tapping mode operates with a larger separation from the sample and because of this it may be preferred in some applications as it leads to less tip wear and greater tip longevity. For this reason and because the soft polymer resist films may be damaged while imaging in contact mode, tapping mode was used exclusively in this work.

4.8.2 Scanning Electron Microscopy

With scanning electron microscopy (SEM) the sample to be imaged is placed into a vacuum chamber and an accelerated tightly focussed beam of electrons is scanned across the sample surface in a raster pattern. This beam produces secondary electrons

as it interacts with the sample which are accelerated towards a nearby detector biased at a positive voltage. The recorded signal is displayed against the position in the scan and in this way an image can be produced with very high magnification. Reducing the dimensions of the raster scan increases the magnification of the image.

The electron wavelength is far smaller than that of visible light making SEM a powerful tool allowing for an image of a sample to be taken with a much higher resolution than possible with optical microscopy. An inherent disadvantage of SEM is that the beam can charge non-conductive samples which deflects the incoming electron beam and compromises image quality and resolution. It may be necessary to coat the sample with a thin layer of gold or carbon in order to avoid charging.

Electromigrated Permalloy and Co Nanogaps

5.1 Permalloy Nanogaps

Chapter 5

Initially, feedback controlled electromigration was performed in ambient conditions in a probe station with Permalloy nanojunctions. These devices were mainly used as tests in order to gain experience of the electromigration process and gain a greater understanding of appropriate pulse lengths and voltages needed in order to obtain a smooth narrowing of the nanojunction and breakage to form a nanogap.

Since the eventual aim is to incorporate molecules within the nanogap and measure their electronic properties, carrying out smooth electromigration is a requirement of producing molecular nanogap devices since this has been shown to avoid the formation of metallic clusters which can mimic molecular behaviour as discussed in chapter 2 (see figure 2.7). An example of a device where this smooth electromigration did not occur is shown in figure 5.1 a).

An uncontrolled breaking process can clearly be distinguished from one in which a controlled thinning of a nanojunction has occurred by identifying several clear conduction regimes in the resistance vs time plot during electromigration. An initial increase in the nanojunction resistance up to a few hundred Ohms which is then followed by an abrupt break where the resistance increases to very high values is a clear indication of an uncontrolled process. In addition, preceding the breakage, a large separation between the nanojunction resistance when measured during and between pulses indicates that a large amount of Joule heating is occurring.

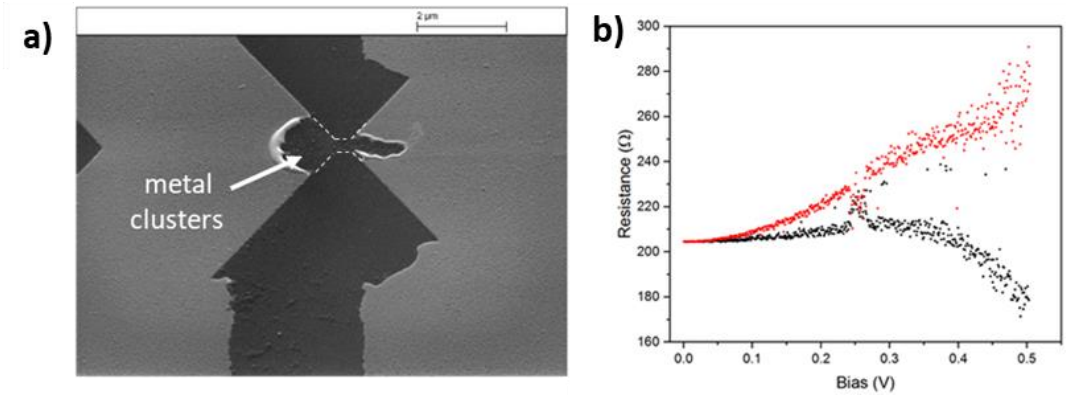

Figure 5.1 *- a) SEM image of a Permalloy nanojunction after breaking due to runaway Joule heating, a large gap is present along with presence of metallic clusters likely formed from melting and aggregation of the electrode material. Note: white dashed lines show origin geometry of nanojunction b) Resistance vs bias voltage showing large separation between resistance measured during pulse (red points) and at zero pulse bias (black points).*

This is shown in figure 5.1 b). Interestingly it can also be seen that the device resistance measured between pulses decreases from the original starting value. This is likely as a result of a recrystallizing process driven by heating of the conductor.[45]

Uncontrolled breakage of the nanojunctions occurred when the junction areas are very large such that heating takes precedence over electromigration, or when the pulse length was set to a value greater than 100 ms. Uncontrolled breakages also occurred in trials when a feedback mechanism was not present or was intentionally deactivated in these pulses driven system and also in cases where the bias was simply ramped linearly.

Permalloy devices were fabricated with the single step NIL process as this material has very good adhesion to a SiO_2 substrate. Although work along this path was not pursued, Permalloy is an ideal material to investigate spin injection and transport in nanogap devices as it shows zero magnetostriction while being ferromagnetic. The idea being that the opening and closing of the nanojunction as a result of applied magnetic field

can be excluded from actual spintronic effects shown by a molecule or other structure confined within the nanogap electrodes.

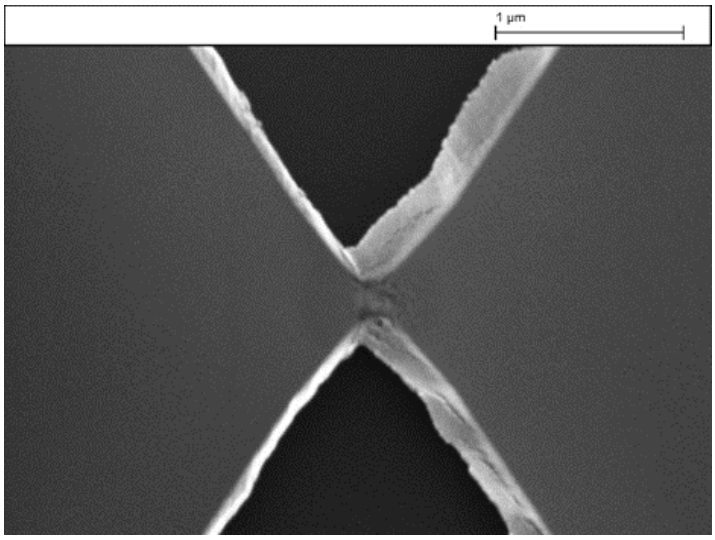

Figure 5.2 *- SEM image of a Permalloy nanojunction after undergoing feedback controlled electromigration. The gap is poorly defined but is indicated by a change in surface texture of the metal electrodes.*

Electromigration of these devices is carried out using the feedback control setup. A pulse length of 10 ms and a delay of 50 ms between pulses gave reliable results after optimisation of the parameters and an SEM image of an electromigrated Permalloy nanojunction is shown in figure 5.2. A plot of the junction resistance measured as the bias voltage is increased is shown in figure 5.3 a). In the data a sudden transition in the resistance of the junction is present as the bias voltage is increased beyond 0.4 V. This indicates that electromigration has thinned the nanojunction so that its dimensions are now comparable to the electron scattering length. This step is well documented to show that electromigration has progressed smoothly and corresponds to electron transport in a quasi-ballistic regime.[45] In some cases, we can observe a small decrease or increase in resistance before this transition has been attributed to a heating driven recrystallisation process occurring within the nanojunction.[150]

Conduction plateaus around multiples of G_0 are apparent in some plots of junction resistance as a function of time when carrying out electromigration. These signify the formation of a multiple atom contact and eventually a single atomic point contact as the junction becomes thinned. In one example, shown in figure 5.3 b), a sudden drop in conductance at a voltage bias of 0.43 V to a conductance value of 3 G_0 is observed. Repetitive reductions in conductance are present in the data and, although these are under-sampled by our measurement setup due to their very rapid nature, are most likely transitions to a value of 1 G_0 before the value stabilizes. This is reminiscent of the behaviour seen in atomic switch-based memory where the conductance can be cycled between two well defined and quantized conductance values by a voltage induced rearrangement of a few atoms.[151] As the pulse voltage is further increased and after a period of further instability, the junction finally breaks to form a tunnel gap.

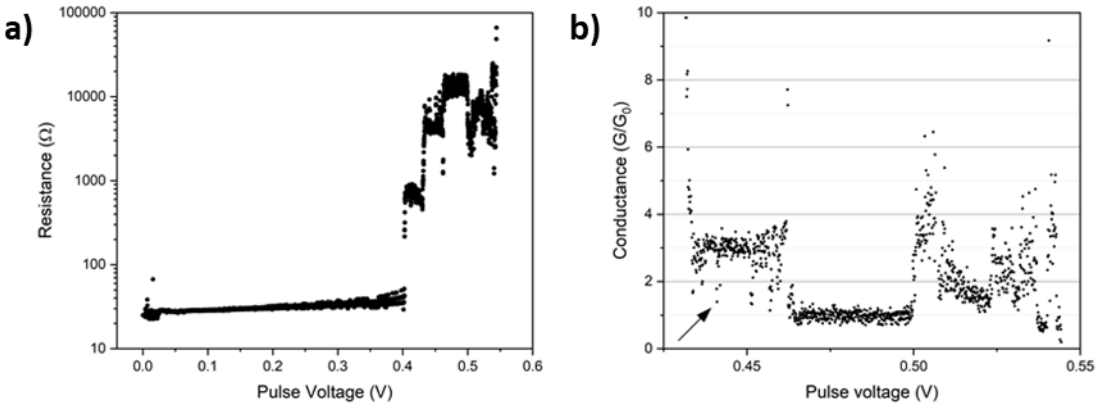

Figure 5.3 *- a) Resistance vs pulse voltage during electromigration for a Permalloy nanojunction. b) Plot of junction conductance in terms of G/G_0 showing conductance of junction evolving in a step like manner before the opening of a tunnelling gap. Arrow indicates the region of conductance switching between $3G_0$ and possible $1G_0$.*

In total electromigration was successfully carried out in 28 Permalloy nanojunctions. From resistance vs pulse voltage plots, it is possible to determine that the transition

from a diffusive to a quasi-ballistic regime occurs at a pulse voltage of 0.52 ± 0.08 V. The voltage at which this first transition occurs is very repeatable. For example, neighbouring nanojunctions fabricated on the same substrate show a difference as small as 1 mV in applied bias. This indicates that it is the nanojunction geometry and microstructure of the thin film that is responsible for determining the point at which the first transition occurs, since neighbouring nanojunctions share very similar processing conditions and hence should have a very similar geometry and structural composition.

The voltage at which the junction breaks to form a tunnel gap shows greater variability and occurs at a mean value of 0.700 ± 0.22 V, again measured for 28 nanojunctions. The most likely reason for this large range is due to the fact that the motion and breakage of the final few atoms forming the constriction is a stochastic process, not dependent on the sample geometry or structure but on a voltage induced diffusion process acting on the remaining atoms in the thinned nanojunction.[47]

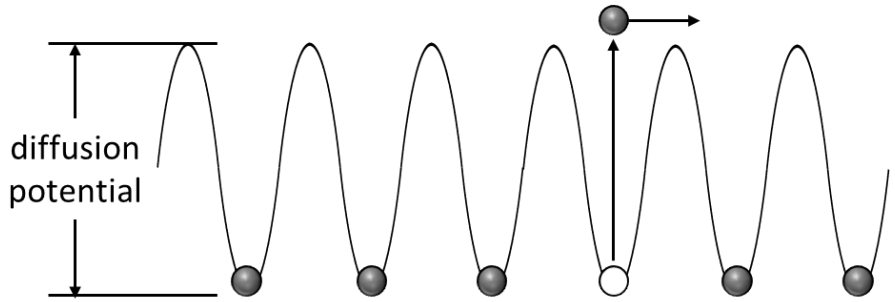

Figure 5.4 *- Atom diffusion driven by microscopic kinetic energy transfer from conduction electrons to a single metal atom.*

This is the description given by Umeno *et al.* whereby in the quasi-ballistic conduction regime, the applied voltage drives the motion of material via a microscopic transfer of kinetic energy that overcomes the interatomic diffusion barrier within the metal.[152]

This is illustrated in figure 5.4. In this way it is different from the usual momentum transfer processes in that it acts on individual atoms and not scattering centres.

In the extreme case, when the junction has been thinned to just a few atoms and the conductance is few multiples of G_0 and lower, it has been shown that an applied bias is not even necessary to perform the final breakage and residual thermal energy at room temperature can be sufficient to cause motion of the remaining few atoms.[64][49][62] Here the junction can undergo a self-breaking process whereby thermal energy at room temperature is sufficient to remove the final atoms. This occurs typically in a time span of several minutes to a few hours.

5.1.1 Stability of Permalloy Nanogaps

Overall the lifetime of Permalloy devices was not long, with resistance values being stable for a maximum of several minutes after electromigration had formed a nanogap. This was long enough to measure the I-V characteristics of the junction but most of the devices re-formed and showed a resistance of several hundred Ohms after approximately one hour at room temperature. This occurred in the absence of applied voltage and is likely driven by thermal motion at room temperature. Electromigration could be carried out again and another I-V measurement made again but this behaviour limited the use of this type of nanogap for further measurements.

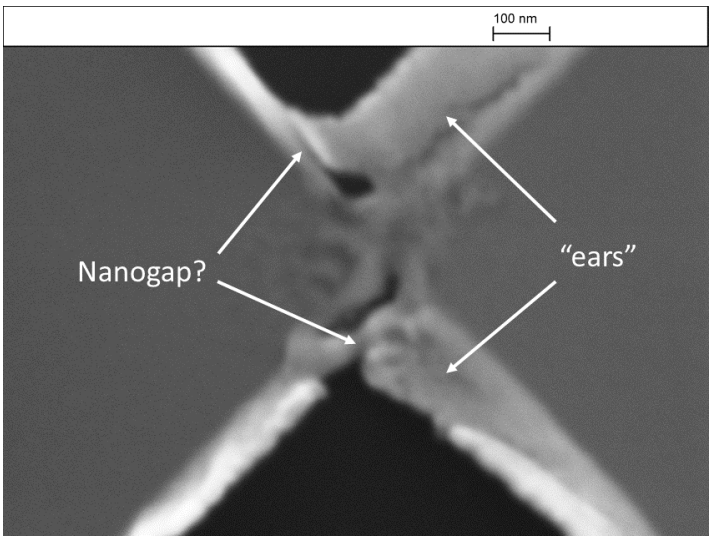

Figure 5.5 *- SEM image of a Permalloy nanojunction after feedback controlled electromigration. Annotations show possible locations of a nanogap formed between unsupported regions of the device.*

This poor stability is likely due to several factors. Firstly, the geometry of the nanojunction was poor as a result of the fabrication technique. As shown in figure 5.5, the poor edge quality of the devices could lead to the scenario where the nanogap forms in a region not in contact with the substrate. Another possibility is that the electromigration process induces localised stress within the nanogap electrodes. At a microscopic level, and given time, these stresses may relax resulting in material motion and closing of the nanogap.

5.2 Electromigrated Co Nanogaps

Based on the poor stability of Permalloy nanogap devices, we investigrated modifying the fabrication technique to imporve the quality of the nanojunctions. Several Co devices were produced using bilayer NIL technique. Devices were investigated using SEM and AFM and were free of sidewall deposition “ears”.

Smooth electromigration in Co devices was not observed in the 8 devices measured. All appeared to undergo a runaway breaking process with no intermediate quazi-ballisitic regime and no observed quantised conductance values as was observed with the Permalloy devices. A plot of the junction resistance showing a sudent jump to high resistance is shown in figure 5.6 a). It is not possible to determine a point at which the resistance and hence electromigration begins for these devices as it appeared to occur randomly. Some junctions break at a low voltage of around 0.2 V, while others were very resilient and break only when large voltages over 1.2 V were applied. One explanation for this behaviour is that Co may be very suceptible to Joule heating with the sudden onset of the heating being faster than the feedback mechanism of our system. Another possibility is that the grain structure of Co devices varied considerably with some devices having a "bamboo" like structure while others may have a multigrained structure.[56]

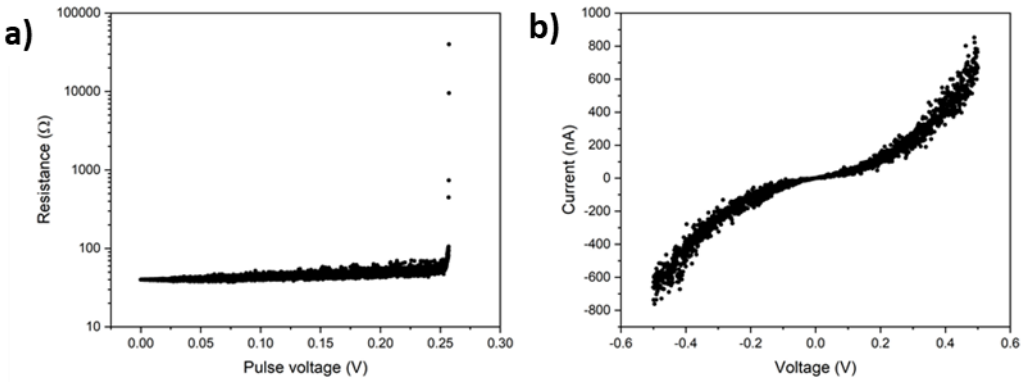

Figure 5.6 *- a) Resistance vs pulse voltage for a Co nanojunction showing direct transition to a tunnel gap without intermediate quasi-ballistic regime. b) Tunnelling current measured after uncontrolled electromigration for the same device.*

Despite this inability to control the electromigration process in Co in the same way as with Permalloy devices, these nanogaps proved far more stable, allowing time to measure the characterisitics of the formed nanogaps in detail with tunnel current

measurement and later performing temerature cycling over many hours. In all 5 out of the 8 Co devices showed a tunnelling current measurable after the sharp increase in resistance as the nanojunction broke. An example of the corresponding tunnelling curves are shown in figure 5.6 b).

5.3 Electromigrated Au Nanogaps

Au nanojunctions were also fabricated using a bilayer NIL process. As with Co devices, the resulting Au devices were inspected with SEM and tapping mode AFM and all showed well defined boundaries that were free of metal “ears”.

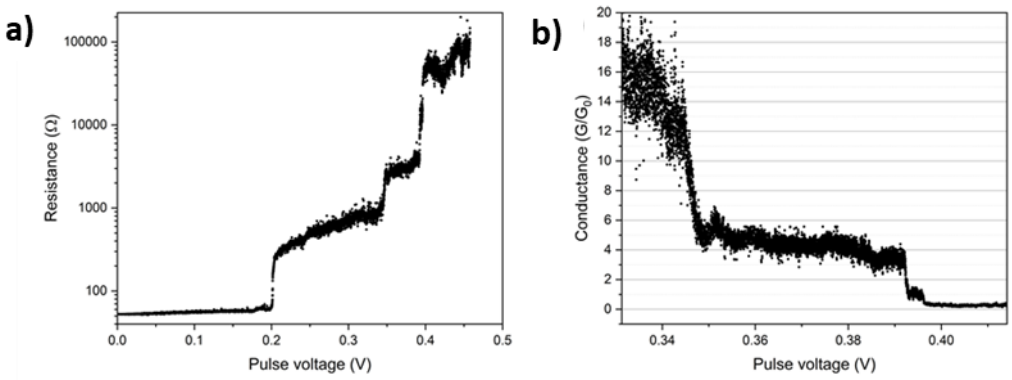

Figure 5.7 *- a) Resistance vs pulse voltage during electromigration for a Au nanojunction b) Plot of junction conductance in G/G_0 showing conductance of junction evolving in a step like manner before the opening of a tunnelling gap.*

Figure 5.7 a) shows the resistance of a gold nanojunction as pulse voltage is increased. Electromigration with Au preceded very similar to Permalloy nanojunctions. An increase in resistance is observed as the bias is increased indicating the onset of electromigration. Again, this is followed by a sudden transition into a quasi-ballistic regime. However, the voltage at which the transition occurs is much lower, in the region of 0.2 V. This is likely

due to the enhanced rate of electromigration of Au compared to that of Permalloy.[153][154]

As shown in figure 5.7 b), quantised conductance values are also observed as electromigration is carried out. This feature, in addition, with the appearance of a quasi-ballistic resistance regime, indicates that the electromigration procedure is carried out smoothly for Au nanojunctions. The voltage at which the nanojunction finally breaks is in good agreement with the self-diffusion potential for Au measured by Günther *et al.* at 0.4 V and agrees well with the model proposed by Umeno *et al.*.[155] An AFM image of a Au nanojunction is shown in figure 5.8. Although the nanogap cannot be resolved, a clear constriction is present and contrasts with the as prepared nanojunctions.

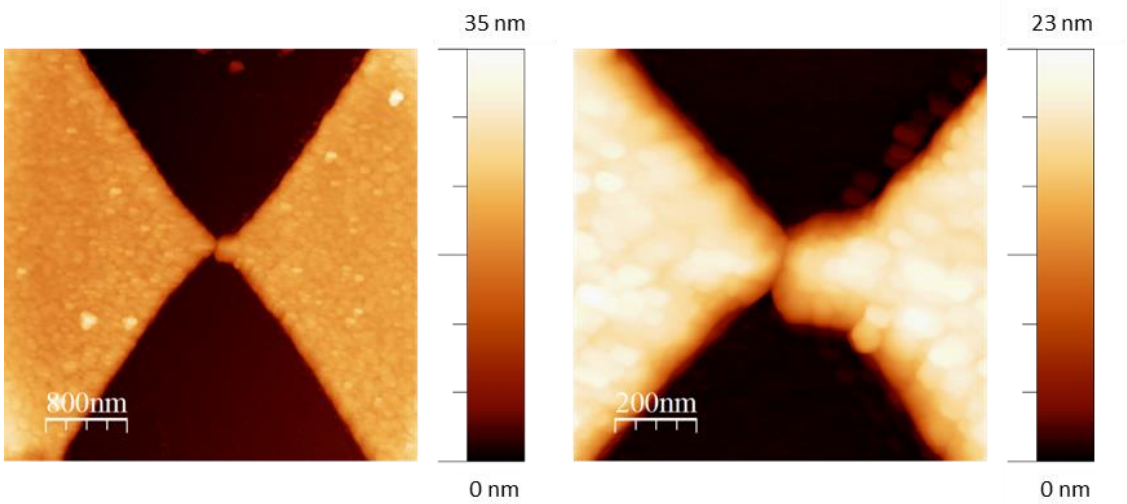

Figure 5.8 *- Tapping mode AFM images of a Au nanojunction after electromigration.*

5.4 Results and Discussion

Now that the nanogap fabrication method has been refined, it is now possible to investigate the behaviour of electromigrated Co and Au nanogaps. In order to improve stability and reduce the possibility of contamination of our devices, the electromigration

process is carried out in vacuum (1×10^{-7} mbar) and after extensively plasma cleaning devices before forming nanogaps in the two materials.

5.4.1 Resonant States in Electromigrated Co and Au Nanojunctions

A common feature observed in electromigrated Co and Au nanojunctions is the appearance of resonances in the dI/dV curves. These resonances were particularly well defined when the conductance values of the device were in the range $0.1\ G_0 < G < 5\ G_0$. Although devices showing this behaviour lacked sample to sample reproducibility, the peak positions for single device were stable when held at decreased temperatures (77 K) and vacuum conditions, displaying reproducible I-V sweeps for around 1 hour in some cases. However, at increased temperature, and after prolonged voltage cycling, the characteristics of a single device evolves, displaying new peaks at different voltages. This is shown in figure 5.9.

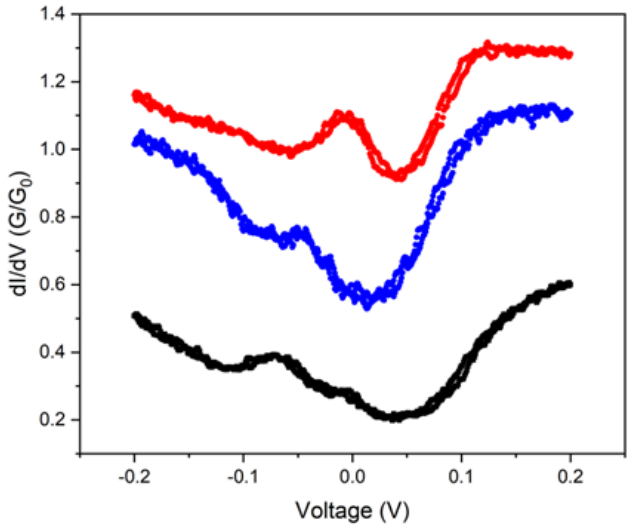

Figure 5.9 *- dI/dV behaviour to resonant states observed in electromigrated Co nanojunctions with a conductance value less than $1G_0$. The red and blue curves are recorded from a single electromigrated device separated in time and are offset from black curve by $0.25G_0$ for clarity.*

Similar behaviour is reported in literature for devices with a conductance value > $1G_0$ but here we see that this behaviour is also preserved in a device even as the conductance values are below $1G_0$. This is a poorly explored regime characterised by an extremely small tunnel gap (based on the values of conductance being quite large in relation to typical tunnel gap formed using the electromigration process) or possibly a mixed regime between metallic and tunnelling processes.[52] The underlying physics governing conduction in this regime are complex, described by Kondo physics and quantum interference effects.[156][157]

The temperature dependence of an observed resonance at zero bias is shown in figure 5.10. Overall the conduction increases as temperature increases and the resonance feature display strong temperature dependence, with the dI/dV peak becoming broadened and reduced in magnitude as temperature is increased.

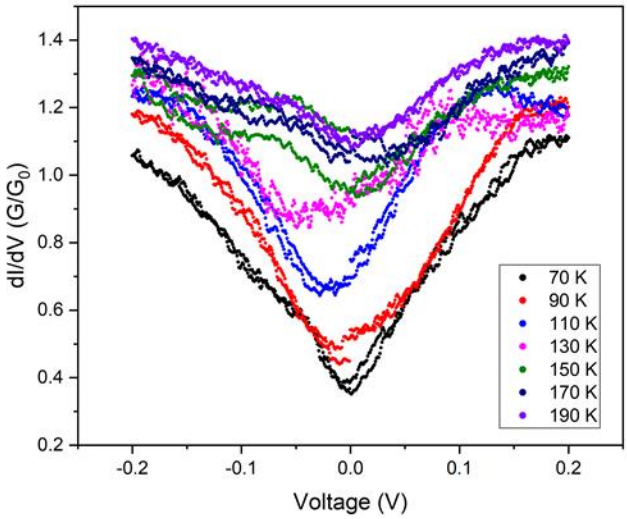

Figure 5.10 *- Temperature dependence of a resonant peak around zero-bias in an electromigrated Co device.*

Our results presented in this section resemble very closely those seen in electromigrated Ni nanojunctions by Beaufrand *et al.* [158] and also by Shi *et al.* in Ni, Permalloy and Co

devices.[159] The wide variation from sample to sample and as well as variation in the behaviour of a single sample over the course of several hours indicated this this is a very sensitive effect, the origin of which is not attributed to a bulk property of Co. Likely these resonant states are as a result of disorder, dopants or as a result of the geometry of the two electrode surfaces.[158] The latter process has been studied as it has a crucial role in scanning tunnelling spectroscopy (STS) whereby the sharpness of a W tip has an influence on the recorded dI/dV spectrum. [160]

These features in the dI/dV are present only when the conductance of the nanogap is approximately in the range of $1G_0$ to 0.1 G_0 (resistance values of 12.9 kΩ to approximately 100 kΩ). As shown in figure 5.11, nanogaps with lower conductance values showed a smooth dI/dV behaviour.

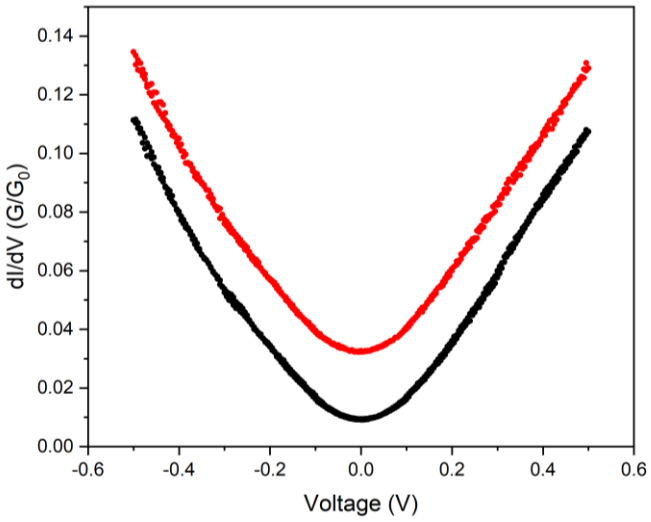

Figure 5.11 *- dI/dV behaviour of two electromigrated nanogaps, one Co (black) and another Au (red). Measurement was performed at 70 K for both curves. Both curves show a smooth behaviour and have a zero-bias conductivity below 0.1 G_0. Red curve is offset by 0.02 G_0 for clarity.*

5.4.2 I-V characteristics of Au nanogaps

The I-V characteristics of the formed nanogaps show a very non-linear behaviour indicating the presence of a tunnelling gap. Fitting of the data to the Simmons tunnelling equation (see section 3.1.1) is shown in figure 5.12. This is carried out using the graphing and analysis software Origin 2019, applying a Levenberg–Marquardt fitting algorithm to the experimental data.

Unfortunately, because the tunnel equation depends upon three independent variables as well as the voltage applied to the device, it means that several satisfactory curve fits can be found for each set of results. However, what is found is that the gap distance is a more stable fitting parameter and while φ and A can vary significantly the gap size remains in the range of 1.5 to 2 nm. A value for A is chosen similar to literature values.[50][56]

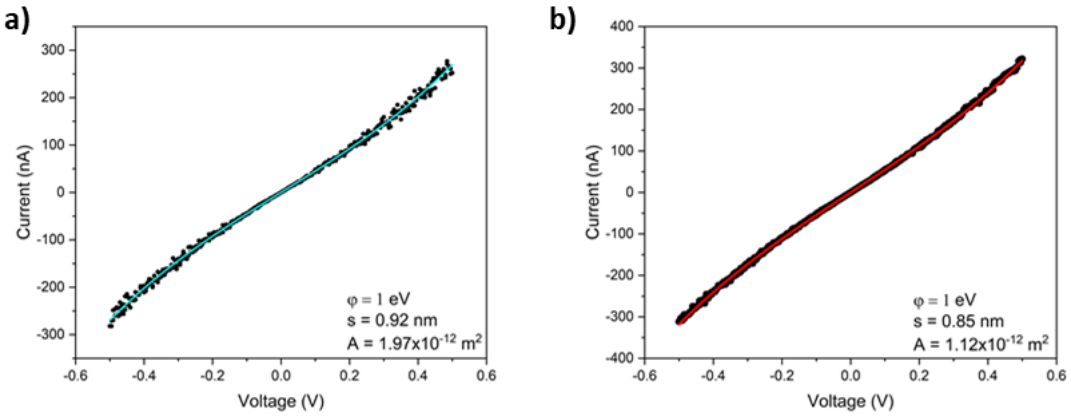

Figure 5.12 *- Fits for two different Au nanogap electrodes formed using feedback controlled electromigration fitted to equation 3.2.*

In both fits, the values used for φ, the work function of Au, is much lower than the accepted for bulk Au, with the literature value of 5.4 eV being a commonly reported

value.[161] This discrepancy is to be expected however, since it has been shown that the work function of a metal can be drastically modified by the presence of surface contaminants as well as changes away from the bulk crystal structure of the metal. The latter is especially true since the electromigration process is likely to form electrodes with surfaces very different from the regular crystal structure of a flat gold surface with the possibility of introducing a localized non-homogeneous work function in the nanogap region. [60][55][162]

Although the Simmons fitting procedure applied to this device type is lacking, through a combination of factors including the fact that the gap size lies below the resolution of SEM and AFM, is produced using a controlled electromigration procedure that shows quantised conductance for Au and Permalloy devices and also showing a tunnelling type behaviour after breaking, there is high degree of confidence that the nanogaps produced in this work are extremely small and are certainly below 5 nm in size.

5.4.3 Temperature Stability of Au Nanogaps

The temperature dependence of the resistance of an Au nanogap devices was also investigated. Figure 5.13 shows the resistance of an electromigrated nanogap device after being formed at room temperature and then immediately cooled to 70 K. It was then allowed to warm slowly to 293 K over a period of 12 hrs. The unbroken-nanojunction device was O_2 plasma cleaned before being transferred to the measurement setup and broken using the feedback electromigration process. In these devices we see only a weak temperature dependence on the overall resistance of the device likely as a result of a narrowing of the available states across the barrier or as a result of the barrier height being temperature dependant. Furthermore, the device does

not show any switching behaviour indicating that the clean nanogaps have a high degree of stability.

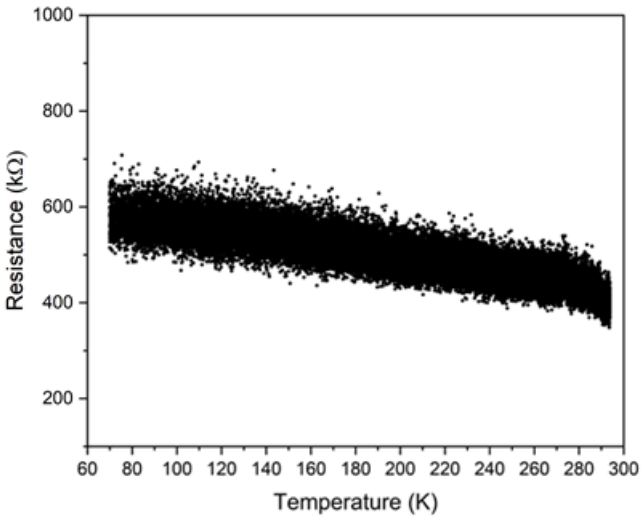

Figure 5.13 *- Resistance as a function of temperature for a Au nanogap formed using feedback controlled electromigration. Resistance of the device is sampled every 200 ms with an applied bias of 8 mV.*

Benzenethiol Molecular Junctions

Chapter 6

As a proof of concept of our fabrication process for carrying out measurements on single molecules electronic devices were made containing benzenethiol (BT) molecules.

6.1 Device Preparation

To measure the electronic transport through BT molecules a 0.04mM solution of diphenyl disulphide (DPDS) is prepared. The DPDS compound consists of two phenyl rings joined via two thiol groups. It has been well documented that upon exposure to a Au surface the S-S bond of the DPDS molecule oxidizes forming BT which can then self-assemble onto electrode surfaces to produce high quality monolayers .[163][164][165] The structure of these two complexes is shown in figure 6.1.

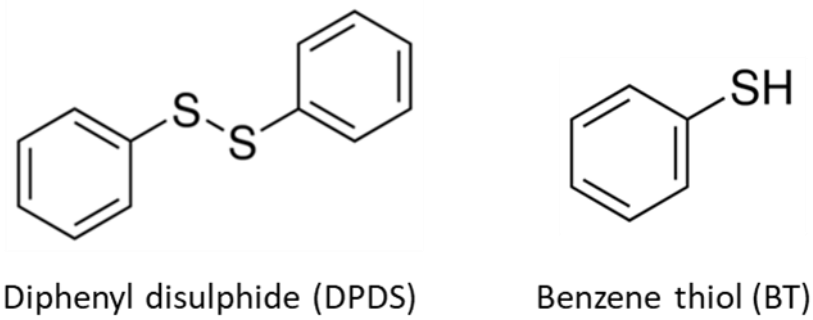

Figure 6.1 *Structure of diphenyl disulphide (DPDS) and benzene thiol (BT).*

Residual contamination left over from the lithography processes is removed by first O_2 plasma cleaning the unbroken nanojunctions (15 minutes, 50 W, 0.35 mbar). Immediately after removing the devices from the chamber the devices are immersed into a 0.04 mM solution of DPDS prepared in ethanol and the self-assembly of BT process

is allowed to occur over 30 minutes. The electromigration process is then carried out and the I-V characteristics of a device are recorded.

6.2 Results and Discussion

Molecular junctions exhibit characteristic transport features that allow us to discriminate electron tunnelling through vacuum from that of true molecular transport. The most familiar of these features is described by the single level model as discussed in section 3.1.3.

6.2.1 Resonant Transport in Benzenethiol Molecular Junctions

Out of 10 electromigrated nanogaps exposed to DPDT, two nanogaps displayed behaviour that was suggestive of molecular transport i.e. current suppression at low voltage with the complex acting as a tunnel barrier and an increase in current at higher voltages due to on resonant transport. In contrast, devices that contained no DPDT molecules exhibited much lower conductivity with a typical I-V characteristic similar to that shown in figure 5.12. At a voltage of 0.5 V, empty junctions typically had a current of 300 nA compared to 1 µA for a junction exposed to DPDT, as shown in figure 6.2 a).

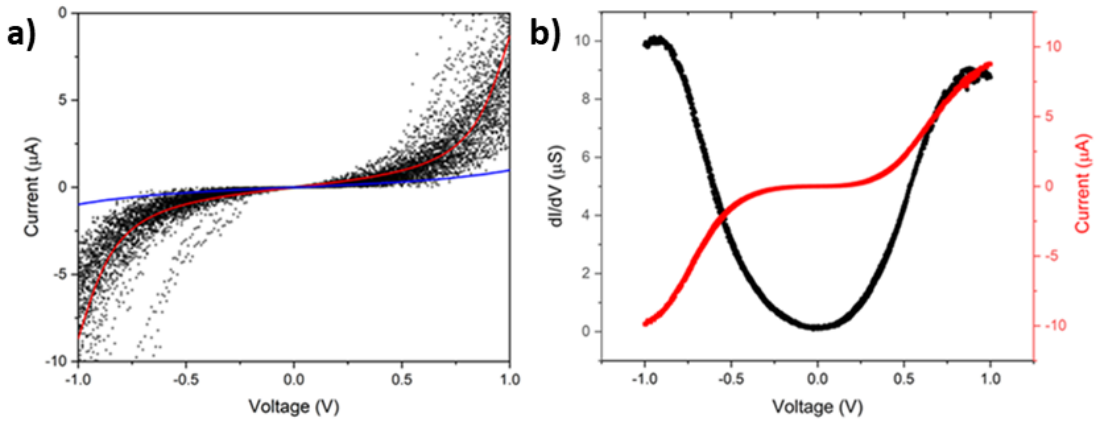

Figure 6.2 *- a) Repeated I-V measurements made over a 12 hr period on an electromigrated nanogap containing DPDS, (lock-in technique 4 mV at 1447 Hz). Current is extracted from dI/dV measurement. Red curve is a fit to the resonant tunnelling model (equation 3.9) with* $\Gamma_{S,D}$ *= 34 meV,* ε_0 *= -0.49 V. The blue curve, showing the lack of a good fit using the Simmons model (*ϕ *= 1 eV, s = 0.85 nm, A =* 1.12×10^{-12} m^2*) indicates that the junction is not an empty tunnel gap. b) Selected single I-V curve (red) and dI/dV (black) from a second junction showing similar current suppression. Measurements are carried out at room temperature.*

Figure 6.3 a) shows the I-V behaviour of another device exposed to DPDS, electromigrated and then measured continuously over a 12 hr period. The I-V curves show some variation, mostly liked due to minor movement of the molecules due to thermal effects, but the current suppression expected at low voltage is clearly visible.

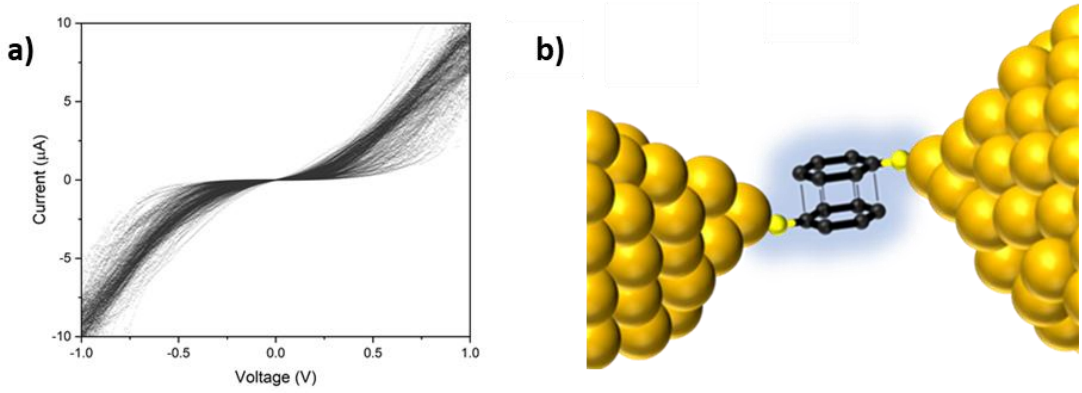

Figure 6.3 *- a) I – V measurements on a different BT junction showing similar device behaviour. b) Proposed molecular configuration of the nanojunction consisting of overlapping* π *orbitals s from stacked benzene rings of opposite electrode represented by dotted lines.*

To the best of our knowledge, these are the first reported results of BT measured in Au break junction devices. The shape of the I-V curves are very consistent with measurements on similar phenyl compounds in mechanically controlled break junctions [36] and agree well with *ab initio* calculations.[39] However, there are a number of

differences due to the different molecules used in this study. In contrast to previous work that had molecules with two thiols that could bridge on opposite sides of the nanogap electrodes, the molecules used in this study can only bind to Au on one side. The large current (10 μA at 1.0 V) exhibited in conjunction with the on/off resonant transport is indicative of a highly conducting pathway between the source and drain electrodes. This current is much larger than that observed for a linear bridged bi-phenyl dithiol [166], having an experimentally measured conductance value of 1.7×10^{-4} G_0, which further indicates the molecules are in a different geometry. The strong symmetry in the current-voltage curves also provides further evidence of a transmission function that is independent of the direction of current flow, as expected in a symmetric system having similar thiol-gold barriers on the drain and source electrodes. This high conduction (≈ 0.13 G_0 at 1.0 V) is likely due to overlapping π-orbitals from the stacked benzene rings that are bound from opposing electrodes, as shown in figure 6.3 b). This has similarly been observed in π-folded molecular junctions.[167]

6.2.2 Transition voltage spectroscopy

Further information can be gained by examining the data using Transition Voltage Spectroscopy (TVS), which is now a commonly used tool for probing the position of the frontier molecular orbitals (HOMO or LUMO) in molecular devices. Since the necessary voltage is likely to result in breakdown of the molecular junction before resonance can be achieved, TVS is envisaged as a means by which this information can be extracted while subjecting the device to greatly reduced electric fields. The knowledge of these energy levels will allow for tailoring of charge injection in molecular electronic devices.

TVS was first discussed in terms of tunnelling over an energy barrier by Beebe *et al.*[168][169] but is now understood to be better interpreted in terms of coherent Landauer transport.

The main assumption with early interpretations of the TVS technique was that the molecule is represented as a featureless potential barrier with a resultant linear voltage drop across the junction. This is not the case as discussed in section 3.1.2, where molecular junctions are more accurately described within a coherent Landauer treatment. Transport occurs via a transmission function that is explicitly energy dependant with the transmission function is peaked around energy levels which can be represented as a series Lorentzian peaks. In this case the voltage drop occurs at the interfaces between molecule and electrode and no voltage is dropped "within" the molecule. This discrepancy is particularly well revealed in studies on length dependant conduction in alkanethiols which finds that V_{trans} is independent of molecular length as expected for Landauer transport.[170] A thorough review of the TVS technique, and in particular the lacking of its original interpretation, can be found in the work of Huisman *et al.*.[171]

While TVS does not include effects related to the absorption geometry of molecules within nanogap devices or does it capture effects related to… , the TVS technique has successfully been used both experimentally and theoretically to investigate a variety of partially bridged and fully bridged electrode-molecule-electrode systems. Studies are typically based on traditional gold electrodes [172] but also make use of novel approaches with contacts made of graphene or carbon nanotubes. [173][174][175]

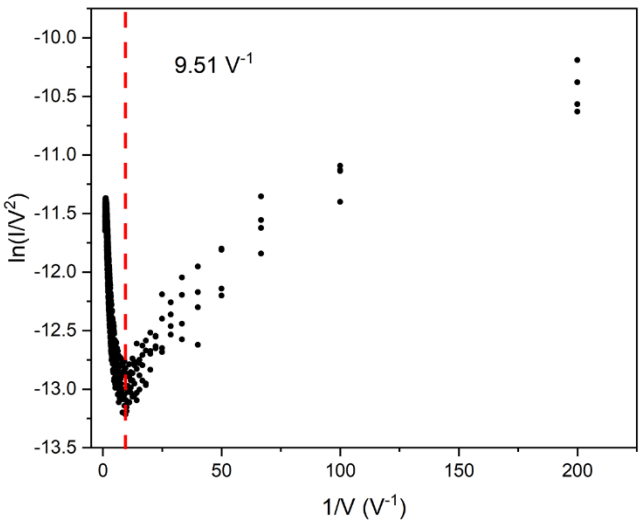

Figure 6.4 *- Transition Voltage Spectroscopy plot showing a voltage minimum at 9.51 V^{-1} corresponding to a transition voltage of V_{trans} = 0.11 V. The transition voltage relates to the difference between the energy of the highest occupied molecular orbital (HOMO) and the Fermi energy of the electrode.*

In figure 6.4, the I-V graphs are analysed by plotting $\ln\left({}^{1}/_{V^2}\right)$ vs ${}^{1}/_{V}$, the so-called Fowler-Nordheim (F-N) plot that is used to study the tunnelling to field-emission transition in solid-state junctions. A key feature of the TVS plot is the transition voltage, V_{trans}, which is the position of the first minimum and is linearly proportional[169] to the relative difference between the energy of the highest occupied molecular orbital (HOMO) and the Fermi energy. Physically this minimum in a F-N plot corresponds to the rectangular potential barrier becoming triangular as is depicted in section 3.1.1 (figure 3.1). Figure 6.3 shows a TVS plot for the data of several I-V sweeps shown in figure 6.2 a). From the graph there is a clear minimum at a voltage 9.51 V^{-1}, which gives a transition voltage of V_{trans} = 0.11 V.

Although no previous data exists for the system investigated in this article, a comparison of experimental and theoretical values of V_{trans} with molecules of similar type can be

made. In the case of a single phenyl-SH molecule, bonded only to a single gold electrode, a range of theoretical values based on *ab initio* calculations exist, including 0.35V [176], 0.9V [177] and 1.69 V [178]. In terms of experimental measurements, a value of 0.95±0.11 V [168] has been found, which would indicate a midpoint value of the theoretical range is appropriate.

In bridged systems, whereby the phenyl molecules have thiols attached to both drain and source electrodes, experimentally determined TVS values of 0.16 V [179] and 0.79±0.2 V [172] have been found for a single phenyl molecule (benzene-1,4-dithiol) and for two phenyl molecules (biphenyl-4,4'-dithiol) respectively. Thus, from these literature values, our TVS value of 0.11 V is of closest match to the bridged single phenyl molecule (benzene-1,4-dithiol), having a TVS minimum at 0.16 V. This comparison suggests the TVS value is largely unaffected when either two phenyl molecules are directly bridged via σ-bonds or indirectly bridged via vertical stacking. Because of the nature of the sp^2 hybridized carbon atoms within the benzene molecule, a ring of delocalized π electrons is formed above and below the plane of the benzene molecule. In the case of two or more stacked aromatics, such a π – stacked configuration supports through-space transfer which allows the exchange of electrons [180] over sometimes exceptional distances.[181]

The importance of π-π overlap has long been recognized in thin-film organic electronics when investigating small molecules and polymeric systems. More recently it has been recognised as a transport mechanism in tailored graphene devices [182], structures formed in supramolecular chemistry and also electron transport in biological systems. It has also been used to guide the formation of molecular bridges [183] in single molecule electronics. The low value of the TVS minimum is likely due to the close alignment

between the HOMO level (transport through the HOMO level is known to dominate in these systems [184]) of the molecule and the electrodes which is hybridized because of the strong coupling between the thiol and electrode. The strong level of coupling is expected in the case of small molecules especially those incorporating a thiol group due to its high affinity with the Au electrode surface.[38]

SCO Molecular Junctions

7.1 [Fe(L)NCS] complex

Chapter 7

The choice of which SCO compound investigated was based on several factors. Firstly, a solution processable material is very beneficial. A compound which is able to be deposited as a thin film from solution greatly simplifies processing since it allows the use of spin coating or drop casting and avoids the need for complex deposition techniques such as thermal sublimation cells or electrospray sources. The chosen complex should therefore have moderate solubility while also being stable when dissolved and deposited onto a surface.

In addition, any observed switching behaviour seen in a nanogap device must be confidently attributed to the spin transition of a trapped SCO molecule within the nanogap. A switch like behaviour resulting from the diffusion of atoms can be eliminated or at least reduced by performing measurements at cryogenic temperatures. Therefore, the SCO complex should have a transition temperature well below room temperature but within the experimentally accessible temperature range of our cryostat setup.

A compound that meets these criteria is [Fe(L)NCS] where L = N,N'-bis(3-ethoxy-2-hydroxybenzylidene)-1,6-diamino-3-azahexane. This compound belongs to a group of Schiff base complexes in which the sixth Fe coordination site is taken up by a pseudohalide ligand as shown in figure 7.1.

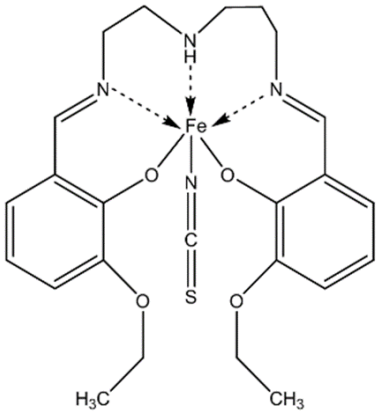

Figure 7.1 *- Schematic representation of the [Fe(L)NCS] complex.*

In the compound used in this study, this site is occupied by an NCS (isothiocyanate) group allowing the molecule to bind to a Au surface. This is also a neutral complex that can be dissolved in acetone to form a solution suitable for the preparation of thin films through spin coating or drop casting from a solution. This compound has a sharp spin transition located well below 100 K, therefore meeting our stability requirement imposed by the electrode material. The complete synthesis as well as a detailed structural and magnetic characterisation of this SCO compound in the bulk form and also of the related family of Schiff base complexes can be found in work by Masárová *et al.*.[185]

7.2 [Fe(L)NCS] Thin films

The [Fe(L)NCS] complex can readily be prepared into thin films. The crystalline material is ground into a fine powder which can then be dissolved in acetone overnight with magnetic stirring (2% solution by weight). The solution can then be drop cast or spin coated to produce thin films. It was found that heating the solution to around 60 °C prior to deposition improved the morphology of the films as shown in figure 7.2. Likley this

heating step increased the solubility of aggregates in the solvent, reducing the formation of streaks and large undissolved particles in the spin coated films. A continuous film thickness down to 40 nm could readily be achieved which was confirmed using AFM.

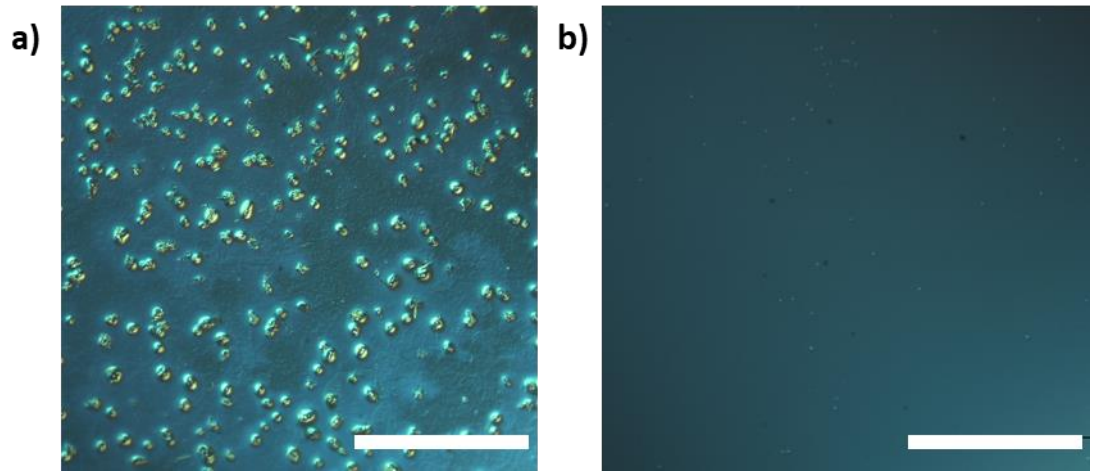

Figure 7.2 *[Fe(L)NCS] thin films prepared a) without heating and b) with heating prior to spin coating. Note: scale bar is 100 µm for both images and film thickness is 40 nm.*

7.3 Magnetic Properties of [Fe(L)NCS]

Temperature dependent magnetometry was performed on both bulk (powder) samples as well as thin films of the [Fe(L)NCS] compound. For the thin films, the material was drop cast onto a Au thin film (50 nm thickness) on a silicon substrate. This was carried out in order to verify that the SCO behaviour is maintained when this compound is dissolved into solution and deposited as thin film directly onto a metal substrate.

For the magnetic measurements, a Quantum Design MPMS-SVSM system is used with an applied magnetic field of 0.1 T. This system uses the superconducting quantum interference device (SQUID) technique to detect extremely small variations in a sample magnetic moment, allowing us to probe the magnetic behaviour of thin film samples which, due to the small amount of material present, generate a very small change in

overall signal during the spin transition. Heating and cooling of the sample was carried out using the inbuilt helium flow cryostat at a rate of 3 $Kmin^{-1}$. The contribution from the substrate was subtracted from the signal. A Kel-F holder was used to contain the samples and has a negligible contribution towards the measurements.

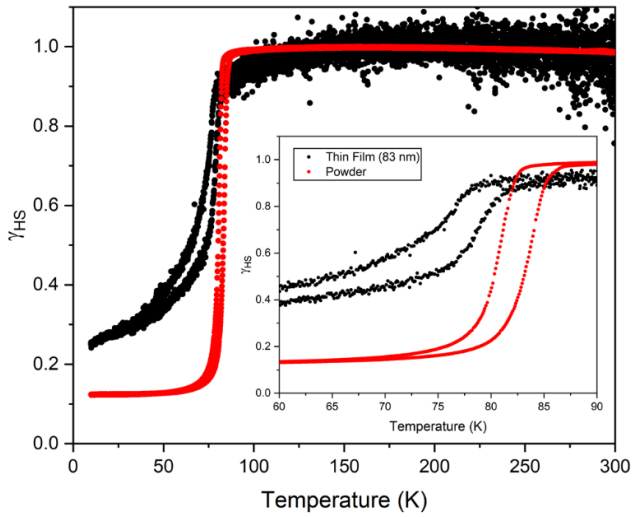

Figure 7.3 *- γ_{HS} (high spin fraction) as a function of temperature for powder sample (red dots) and 83 nm thin film (black dots) of [Fe(L)NCS]. For the thin film sample, due to the low signal level and large amount of noise in the signal, the data is normalised to the mean signal value over the temperature range 300 K to 100 K. Insert shows a reduced temperature range from 60 K to 90 K showing the hysteresis behaviour of the two samples.*

Figure 7.3 shows the high spin fraction as a function of temperature for both the powder and thin film sample. A clear dependence on the sample morphology exists with both a suppression of the transition temperatures (83 K vs 68 K during cooling) and an increase in the width of the hysteresis loop (3 K compared to 7K).

Although these measurements are still probing the behaviour of a thin film and not the behaviour of a single molecule, these measurements serve to prove that our sample preparation process using drop casting from solution still preserves the spin crossover.

These results qualitatively agree with magnetic studies of thermally deposited $[Fe(phen)_2(NCS)_2]$ by Shi *et al.* whereby a rounding of the spin transition curve is observed for thin film samples. In the former study, the authors were able to prove the spin transition is preserved in samples with a thickness down to 7 nm using optical techniques. However, in order to probe the spin state behaviour of single molecules, more advanced techniques are necessary. X-ray magnetic circular dichroism (XMCD) measurements maybe a suitable technique in order to determine the behaviour of isolated SCO complexes deposited with sub-monolayer coverage.[186][113][187]

Within the bulk SCO material, an individual switching molecule produces a localised elastic distortion within the crystal lattice. These distortions propagate through the entire material with the result being a cooperative phase transition. It is therefore unsurprising that the sample morphology will have some an effect on the SCO behaviour. For a thin film material, reducing the sample thickness results in a greater surface to volume ratio and similarly, for a film comprised of clusters, reducing the cluster size will again have the effect of reducing cooperativity as well as modifying the SCO transition temperature. In the extreme case, a single isolated spin crossover molecule will of course be completely absent of any crystal interactions with only substrate interactions being present.

7.4 Electrical properties of [Fe(L)NCS] Drop Cast Films

Interdigitated Au electrode arrays were fabricated using UV-lithography on high purity quartz substrates. The device consisted of an array 40 interdigitated electrodes of dimension 500 x 5 x 5 µm (length x separation x width) with a film thickness of 50 nm. Devices were measured both after fabrication and after drop casting of [Fe(L)NCS].

Devices were measured in a custom built low-noise probe station using a Keithley 487 picoammeter source measurement unit. The I-V characteristics of an interdigitated device is shown in figure 7.4. The drop cast film was approximately 50 µm thick and covered the interdigitated region of the device leaving the contact pads exposed.

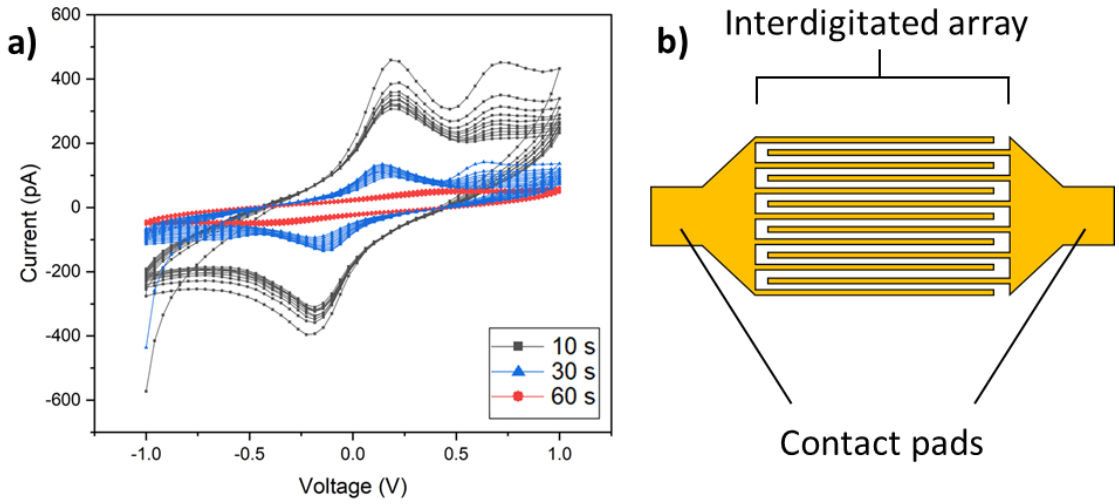

Figure 7.4 *- a) I-V characteristics of an interdigitated electrode array with drop cast* [Fe(L)NCS]. *A delay of 10 s, 30 s and 60 s between setting the voltage and measuring the current was used. Voltage steps of 0.02 V (red data points) and 0.04 V (blue and black datapoints) are used with the sweeps repeated 100, 50 and 20 times for the red, blue and black curves, respectively. b) Schematic of the Au interdigitated electrodes. Note in actual devices, there are 40 interdigitated electrodes and the diagram is merely to illustrate the overall layout of these arrays and contact pads.*

Drop cast devices exhibit very low conduction values 1×10^{-10} S (10 GΩ at +0.5V figure 7.4 red curve). The I-V data also displays loops characteristic of material charging and as such analysis of the data is challenging. However, it is likely that conduction in this material as with most SCO materials takes place through a number of thermally activated conduction processes such as NNH and VRH (see section 3.3.5).[132] The low value of conductivity of these devices prevented further temperature dependent studies

mainly due to the fact that the cryostat measurement setup did not meet the required electrical insulation for measurements on devices that were this poorly conducting, with leakage currents dominating any measurements in the cryostat setup due to the choice of insulation on wiring and vacuum feedthroughs which limits measurements to devices with resistance values below approximately 100 MΩ. Regardless, it is unlikely that thin films of the[Fe(L)NCS] compound will display a measurable conductivity changes at the transition temperature of approximately 80 K. This is because any thermally induced bulk conduction mechanisms will be practically absent at this low temperature and is likely the reason that most literature reports of conductivity changes in thin film SCO devices use SCO materials with around or above room-temperature transition temperatures where thermally activated processes raise the conduction levels to detectable levels.[133]

7.5 [Fe(L)NCS] in Nanogap Electrodes

Investigations of the charge transport of individual or small numbers of SCO molecules, with the hope of using the magnetic bistability as a means to modulate the electrical conductivity of a device. To do this the [Fe(L)NCS] complex is incorporated into nanogap electrodes in a similar manner to BT molecular junctions as discussed in chapter 6. First a 0.01 mM acetone solution of [Fe(L)NCS] is prepared. A gold nanojunction device is plasma cleaned and approx. 2 µl of the solution is drop cast onto the device. Afterwards the solvent is allowed to evaporated under a nitrogen flow and the device is then mounted on the cryostat sample holder. The sample chamber is evacuated to a pressure around 1×10^{-7} mbar. Electromigration is then carried out at room temperature until a conduction value much less 1 G_0 indicates that a nanogap has formed in the device.

Helium exchange gas is slowly introduced to a pressure of 1 – 2 mbar so that heating and cooling of the deice can be carried out.

Figure 7.5 a) shows the behaviour of a device when cooling from room temperature to 66 K. The resistance of a device is sampled with an applied bias of 8 mV. The device shows a gradual increase in resistance from around 150 kΩ at room temperature to a value of around 600 kΩ at low temperature. When cooled below 160 K a bistability in the resistance becomes increasingly apparent. The separation in terms of resistance becomes more distinct as temperature is reduced and the time spent in each of the resistance states also increases.

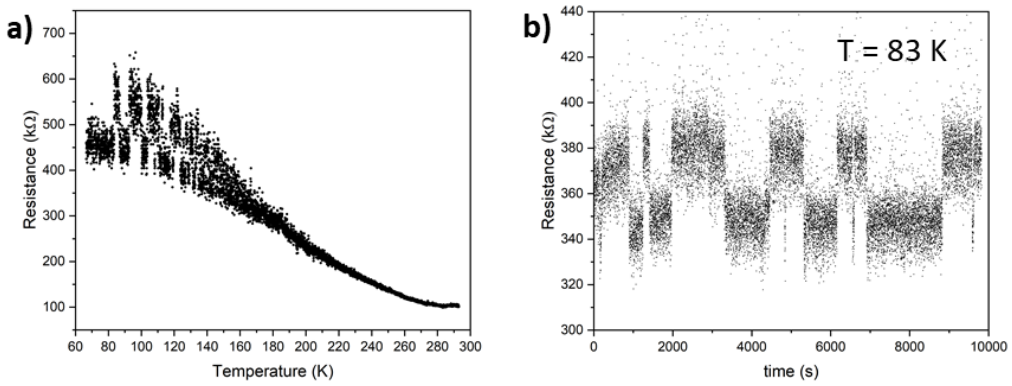

Figure 7.5 *- a) Resistance vs temperature during cooling from 293 K to 66 K for an electromigrated Au nanogap containing SCO1 compound. b) Resistance vs time for the same device as the temperature is held at 83K.*

While resistance fluctuations are a feature of clean nanogap devices, the time evolution of the resistance of a clean nanogap device occurs in a random manner and also with a strong temperature dependence. At room temperature the resistance of a Au nanogap device is likely to change drastically in the timespan of a few minutes to a few hours due to thermal motion of the electrode material. However, at cryogenic temperatures the

devices are stable enough to measure long term behaviour. This is not the case when [Fe(L)NCS] complexes are present. In the low temperature regime resistance fluctuations are observed. If this behaviour is due to an electrode diffusion processes it would be strongly temperature dependent and take on a behaviour unlike that shown in figure 7.5.

In devices broken without molecules present, there is only a weak temperature dependence of the tunnelling resistance after cooling of the device to 70 K and multi-level resistance states is only observed in devices exposed to the SCO complexes. This suggests that there is a strong correlation between tunnelling electrons interacting with states on the complex and temperature.

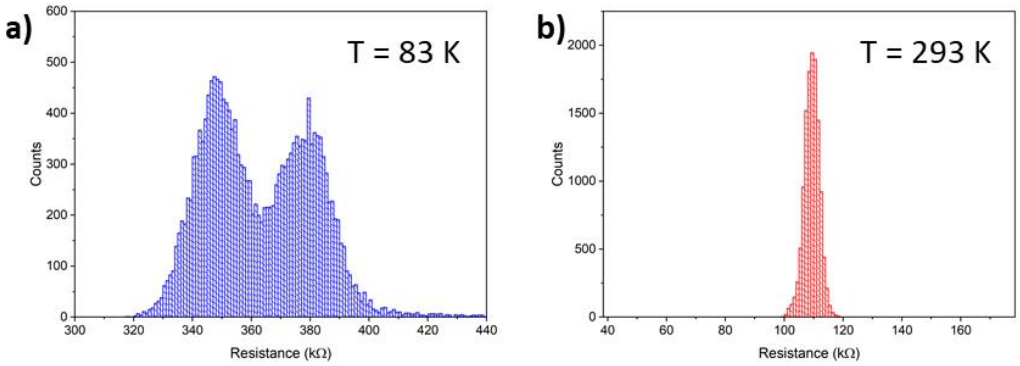

Figure 7.6 *- Resistance histograms at a) 83K and b) 293K. (Note: Bin size is 1 kΩ for each of the histograms with 1.2×10^4 total samples).*

As shown in figure 7.5 b) the lifetime of each state is well defined at 83 K and also long-lived, with the lower resistance state being occupied for a maximum of 30 minutes and with the low resistance state being occupied for 54% more time than the high resistance state. A resistance histogram at fixed temperature is constructed from figure 7.5 b) and is shown in comparison to a repeated measurement made after slowly heating the device to room-temperature. This is shown in figure 7.6.

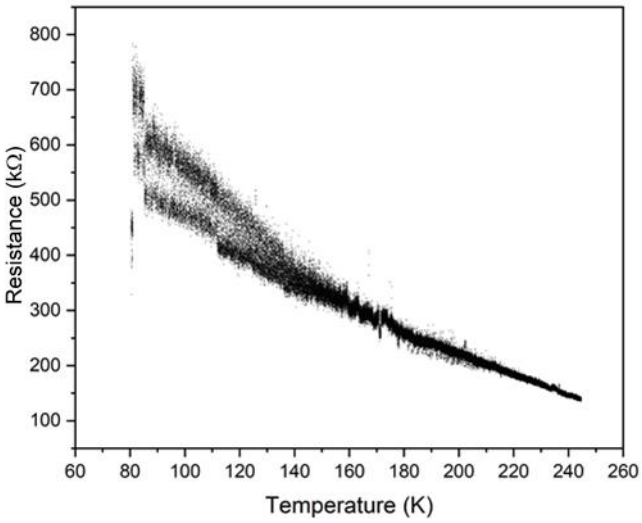

This behaviour is reproducible over several cooling and heating cycles. Figure 7.7 shows the resistance as a function of temperature plotted for the same device after repeating the cooling and heating cycle four times. The bistability is still apparent as well as several discontinuities. While thermal motion of the device is greatly reduced at cryogenic temperatures, it is not totally absent and is likely the origin behind the discontinuities. The behaviour was also observed in several devices electromigrated with [Fe(L)NCS] deposited, one such example is shown in figure 7.8 a) which shows the resistance as a function of time during heating from around 80 K to room temperature. Although the telegraph-like switching not as clear as the behaviour shown in figure 7.5, the switching is apparent in the data presented in figure 7.8 b), which shows a reduced section of the recorded data. Possibly this occurs due to the [Fe(L)NCS] molecule taking a different binding arrangement within the nanogap electrode which results in the spin transition having a reduced influence on the conduction through the device.

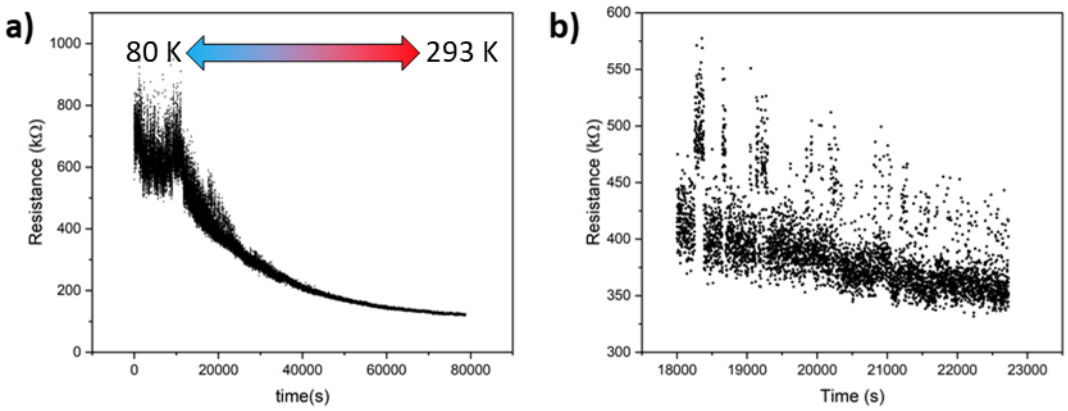

Figure 7.8 *a) Resistance as a function of time for a second electromigrated nanogap device with [Fe(L)NCS] deposited. During the measurement of the resistance, the temperature of the device is allowed to vary from approximately 80 K at t = 0 s, to room temperature over the 21 hr measurement period. b) A reduced section of data taken between 18000 s and 22732 s showing resistance switching.*

7.6 Discussion

Fluctuations between well-defined conductance levels is a commonly observed behaviour in nanoscale devices and is believed to be the physical origin of burst noise (also called random telegraph noise or popcorn noise) in electronic circuits. In nanogap devices, these stochastic or random fluctuations have been attributed to a variety of processes including variations in molecular conformation and surface orientation,[188][189][190] charge trapping in bridged polymer devices,[191] molecular oscillations as a result of inelastic tunnelling processes,[192] and, especially in the case of surface probe measurements, the formation and breakage of a chemical bond with the probe tip.[193] The fundamental origin of the switching behaviour in our devices is likely due to a combination of two processes occurring. Firstly, a reduction in the energy of the ligand field splitting parameter, Δ_O, as a result of the reduced temperature then

allows for thermal perturbations of the ligand structure around the central ion to induce a spin transition of the complex. As predicted by numerous DFT calculations on similar complexes, the two spin states differ in electronic properties resulting in the appearance of two different conducting states.

In contrast to previous work which reported telegraphic-like switching within I-V sweeps,[139] this work used only a small bias voltage to avoid the effects of voltage triggered conformational changes[92] and resistance switching memory effects from filamentary formation as is commonplace in ReRAM memory devices.[194] Additionally, the telegraphic-like switching process has been observed in empty graphene nanogaps with the origin of this behaviour likely resulting from interfacial defects.[101] In this study clean gold nanojunctions have been used yet still observe telegraphic-like switching at very low bias (8 mV).

Previously reported studies on voltage triggered switching has occurred only for complexes which are either specifically tailored heteroleptic metal complexes which have large intrinsic dipole moments[92] and are hence susceptible to a voltage driven distortion of the octahedral structure or in STM studies on specially prepared substrates which decouple the SCO complexes from the strong surface interactions[188][84]. In both types of measurement, switching still occurs at a fairly high bias voltage, typically between 0.5 V and 1 V in MCBJ experiments and up to 1.5 V is reported in STM studies.[70] This is in line with theoretical predictions that a critical field strength upwards of 1 GVm^{-1} is needed in order to electrostatically induce the spin transition[195] when typical electrode – molecule distances are considered.

The fact that the transition temperature in these measurements is vastly different from that of the bulk material is unsurprising. The behaviour of a small number of molecules or an individual molecule is different from that of the bulk material as no cooperative effects are present. This is illustrated by measurements of thin films of [Fe(L)NCS]. Because the stabilising effect of the surrounding crystal lattice is not present for an isolated [Fe(L)NCS] complex, the spin state is likely to be free to switch between states rapidly and at a temperature vastly different than that at which the bulk complex undergoes a spin-transition. A possible explanation for the temperature dependence of these measurements which is in contrast with the measurements presented in a previous report is likely due to the choice of molecule. The large protracted $[Fe(L')_2](BF_4)_2$ CH_3CN H_2O molecule and its extended arrangement across electrodes is potentially more susceptible to thermal perturbations than the far smaller [Fe(L)NCS] complex used here. Also of note is that the [Fe(L)NCS] complex binds to Au surface via a single NCS ligand whereas complex reported by Miyamachi *et al.* and Burzurí *et al.* bind to surfaces via two functional groups.[84] Because the SCO phenomenon relies heavily on the splitting energy, Δ_O, due to the octahedral symmetry of the ligands surrounding the central Fe ion, it is not surprising that binding onto the surface kills the SCO phenomenon. This is avoided in our complex making it possible that the necessary structural changes are still maintained.

While the [Fe(L)NCS] complex is likely to be bound to the Au surfaces via the NCS group, the possibility of the SCO complex also occupying an alternative binding arrangement cannot be eliminated. Because of the small size of the [Fe(L)NCS] molecule in relation to other functionalised SCO complexes, it may be possible that it occupies a site on the oxide substrate surface between the Au electrode. In such an arrangement it will be

attached weakly via physisorption. In this way the SCO mechanism is preserved in a similar way to that seen in STM measurements by the introduction of a decoupling CuN spacer layer. In this arrangement current flow is laterally through the SCO complex.

7.7 Multilevel Switching

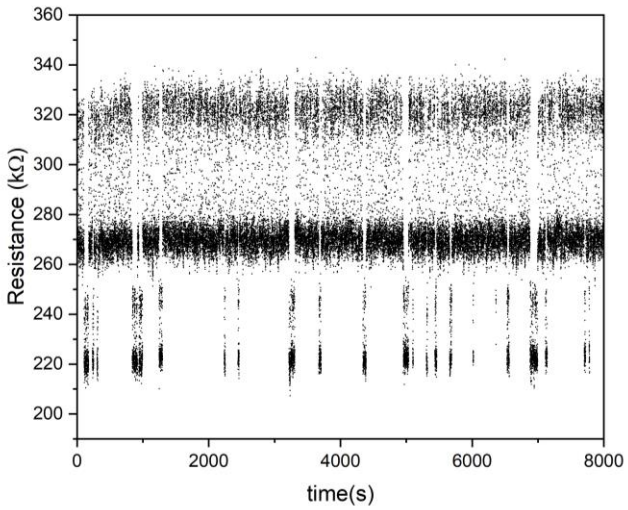

Figure 7.9 *- Resistance vs time for a Au nanogap device containing [Fe(L)NCS] displaying multilevel resistance switching, measured at a temperature of 83 K. Applied bias is 8 mV.*

Many repeated cooling and heating cycles were performed on a single electromigrated device. Figure 7.9 shows the low temperature behaviour of a device exhibiting multi-level switching behaviour. This behaviour was observed in a device that previously showed two level switching in resistance similar to that presented in figure 7.9. After heating the device to room temperature and maintaining this temperature for several minutes a multilevel resistance switching behaviour was measured when cooled back to low temperature. This is possibly as a result of a second SCO complex either “becoming active” or diffusing into the nanogap after an extended duration at room temperature.

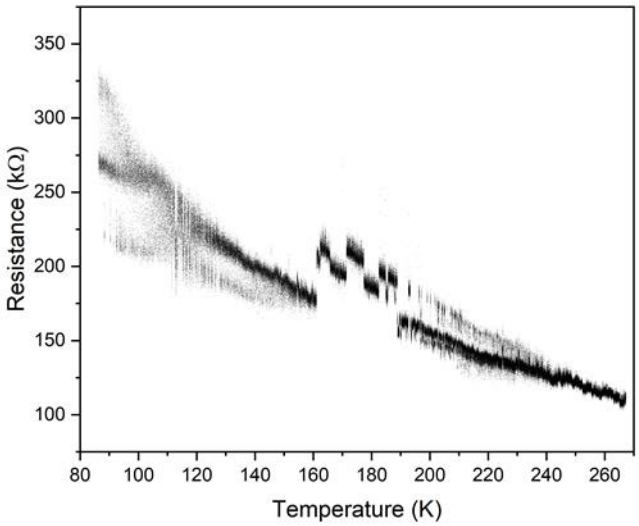

Figure 7.10 *- Nanogap containing [Fe(L)NCS] molecules displaying multilevel switching during warming from low temperature to room temperature. The resistance is measured with a bias voltage of 8mV over a 14 hr period. In some cases, as shown, discontinuities were observed in the resistance measurement, which can be ascribed to either changes in the structure of the electrode interface or changes within the nanogap itself, such as a movement of the attached molecule.*

The temperature dependence of this behaviour is shown in figure 7.10 showing the complex evolution of this behaviour as well as a large discontinuity when the temperature warms above 160 K. Again, this is likely as a result of thermal motion of the SCO complex with respect to the nanogap. If two molecules are present within the nanogap then the total tunnelling current is influenced by the relative contributions from both molecules.

The only previously reported measurement of multilevel switching three distinct states) in a SCO complex by Jasper-Toennies *et al.* with multilevel switching between three distinct resistance states. However, this was attributed to being due to an extrinsic effect due to substrate coupling.[188] The LS state is shown to possess two possible closely

spaced conductance values which arise due to a rotation of the complex on the crystalline substrate. In addition to applying a sufficiently large voltage (> 1.8 V), the complexes must also possess a degree of flexibility and be suitably decoupled from the substrate[196] which is not the case for the [Fe(L)NCS] complex and which is achieved by the authors via the use of a Cu_xN spacer layer. Additionally, the molecules in these measurements are unlikely to exist on a flat crystalline surface due to the nature of the electromigration process[62] eliminating this as a possible mechanism for the appearance of four resistance states.

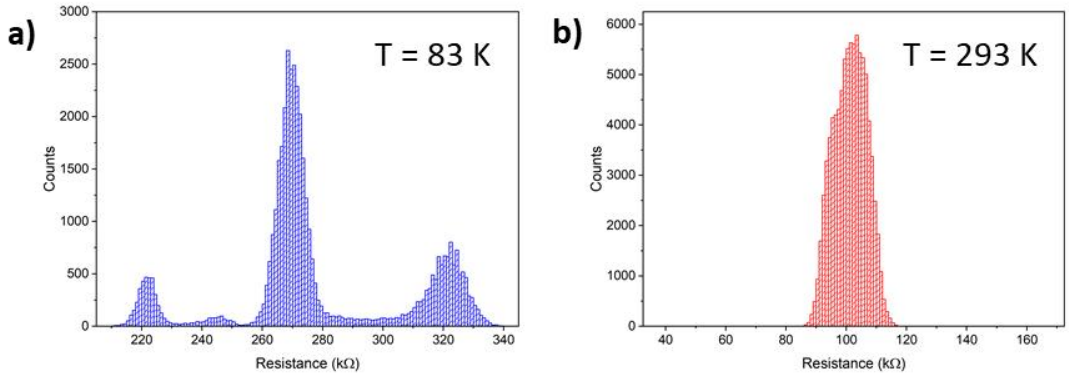

Figure 7.11 *- Resistance histograms at 83K showing four individual peaks, which are expected to be due to the following spin combinations that occurs when two molecules are present within the gap (LS-LS, HS-LS, LS-HS, HS-HS). b) 293 K showing only a single broad peak. (Note: Bin size is 1 kΩ for each of the histograms with 4.3×10^4 total samples).*

Monitoring the resistance over a long period of time at constant temperature allows a resistance histogram plot to be created as shown in figure 7.11 for the device at low temperature and room temperature. In figure 7.11 a) four peaks are clearly visible as can be expected to be due to the following spin combinations of the two molecules within the gap (LS-LS, HS-LS, LS-HS, HS-HS). Figure 7.11 b) shows the resistance histogram of the device before cooling. In this case only a single broad peak is observed,

indicating that all molecules present are in the HS state due to the temperature dependence of the splitting energy, Δ_O.

Conclusion and Future Outlook

8.1 Conclusions

Chapter 8

Hopefully this thesis has given the reader an insightful look at the fabrication techniques used to produce nanogap electrodes with separation below 2 nm and methods to incorporate and measure molecular entities within those structures. A significant part of this thesis work was to develop a low cost, high throughput approach that allows nanoscale devices to be produced in high volumes and over large area substrates. This was demonstrated using a bilayer nanoimprint lithography approach that optimizes the yield of successful devices whilst retaining the nanoscale feature size (< 20 nm). One problem with nanoimprint lithography is that it can be difficult to pattern both large and nanoscale features at the same time because of the manner in which the imprinted polymeric material flows. Using careful design of the stamp and imprinting parameters (pressure, temperature, time, resist material) it was possible to find an optimised approach that allowed patterning of the molecular electronic devices, which require both large-area contact pads and small nanoscale conducting channels for the electromigration process.

Although nanoscale features made using nanoimprint lithography are suitable for many applications, molecular electronics requires feature sizes that are much smaller. In particular, it requires very small nanosized gaps, of just ~1-2 nm, between metal electrodes that can support the bridging and electrical contact to single molecules. In this work, very small sized junctions were made by applying an electromigration process to the devices after the nanoimprint lithography process. The electromigration process

involves applying a series of voltage pulses to conducting channels of very narrow width (50 nm). The large current through the channel causes atoms to migrate away from a central spot within the channel until a pinch-off process starts to occur. Using very fast monitoring with feedback control, the current through the channel is adjusted to avoid thermal runaway. The electromigration processes is continued until a very small nanogap within the conducting channel is formed. As shown in this work, with good control electronics and device design, gap sizes of < 2 nm can be routinely created. The final device, consisting of two metal electrodes with a very small nanogap and called a break-junction or a nanojunction, provides a suitable platform for integrating molecules for molecular electronics studies.

Using the above approach, devices were first made with benzenethiol (BT) molecules bridging across the nanogap. The incorporation of similar thiolated aromatic molecules in devices is often used for benchmarking and is also an important precursor to the integration and study of a wide range of different molecular species. BT molecules are very versatile and can be used to form the initial anchoring unit of a molecular wire, allowing the construction of many types of molecular junctions with differing functionalities through, for example, step-wise chemical synthesis[197]. Incorporation of BT molecules in this work was also used as an important validation step to assess the suitability of our nanojunction fabrication methods, stability of our devices and the precision of the measurement platform. The success of integrating BT molecules within the nanogap was confirmed by the observation of molecular transport signatures in repeated I-V sweeps. A current suppression present in the I-V behaviour at low voltage, which is then lifted at high voltage, signifying on- and off-resonant transport as a function of voltage is a characteristic feature of a successfully formed molecular junction.

After validation of the entire nanofabrication platform, consisting of device fabrication, molecular integration and electronic measurement setup, the work shifted to the study of spin crossover molecule systems. Temperature dependent magnetic and electronic studies were initially carried out on bulk materials and thin-films containing the [Fe(L)NCS] complex used in this study. This was followed by the incorporation of the SCO molecule into electromigrated nanojunctions and variable temperature electronic transport measurements. This work mostly focussed on the [Fe(L)NCS] molecule as we were particularly interested in molecules that are asymmetric in nature and only form a connecting “molecular bonding bridge” to one gold electrode.

Previously only a handful of measurements that focus on SCO compounds at a single molecule level have been reported in the literature. These were carried out using either surface probe techniques, MCBJ’s, electromigrated nanogap devices or electroburnt graphene nanogap devices. Excluding the recent work carried out by Burzurí *et al.,* all previous studies have taken place at very low temperatures. This is unsurprising since single molecule electrical measurements are challenging and low temperature offers greater stability, increased longevity of the molecular junction and smaller amounts of electronic noise.

The SCO switching effects studied in this thesis present a very unique type of switching behaviour. At room temperature, only a single resistance state is measured. As the temperature of a device is reduced below 200 K, telegraphic-like switching occurs with switching between two resistive states. As the temperature is reduced further the two resistance states become more defined and the time spent in each state increases. This is a strong indicator that temperature is the driving stimulus behind this switching process.

This type of switching is completely different for switching from artefacts involving the migration of atoms between the two device electrodes, which typically show increased rates at room temperature and also show evolution in a random manner between many values. Furthermore, switching effects that are related to electrode instability or resistive switching as a result of filamentary formation (from the electrodes) can be eliminated as the measurements were restricted only to very low bias during measurement.

The two well-defined resistance levels observed in nanojunctions containing SCO complexes is expected to be due to the conformational change of the SCO molecule and a modification of the tunnelling processes that occur as the complex undergoes the spin transition. The transition likely arises as a result of thermal perturbations and the reduced energy of the ligand field splitting parameter that occurs at reduced temperature.

This modification of the transition temperature, in contrast to the bulk material, is unsurprising as the co-operative SCO phenomenon is no longer present in the case of a single isolated molecule. The stabilising effect that the surrounding crystal lattice has is totally absent and the interaction of the complex with the surface instead dominates, drastically increasing the temperature at which the SCO phenomenon occurs.

The [Fe(L)NCS] devices are characterised only at low bias, which avoids the possibility of resistive switching effects that are not discussed in other papers on nanogap devices. In addition, the efforts used to decouple the SCO complex from the extended electronic states of the leads has been shown to be not necessary to preserve the SCO effect. This was observed in our case and is likely due to the different choice of SCO complex. The [Fe(L)NCS] complex used in this work is compact with respect to other functionalised

SCO complexes such as the $[Fe(L')_2](BF_4)_2$ CH_3CN H_2O molecule. Unlike other SCO complexes that have been investigated electrically and at a single molecule, the [Fe(L)NCS] binds to the Au electrode via only one ligand. The result of this is that the octahedral symmetry around the spin transition core remains unchanged when it is deposited onto a surface. The long extended structure of the $[Fe(L')_2](BF_4)_2$ CH_3CN H_2O complex in particular makes it unsurprising that this complex loses its temperature dependent SCO behaviour when placed in a nanogap device. Non-symmetrical binding arrangements are likely and localised perturbations of these extended ligands could be large enough to induce the spin transition at all temperatures since they are in contact to a relatively large area of the electrode surface via pyrene end groups.

In some cases, switching between four resistance states was observed in these devices. In this case, we propose that two SCO molecules are present within the nanogap and are participating in the electron tunnelling and the spin-transition process with the four resistance states corresponding to different spin state combinations of the two complexes. This type of behaviour, when controllable, could facilitate multi-level resistance switching and the development of ultra-small molecular memory devices having more than two binary states.

8.2 Future Outlook

Molecular spintronics is a rapidly evolving field. Even in the course of this work several breakthroughs have been made in the area of molecular electronics and SCO devices. Examples of these achievements include advances in the fabrication of high quality large area thin films,[198] development of electroburnt and MCBJ graphene

devices,[139][199] electrical detection of SCO in nanoparticle thin films, [75] and the incorporation of a SCO complex into a planar device while preserving the SCO.[139]

The observation of this resistance switching mechanism, in particular the measurement of four-level resistance switching in devices which we theorise contain two molecules, has prompted a collaboration with the group of Jürgen König at the University of Duisburg-Essen (UDE). The aim of this collaboration is to apply a technique which analyses correlations between the switching events by analysing quantities known as factorial cumulants to extract information about the switching process.[200]

This technique has been demonstrated already in the single-electron tunnelling processes in semiconductor quantum-dot devices where non-equilibrium properties, namely the spin-relaxation rate, is extracted from monitoring the telegraph-like optical signal produced by time-resolved resonance fluorescence on a single quantum dot.[201] Although work is largely ongoing and a manuscript is in preparation, initial analysis suggests that there is correlation between the switching and therefore two interacting molecules. This suggests that the molecules must be localised within a nanogap since the interaction is likely to be short range.

In addition to this ongoing work, there are several areas where I believe there is room to carry out further work based on the general theme explored in this work. Firstly, chemical modification of SCO compounds themselves or the manner in which the molecules bind to the electrodes may be advantageous in both tuning the SCO phenomenon or preserving the spin transition behaviour when single molecules are constrained within nanogap electrodes. Although we have presented a device that showed conductance switching as a function of time and temperature, the success rate was low and we discussed alternative binding arrangements within the nanogap as a

means of explaining our observed switching behaviour. As discussed extensively in the literature, binding of these complexes with metallic surfaces is likely to modify the spin transition behaviour of the devices and in some cases even block it. This was also partly the motivation behind the work in this thesis involving the self-assembled monolayers (BT), since these can be used as a means by which molecules can be soft-coupled to electrodes so as to preserve the SCO effect.

The emergence in the last few years of electroburnt graphene nanogaps is also very promising and represents a continuation of the idea of this soft-coupling approach to electrically connect molecules within devices. These devices also show remarkable stability allowing for temperature dependent measurements as well as a wide variety of other possibilities.[10] This is certainly an area of viable future work.

It has also recently been shown that it is possible to induce the spin transition at temperatures far higher than their usual bulk spin transition temperature through chemical substitution within SCO materials, possibly opening the route to room temperature devices.[91] This would avoid the need of cryogenic systems for device operation and could lead to real device applications in memory technologies. Work is currently underway to incorporate these compounds into devices, but, as yet single molecule devices have not been made. This would be an obvious area of future research and perhaps, in this respect, a step-wise synthesis and integration method for inclusion of the molecule within a nanogap could be a suitable method of choice.[197]

Finally, it has been realised by several groups through *ab initio* calculations[202][19][203] that SCO molecules behave as spin filters and that this effect is largely responsible for the conductivity change in devices.[138] This has not yet been taken advantage of in a

practical SCO based device but may prove to be a very powerful method of generating localised spin-polarised currents at an interface within a molecular electronic device.

As discussed, the LIESST effect is limited to very low temperatures,[204] making the prospect of using this in a practical device unlikely but it is still worth exploring the possibility of photo-switching of a SCO complex in a nanogap device. The absence or preservation as well as lifetime measurements of the LIESST and/or inverse-LIESST effect could reveal insights into the binding of the complex on surfaces. An alternative route could also be envisioned that utilises a light-driven conformational change to induce the SCO in the complex. Light induced spin state photoconversion has already been observed in [Ni(^{F}TPP)] complexes, (where ^{F}TPP=tetrakis(pentafluorophenyl)porphyrinato(2-)).[205] This would not only preserve the beneficial qualities of a SCO based molecular devices but also add an optical stimulus as a means to drive switching. Chemical modification has also been shown to be able to modify the behaviour of SCO complexes, with examples including pH induced spin transitions,[206] ligand addition,[207][208] ligand exchange [209][210] and non-covalent guest molecule interactions.[211] In general, the observation of chemically induced SCO phenomenon occurs in the liquid state but perhaps could be applied to a molecular electronic device, for example, in a nanogap device incorporating a microfluidic system.[29]

References

[1] P. Gütlich and H. a. Goodwin, *Spin Crossover in Transition Metal Compounds I*, vol. 233. 2004.

[2] P. Gütlich, A. B. Gaspar, and Y. Garcia, "Spin state switching in iron coordination compounds," *Beilstein J. Org. Chem.*, vol. 9, no. Ii, pp. 342–391, 2013.

[3] J.-F. Létard, P. Guionneau, and L. Goux-Capes, "Towards Spin Crossover Applications," *Spin Crossover Transit. Met. Compd. III*, vol. 1, pp. 221–249, 2006.

[4] G. E. Moore, "Cramming more components onto integrated circuits (Reprinted from Electronics, pg 114-117, April 19, 1965)," *Proc. Ieee*, vol. 86, no. 1, pp. 82–85, 1965.

[5] B. Y. M. M. Waldrop, O. F. M. S. Law, and M. Interesting, "More Than Moore," *Nature*, vol. 530, p. 145, 2016.

[6] C. Grupe, "Visions for a molecular future," *Nat. Nanotechnol.*, vol. 8, no. 6, pp. 385–389, 2013.

[7] G. Puebla-Hellmann, K. Venkatesan, M. Mayor, and E. Lörtscher, "Metallic nanoparticle contacts for high-yield, ambient-stable molecular-monolayer devices," *Nature*, vol. 559, no. 7713, pp. 232–235, 2018.

[8] J. Cuevas and E. Scheer, *Molecular Electronics: An Introduction to Theory and Experiment*, vol. 53, no. 9. 2013.

[9] Y. Chen *et al.*, "Nanoscale molecular-switch crossbar circuits," *Nanotechnology*, vol. 14, no. 4, pp. 462–468, 2003.

[10] C. Jia *et al.*, "Covalently bonded single-molecule junctions with stable and reversible photoswitched conductivity," *Science (80-.).*, vol. 352, no. 6292, pp. 1443–1446, 2016.

[11] J. Trasobares, D. Vuillaume, D. Théron, and N. Clément, "A 17 GHz molecular rectifier," *Nat. Commun.*, vol. 7, pp. 1–9, 2016.

[12] A. Fert, "Giant Magnetoresistance of (001)Fe/(001)Cr Magnetic Superlattices," *Phys. Rev. Lett.*, vol. 61, no. 21, p. 2471, 1988.

[13] G. Binasch, P. Grünberg, F. Saurenbach, and W. Zinn, "Enhanced magnetoresistance in

layered magnetic structures," *Phys. Rev. B*, vol. 39, no. 7, pp. 4828–4830, 1989.

[14] A. Fert, "The present and the future of spintronics," *Thin Solid Films*, vol. 517, no. 1, pp. 2–5, 2008.

[15] M. Urdampilleta, S. Klyatskaya, J. P. Cleuziou, M. Ruben, and W. Wernsdorfer, "Supramolecular spin valves," *Nat. Mater.*, vol. 10, no. 7, pp. 502–506, 2011.

[16] L. Bogani and W. Wernsdorfer, "Molecular spintronics using single-molecule magnets.," *Nat. Mater.*, vol. 7, no. 3, pp. 179–186, 2008.

[17] S. Kyatskaya *et al.*, "Anchoring of rare-earth-based single-molecule magnets on single-walled carbon nanotubes," *J. Am. Chem. Soc.*, vol. 131, no. 42, pp. 15143–15151, 2009.

[18] N. Baadji and S. Sanvito, "Giant resistance change across the phase transition in spin-crossover molecules," *Phys. Rev. Lett.*, vol. 108, no. 21, pp. 1–5, 2012.

[19] J. Huang, R. Xie, W. Wang, Q. Li, and J. Yang, "Coherent transport through spin-crossover magnet Fe2 complexes," *Nanoscale*, vol. 8, no. 1, pp. 609–616, 2016.

[20] I. Díez-Pérez *et al.*, "Rectification and stability of a single molecular diode with controlled orientation," *Nat. Chem.*, vol. 1, no. 8, pp. 635–641, 2009.

[21] R. M. Metzger *et al.*, "Unimolecular electrical rectification in hexadecylquinolinium tricyanoquinodimethanide," *J. Am. Chem. Soc.*, vol. 119, no. 43, pp. 10455–10466, 1997.

[22] A. S. Martin, J. R. Sambles, and G. J. Ashwell, "Molecular Rectifier," *Phys. Rev. Lett.*, vol. 70, no. 2, pp. 218–221, 1993.

[23] B. Capozzi *et al.*, "Single-molecule diodes with high rectification ratios through environmental control," *Nat. Nanotechnol.*, vol. 10, no. 6, pp. 522–527, 2015.

[24] A. E. Grigorescu, M. C. van der Krogt, C. W. Hagen, and P. Kruit, "10 nm lines and spaces written in HSQ, using electron beam lithography," *Microelectron. Eng.*, vol. 84, no. 5–8, pp. 822–824, 2007.

[25] Y. Jiang, B. Luo, and X. Cheng, "Enhanced Thermal Stability of Thermoplastic Polymer Nanostructures for Nanoimprint Lithography," *Materials (Basel).*, vol. 12, no. 3, p. 545, 2019.

[26] G. Binnig, H. Rohrer, C. Gerber, and E. Weibel, “Surface studies by scanning tunneling microscopy,” *Phys. Rev. Lett.*, vol. 49, no. 1, pp. 57–61, 1982.

[27] X. D. Cui *et al.*, “Reproducible measurement of single-molecule conductivity,” *Science (80-.).*, vol. 294, no. 5542, pp. 571–574, 2001.

[28] A. Avila and B. Bhushan, “Electrical measurement techniques in atomic force microscopy,” *Crit. Rev. Solid State Mater. Sci.*, vol. 35, no. 1, pp. 38–51, 2010.

[29] P. Lunca Popa *et al.*, “Heteronanojunctions with atomic size control using a lab-on-chip electrochemical approach with integrated microfluidics,” *Nanotechnology*, vol. 22, no. 21, 2011.

[30] L. De Los Santos Valladares *et al.*, “Controlled electroplating and electromigration in nickel electrodes for nanogap formation,” *Nanotechnology*, vol. 21, no. 44, 2010.

[31] Y. Kashimura, H. Nakashima, K. Furukawa, and K. Torimitsu, “Fabrication of nano-gap electrodes using electroplating technique,” *Thin Solid Films*, vol. 438–439, no. 03, pp. 317–321, 2003.

[32] S. Hassan, M. Jafri, T. Blom, and K. Leifer, “Shrinking of FIB cut nanogaps in gold wires down to 5nm by electrodeposition,” no. April 2015, pp. 5–7.

[33] P. Lunca Popa *et al.*, “The magnetoelectrochemical switch,” *Proc. Natl. Acad. Sci.*, vol. 111, no. 29, pp. 10433–10437, 2014.

[34] F.-Q. Xie, L. Nittler, C. Obermair, and T. Schimmel, “Gate-Controlled Atomic Quantum Switch,” *Phys. Rev. Lett.*, vol. 93, no. 12, pp. 1–4, 2004.

[35] D. Xiang, H. Jeong, T. Lee, and D. Mayer, “Mechanically controllable break junctions for molecular electronics,” *Adv. Mater.*, vol. 25, no. 35, pp. 4845–4867, 2013.

[36] M. A. Reed, C. Zhou, C. J. Muller, T. P. Burgin, and J. M. Tour, “Conductance of a molecular junction,” *Science (80-.).*, vol. 278, no. 5336, pp. 252–254, 1997.

[37] C. A. Martin, D. Ding, H. S. J. Van Der Zant, and J. M. Van Ruitenbeek, “Lithographic mechanical break junctions for single-molecule measurements in vacuum: Possibilities and limitations,” *New J. Phys.*, vol. 10, 2008.

[38] M. L. Perrin, E. Burzurí, and H. S. J. van der Zant, “Single-molecule transistors,” *Chem. Soc. Rev.*, vol. 44, no. 4, pp. 902–919, 2015.

[39] M. Di Ventra, S. T. Pantelides, and N. D. Lang, “First-Principles Calculation of Transport Properties of a Molecular Device,” *Phys. Rev. Lett.*, vol. 84, no. 5, pp. 979–982, 2000.

[40] X. Xiao, B. Xu, and N. J. Tao, “Measurement of Single Molecule Conductance: Benzenedithiol and Benzenedimethanethiol,” *Nano Lett.*, vol. 4, no. 2, pp. 267–271, 2004.

[41] E. Lörtscher, H. B. Weber, and H. Riel, “Statistical approach to investigating transport through single molecules,” *Phys. Rev. Lett.*, vol. 98, no. 17, pp. 12–15, 2007.

[42] Y. Komoto, S. Fujii, H. Nakamura, T. Tada, T. Nishino, and M. Kiguchi, “Resolving metal-molecule interfaces at single-molecule junctions,” *Sci. Rep.*, vol. 6, p. 26606, 2016.

[43] J. Tomfohr and O. F. Sankey, “Theoretical analysis of electron transport through organic molecules,” *J. Chem. Phys.*, vol. 120, no. 3, pp. 1542–1554, 2004.

[44] H. Park, A. K. L. Lim, A. P. Alivisatos, J. Park, and P. L. McEuen, “Fabrication of metallic electrodes with nanometer separation by electromigration,” *Appl. Phys. Lett.*, vol. 75, no. 2, pp. 301–303, 1999.

[45] Z. M. Wu, M. Steinacher, R. Huber, M. Calame, S. J. Van Der Molen, and C. Schönenberger, “Feedback controlled electromigration in four-terminal nanojunctions,” *Appl. Phys. Lett.*, vol. 91, no. 5, pp. 11–14, 2007.

[46] J. M. Campbell and R. G. Knobel, “Feedback-controlled electromigration for the fabrication of point contacts,” *Appl. Phys. Lett.*, vol. 102, no. 2, pp. 1–5, 2013.

[47] R. Hoffmann, D. Weissenberger, J. Hawecker, and D. Stöffler, “Conductance of gold nanojunctions thinned by electromigration,” *Appl. Phys. Lett.*, vol. 93, no. 4, pp. 91–94, 2008.

[48] H. Masuda and T. Kizuka, “Distance control of electromigration-induced silver nanogaps,” *J. Nanosci. Nanotechnol.*, vol. 14, no. 3, pp. 2436–2440, 2014.

[49] F. Prins, A. J. Shaikh, J. H. Van Esch, R. Eelkema, and H. S. J. Van Der Zant, “Platinum-nanogaps for single-molecule electronics: Room-temperature stability,” *Phys. Chem. Chem. Phys.*, vol. 13, no. 32, pp. 14297–14301, 2011.

[50] F. Prins *et al.*, “Room-temperature stability of Pt nanogaps formed by self-breaking,” *Appl. Phys. Lett.*, vol. 94, no. 12, pp. 2009–2011, 2009.

[51] K. Ienaga *et al.*, “Zero-bias anomaly in ferromagnetic Ni nanoconstrictions,” *Phys. Rev. B - Condens. Matter Mater. Phys.*, vol. 86, no. 6, pp. 1–4, 2012.

[52] K. I. Bolotin, F. Kuemmeth, A. N. Pasupathy, and D. C. Ralph, “From ballistic transport to tunneling in electromigrated ferromagnetic breakjunctions,” *Nano Lett.*, vol. 6, no. 1, pp. 123–127, 2006.

[53] C. Gärtner, R. Hoffman, F. Prez-Willard, M. Sauter, C. Sürgers, and H. V. Löhneysen, “Fully ultrahigh-vacuum-compatible fabrication of submicrometer-spaced electrical contacts,” *Rev. Sci. Instrum.*, vol. 77, no. 2, pp. 1–4, 2006.

[54] S. Egger, A. Ilie, Y. Fu, J. Chongsathien, D. J. Kang, and M. E. Weiland, “Dynamic shadow mask technique: A universal tool for nanoscience,” *Nano Lett.*, vol. 5, no. 1, pp. 15–20, 2005.

[55] R. Hoffmann-Vogel, “Electromigration and the structure of metallic nanocontacts,” *Appl. Phys. Rev.*, vol. 4, no. 3, 2017.

[56] Z. M. Wu, “Formation mechanism and resistance fluctuations of atomic sized junctions,” University of Basel, 2008.

[57] N. Agraït, A. L. Yeyati, and J. M. van Ruitenbeek, “Quantum properties of atomic-sized conductors,” *Phys. Rep.*, vol. 377, no. 2–3, pp. 81–279, 2003.

[58] D. R. Strachan *et al.*, “Real-time TEM imaging of the formation of crystalline nanoscale gaps,” *Phys. Rev. Lett.*, vol. 100, no. 5, pp. 1–4, 2008.

[59] Y. Oshima and Y. Kurui, “In situ TEM observation of controlled gold contact failure under electric bias,” *Phys. Rev. B - Condens. Matter Mater. Phys.*, vol. 87, no. 8, pp. 1–5, 2013.

[60] H. B. Heersche, G. Lientschnig, K. O’Neill, H. S. J. Van Der Zant, and H. W. Zandbergen, “In situ imaging of electromigration-induced nanogap formation by transmission electron microscopy,” *Appl. Phys. Lett.*, vol. 91, no. 7, pp. 1–4, 2007.

[61] C. N. Liao, K. C. Chen, W. W. Wu, L. J. Chen, and K. N. Tu, “In-situ TEM study of electromigration in Cu lines,” *AIP Conf. Proc.*, vol. 1143, no. June 2009, pp. 12–19, 2009.

[62] D. R. Strachan *et al.*, “Clean electromigrated nanogaps imaged by transmission electron microscopy,” *Nano Lett.*, vol. 6, no. 3, pp. 441–444, 2006.

[63] K. I. Bolotin, F. Kuemmeth, A. N. Pasupathy, and D. C. Ralph, “Metal-nanoparticle single-electron transistors fabricated using electromigration,” *Appl. Phys. Lett.*, vol. 84, no. 16, pp. 3154–3156, 2004.

[64] K. O’Neill, E. A. Osorio, and H. S. J. J. Van Der Zant, “Self-breaking in planar few-atom au constrictions for nanometer-spaced electrodes,” *Appl. Phys. Lett.*, vol. 90, no. 13, pp. 1–4, 2007.

[65] V. Shalabaeva *et al.*, “Vacuum deposition of high-quality thin films displaying spin transition near room temperature,” *J. Mater. Chem. C*, vol. 5, no. 18, pp. 4419–4425, 2017.

[66] K. Senthil Kumar and M. Ruben, “Emerging trends in spin crossover (SCO) based functional materials and devices,” *Coord. Chem. Rev.*, vol. 346, pp. 176–205, 2017.

[67] H. Soyer, C. Mingotaud, M. L. Boillot, and P. Delhaes, “Spin crossover of a Langmuir-Blodgett film based on an amphiphilic iron(II) complex,” *Langmuir*, vol. 14, no. 20, pp. 5890–5894, 1998.

[68] M. Ruben, J. Rojo, F. J. Romero-Salguero, L. H. Uppadine, and J. M. Lehn, “Grid-type metal ion architectures: Functional metallosupramolecular arrays,” *Angew. Chemie - Int. Ed.*, vol. 43, no. 28, pp. 3644–3662, 2004.

[69] M. Matsuda and H. Tajima, “Thin film of a spin crossover complex [Fe(dpp)2](BF4)2,” *Chem. Lett.*, vol. 36, no. 6, pp. 700–701, 2007.

[70] T. G. Gopakumar, F. Matino, H. Naggert, A. Bannwarth, F. Tuczek, and R. Berndt, “Electron-induced spin crossover of single molecules in a bilayer on gold,” *Angew. Chemie - Int. Ed.*, vol. 51, no. 25, pp. 6262–6266, 2012.

[71] H. Naggert, A. Bannwarth, S. Chemnitz, T. von Hofe, E. Quandt, and F. Tuczek, “First observation of light-induced spin change in vacuum deposited thin films of iron spin crossover complexes.,” *Dalton Trans.*, vol. 40, no. 24, pp. 6364–6366, 2011.

[72] S. Shi *et al.*, “Study of molecular spin-crossover complex Fe (phen)2 (NCS)2 thin films,” *Appl. Phys. Lett.*, vol. 95, no. 4, pp. 4–7, 2009.

[73] S. Shi *et al.*, “Study of molecular spin-crossover complex Fe (phen)2(NCS)2 thin films,” *Appl. Phys. Lett.*, vol. 95, no. 4, p. 043303, 2009.

[74] T. E. Keyes *et al.*, “Spin Transition in Arrays of Gold Nanoparticles and Spin Crossover Molecules,” *ACS Nano*, vol. 9, no. 4, pp. 4496–4507, 2015.

[75] J. Dugay *et al.*, “Phase transitions in spin-crossover thin films probed by graphene transport measurements,” *Nano Lett.*, vol. 17, no. 1, pp. 186–193, 2017.

[76] A. Nag, A. Mitra, and S. C. Mukhopadhyay, “Graphene and its sensor-based applications: A review,” *Sensors Actuators, A Phys.*, vol. 270, pp. 177–194, 2018.

[77] S. Ammu and Q. Graphics, “Graphene based chemical sensors,” no. January, 2015.

[78] E. W. Hill, A. Vijayaragahvan, and K. Novoselov, “Graphene Sensors,” *IEEE SENSORS*, vol. 11, no. 12, pp. 3161–3170, 2011.

[79] D. Qiu *et al.*, “Spin crossover-graphene nanocomposites: Facile syntheses, characterization, and magnetic properties,” *RSC Adv.*, vol. 4, no. 59, pp. 31323–31327, 2014.

[80] Y. Murashima *et al.*, “Graphene oxide and reduced graphene oxide hybrids with spin crossover iron(iii) complexes,” *Inorg. Chem. Front.*, vol. 2, no. 10, pp. 886–892, 2015.

[81] C. Cervetti *et al.*, “The classical and quantum dynamics of molecular spins on graphene,” *Nat. Mater.*, vol. 15, no. 2, pp. 164–168, 2016.

[82] L. Poggini, M. Gonidec, J. H. González-estefan, G. Pecastaings, B. Gobaut, and P. Rosa, “Vertical Tunnel Junction Embedding a Spin Crossover Molecular Film,” *Adv. Electron. Mater.*, vol. 1800204, pp. 1–8, 2018.

[83] M. D. Manrique-Juarez *et al.*, “A Bistable Microelectromechanical System Actuated by Spin-Crossover Molecules,” *Angew. Chemie - Int. Ed.*, vol. 56, no. 28, pp. 8074–8078, 2017.

[84] T. Miyamachi *et al.*, “Robust spin crossover and memristance across a single molecule,” *Nat. Commun.*, vol. 3, no. May, pp. 936–938, 2012.

[85] F. Prins *et al.*, “Room-temperature gating of molecular junctions using few-layer graphene nanogap electrodes,” *Nano Lett.*, vol. 11, no. 11, pp. 4607–4611, 2011.

[86] E. Burzurí *et al.*, “Spin-state dependent conductance switching in single molecule-graphene junctions,” *Nanoscale*, vol. 10, no. 17, pp. 7905–7911, 2018.

[87] G. Kuang *et al.*, “Mechanically-Controlled Reversible Spin Crossover of Single Fe-Porphyrin Molecules,” *ACS Nano*, vol. 11, no. 6, pp. 6295–6300, 2017.

[88] V. Meded *et al.*, “Electrical control over the Fe(II) spin crossover in a single molecule: Theory and experiment,” *Phys. Rev. B - Condens. Matter Mater. Phys.*, vol. 83, no. 24, pp. 1–13, 2011.

[89] M. S. Alam *et al.*, “Spin-state patterns in surface-grafted beads of iron(II)complexes,” *Angew. Chemie - Int. Ed.*, vol. 49, no. 6, pp. 1159–1163, 2010.

[90] H. Hao, X. Zheng, L. Song, R. Wang, and Z. Zeng, “Electrostatic spin crossover in a molecular junction of a single-molecule magnet Fe 2,” *Phys. Rev. Lett.*, vol. 108, no. 1, pp. 2–6, 2012.

[91] M. M. Khusniyarov, “How to Switch Spin-Crossover Metal Complexes at Constant Room Temperature,” *Chem. - A Eur. J.*, pp. 1–15, 2016.

[92] G. D. Harzmann, R. Frisenda, H. S. J. Van Der Zant, and M. Mayor, “Single-Molecule Spin Switch Based on Voltage-Triggered Distortion of the Coordination Sphere,” *Angew. Chemie - Int. Ed.*, vol. 54, no. 45, pp. 13425–13430, 2015.

[93] W. M. Sigmund, T. S. Bailey, M. Hara, H. Sasabe, W. Knoll, and R. S. Duran, “Langmuir-Blodgett Films of 3-Alkylpyrroles Studied by Scanning Tunneling Microscopy,” *Langmuir*, vol. 11, no. 8, pp. 3153–3160, 1995.

[94] M. B. Wieland, L. M. A. Perdigão, D. V. Kondratuk, J. N. O’Shea, H. L. Anderson, and P. H. Beton, “Height dependent molecular trapping in stacked cyclic porphyrin nanorings,” *Chem. Commun.*, vol. 50, no. 55, pp. 7332–7335, 2014.

[95] R. Holm, “The electric tunnel effect across thin insulator films in contacts,” *J. Appl. Phys.*, vol. 22, no. 5, pp. 569–574, 1951.

[96] J. G. Simmons, “Generalized Formula for the Electric Tunnel Effect between Similar Electrodes Separated by a Thin Insulating Film,” *J. Appl. Phys.*, vol. 34, no. 6, pp. 1793–1803, 1963.

[97] M. Kumar, O. Tal, R. H. M. Smit, A. Smogunov, E. Tosatti, and J. M. Van Ruitenbeek, “Shot noise and magnetism of Pt atomic chains: Accumulation of points at the boundary,” *Phys. Rev. B - Condens. Matter Mater. Phys.*, vol. 88, no. 24, pp. 1–8, 2013.

[98] E. Scheer *et al.*, “The signature of chemical valence in the electrical conduction through a single-atom contact,” *Nature*, vol. 394, no. April, pp. 154–157, 1998.

[99] M. Brandbyge *et al.*, “Atom-Sized Wires Between Two Metals,” *Phys. Rev. B*, vol. 52, no. 11, pp. 8499–8514, 1995.

[100] B. J. Van Wees *et al.*, “Quantized conductance of point contacts in a two-dimensional electron gas,” *Phys. Rev. Lett.*, vol. 60, no. 9, pp. 848–850, 1988.

[101] P. Puczkarski *et al.*, “Low-Frequency Noise in Graphene Tunnel Junctions,” *ACS Nano*, vol. 12, no. 9, pp. 9451–9460, 2018.

[102] V. Fiks, “Interaction of conduction electrons with single dislocations in metals,” *Sov. Phys. JETP*, vol. 53, no. June 1981, p. 1209, 1981.

[103] K. Doi, K. Iguchi, K. Nakamura, and A. Tachibana, “First-principle dynamical electronic characteristics of Al electromigration in the bulk, surface, and grain boundary,” *Phys. Rev. B - Condens. Matter Mater. Phys.*, vol. 67, no. 11, p. 14, 2003.

[104] T. O. Ogurtani and E. E. Oren, “Electromigration-induced void grain-boundary interactions: The mean time to failure for copper interconnects with bamboo and near-bamboo structures,” *J. Appl. Phys.*, vol. 96, no. 12, pp. 7246–7253, 2004.

[105] J. Cho and C. V. Thompson, “Grain size dependence of electromigration-induced failures in narrow interconnects,” *Appl. Phys. Lett.*, vol. 54, no. 25, pp. 2577–2579, 1989.

[106] J. R. Black, “Electromigration—A Brief Survey and Some Recent Results,” *IEEE Trans. Electron Devices*, vol. 16, no. 4, pp. 338–347, 1969.

[107] J. R. Black, “Electromigration Failure Modes in Aluminum Metallization for Semiconductor Devices,” *Proc. IEEE*, vol. 57, no. 9, pp. 1587–1594, 1969.

[108] L. Pukenas *et al.*, “Bead-like structures and self-assembled,” *J. Mater. Chem. C*, vol. 3, pp. 7890–7896, 2015.

[109] S. Brooker, “Spin crossover with thermal hysteresis: practicalities and lessons learnt,” *Chem. Soc. Rev.*, vol. 44, no. 10, pp. 2880–2892, 2015.

[110] P. Gütlich, Y. Garcia, and H. A. Goodwin, “Spin crossover phenomena in Fe(II) complexes,” *Chem. Soc. Rev.*, vol. 29, no. 6, pp. 419–427, 2000.

[111] L.Cambri, “Über die magnetische Susceptibilität der komplexen Verbindungen,” *Eur. J. Inorg. Chem.*, vol. 64, no. 10, pp. 2591–2598, 1931.

[112] P. Stock *et al.*, “Molecular Spin Crossover in Slow Motion: Light-Induced Spin-State Transitions in Trigonal Prismatic Iron(II) Complexes,” *Inorg. Chem.*, vol. 55, no. 11, pp. 5254–5265, 2016.

[113] S. Ossinger *et al.*, “Vacuum-Evaporable Spin-Crossover Complexes in Direct Contact with a Solid Surface: Bismuth versus Gold,” *J. Phys. Chem. C*, vol. 121, no. 2, pp. 1210–1219, 2017.

[114] P. Weinberger and M. Grunert, “Variable temperature far and mid FT-IR as a valuable tool to determine the spin transition temperature of iron(II) spin-crossover coordination compounds,” *Vib. Spectrosc.*, vol. 34, no. 1, pp. 175–186, 2004.

[115] I. A. Gural’Skiy *et al.*, “Spin crossover composite materials for electrothermomechanical actuators,” *J. Mater. Chem. C*, vol. 2, no. 16, pp. 2949–2955, 2014.

[116] J. Kröber, E. Codjovi, O. Kahn, F. Grolière, and C. Jay, “A Spin Transition System with a Thermal Hysteresis at Room Temperature,” *J. Am. Chem. Soc.*, vol. 115, no. 21, pp. 9810–9811, 1993.

[117] P. Masárová, P. Zoufalý, I. N. Ján Moncol, M. G. Ján Pavlik, R. B. Zdeněk Trávníček, and I. Šalitroš, “Spin Crossover and High Spin Electroneutral Mononuclear Iron(III) Schiff Base Complexes involving Terminal Pseudohalido Ligands Petra,” *New J. Chem.*, vol. 39, no. 1, pp. 508–519, 2015.

[118] I. Šalitroš, N. T. Madhu, R. Boča, J. Pavlik, and M. Ruben, “Room-temperature spin-transition iron compounds,” *Monatshefte fur Chemie*, vol. 140, no. 7, pp. 695–733, 2009.

[119] P. Gütlich, A. Hauser, and H. Spiering, “Thermal and Optical Switching of Iron(II) Complexes,” *Angew. Chemie Int. Ed. English*, vol. 33, no. 20, pp. 2024–2054, 1994.

[120] J. A. Real, A. B. Gaspar, and M. C. Muñoz, “Thermal, pressure and light switchable spin-crossover materials.,” *Dalton Trans.*, no. 12, pp. 2062–2079, 2005.

[121] M. A. Halcrow, “Trapping and manipulating excited spin states of transition metal compounds.,” *Chem. Soc. Rev.*, vol. 37, no. 2, pp. 278–89, 2008.

[122] J. K. McCusker, K. N. Walda, R. C. Dunn, J. D. Simon, D. Magde, and D. N. Hendrickson, “Sub-Picosecond ΔS = 2 Intersystem Crossing in Low-Spin Ferrous Complexes,” *J. Am. Chem. Soc.*, vol. 114, no. 17, pp. 6919–6920, 1992.

[123] J. K. McCusker, A. L. Rheingold, and D. N. Hendrickson, “Variable-Temperature Studies of Laser-Initiated 5T2→1A1 Intersystem Crossing in Spin-Crossover Complexes: Empirical Correlations between Activation Parameters and Ligand Structure in a Series of Polypyridyl Ferrous Complexes,” *Inorg. Chem.*, vol. 35, no. 7, pp. 2100–2112, 1996.

[124] M. A. Halcrow, *Spin-Crossover Materials: Properties and Applications*, 1st ed. Chichester: John Wiley & Sons, 2013.

[125] M. Wuttig and N. Yamada, “Phase-change materials for rewriteable data storage,” *Nat. Mater.*, vol. 6, pp. 824–832, 2007.

[126] M. H. R. Lankhorst, B. W. S. M. M. Ketelaars, and R. A. M. Wolters, “Low-cost and nanoscale non-volatile memory concept for future silicon chips,” *Nat. Mater.*, vol. 4, no. 4, pp. 347–352, 2005.

[127] I. Giannopoulos *et al.*, “8-bit Precision In-Memory Multiplication with Projected Phase-Change Memory,” *Tech. Dig. - Int. Electron Devices Meet. IEDM*, vol. 2018-Decem, pp. 27.7.1-27.7.4, 2019.

[128] J. F. Creemer *et al.*, “Microhotplates with TiN heaters,” *Sensors Actuators, A Phys.*, vol. 148, no. 2, pp. 416–421, 2008.

[129] O. Kahn and C. J. Martinez, “Spin-Transition Polymers: From Molecular Materials Toward Memory Devices,” *Science (80-.).*, vol. 279, no. 5347, pp. 44–48, 1998.

[130] A. Rotaru, I. a. Gural’skiy, G. Molnár, L. Salmon, P. Demont, and A. Bousseksou, “Spin state dependence of electrical conductivity of spin crossover materials,” *Chem. Commun.*, vol. 48, no. 35, p. 4163, 2012.

[131] M. El Hasnaoui, K. Abazine, M. E. Achour, and L. C. Costa, “Mott-hopping processes in polymethylmethacrylate matrices filled with polypyrrole particles,” *J. Optoelectron. Adv. Mater.*, vol. 18, no. 3–4, pp. 389–393, 2016.

[132] N.F.Mott and E.A. Davis, *Electronics Process in Noncrystalline Materials*, 2nd ed. Oxford: Oxford University Publishing, 1971.

[133] C. Lefter *et al.*, “Charge Transport and Electrical Properties of Spin Crossover Materials: Towards Nanoelectronic and Spintronic Devices,” *Magnetochemistry*, vol. 2, no. 1, p. 18, 2016.

[134] P. N. Murgatroyd, “Theory of space-charge-limited current enhanced by Frenkel effect,” *J. Phys. D. Appl. Phys.*, vol. 3, no. 2, pp. 151–156, 1970.

[135] R. O. Jones and O. Gunnarsson, “The density functional formalism, its applications and prospects,” *Rev. Mod. Phys.*, vol. 61, no. 3, pp. 689–746, 1989.

[136] F. Prins, M. Monrabal-Capilla, E. A. Osorio, E. Coronado, and H. S. J. Van Der Zant, “Room-temperature electrical addressing of a bistable spin-crossover molecular system,” *Adv. Mater.*, vol. 23, no. 13, pp. 1545–1549, 2011.

[137] V. Niel, A. B. Gaspar, M. C. Mun, R. Ballesteros, and A. Real, “Spin Crossover Behavior in the Iron (II) − 2-pyridyl [1,2,3] triazolo [1,5-a] pyridine System: X-ray Structure, Calorimetric, Magnetic, and Photomagnetic Studies,” *Society*, vol. 42, no. 15, pp. 200–202, 2003.

[138] D. Aravena and E. Ruiz, “Coherent transport through spin-crossover single molecules,” *J. Am. Chem. Soc.*, vol. 134, no. 2, pp. 777–779, 2012.

[139] E. Burzurí *et al.*, “Spin-state dependent conductance switching in single molecule-graphene junctions,” *Nanoscale*, vol. 10, no. 17, pp. 7905–7911, 2018.

[140] A. C. Aragonès *et al.*, “Large Conductance Switching in a Single-Molecule Device through Room Temperature Spin-Dependent Transport,” *Nano Lett.*, vol. 16, no. 1, pp. 218–226, 2016.

[141] H. Schift and A. Kristensen, “Nanoimprint Lithography – Patterning of Resists Using Molding,” *Springer Handb. Nanotechnol.*, pp. 271–312, 2010.

[142] L. . Heyderman, H. Schift, C. David, J. Gobrecht, and T. Schweizer, “Flow behaviour of thin polymer films used for hot embossing lithography,” *Microelectron. Eng.*, vol. 54, no. 3–4, pp. 229–245, 2000.

[143] N. Chaix *et al.*, “Influence of the molecular weight and imprint conditions on the formation of capillary bridges in nanoimprint lithography.,” *Nanotechnology*, vol. 17, no. 16, pp. 4082–4087, 2006.

[144] F. Lazzarino, C. Gourgon, P. Schiavone, and C. Perret, “Mold deformation in nanoimprint lithography,” *J. Vac. Sci. Technol. B Microelectron. Nanom. Struct.*, vol. 22, no. 6, p. 3318, 2004.

[145] J. L. Keddie, R. A. L. Jones, and R. A. Cory, “Size-Dependent Depression of the Glass Transition Temperature in Polymer Films .,” *Europhys. Lett.*, vol. 27, no. 1, pp. 59–64, 1994.

[146] P. Carlberg, M. Graczyk, E. Sarwe, I. Maximov, M. Beck, and L. Montelius, “Lift-off process for nanoimprint lithography,” *Microelectron. Eng.*, vol. 68, pp. 203–207, 2003.

[147] S. Girod, J. L. Bubendorff, F. Montaigne, L. Simon, D. Lacour, and M. Hehn, “Real time atomic force microscopy imaging during nanogap formation by electromigration,” *Nanotechnology*, vol. 23, no. 36, p. 365302, 2012.

[148] H. S. J. Van Der Zant *et al.*, “Molecular three-terminal devices: Fabrication and measurements,” *Faraday Discuss.*, vol. 131, pp. 347–356, 2006.

[149] G. Esen and M. S. Fuhrer, “Temperature control of electromigration to form gold nanogap junctions,” *Appl. Phys. Lett.*, vol. 87, no. 26, pp. 1–3, 2005.

[150] S. M. Kuo and K. L. Lin, “Recrystallization under electromigration of a solder alloy,” *J. Appl. Phys.*, vol. 106, no. 2, pp. 1–5, 2009.

[151] C. Schirm, M. Matt, F. Pauly, J. C. Cuevas, P. Nielaba, and E. Scheer, “A current-driven single-atom memory,” *Nat. Nanotechnol.*, vol. 8, no. 9, pp. 645–648, 2013.

[152] A. Umeno and K. Hirakawa, “Nonthermal origin of electromigration at gold nanojunctions in the ballistic regime,” *Appl. Phys. Lett.*, vol. 94, no. 16, pp. 1–4, 2009.

[153] M. L. Trouwborst, S. J. Van Der Molen, and B. J. Van Wees, “The role of Joule heating in the formation of nanogaps by electromigration,” *J. Appl. Phys.*, vol. 99, no. 11, 2006.

[154] S. Bae, J. H. Judy, I. F. Tsu, and E. S. Murdock, “Electromigration-induced failure of single layered NiFe Permalloy thin films for a giant magnetoresistive read head,” *J. Appl. Phys.*, vol. 90, no. 5, pp. 2427–2432, 2001.

[155] S. Günther, A. Hitzke, and R. J. Behm, “Low adatom mobility on the (1 x 2) missing-row reconstructed Au (110) surface,” *Surf. Rev. Lett.*, vol. 4, no. 6, pp. 1103–1108, 1997.

[156] F. Pauly, M. Dreher, J. K. Viljas, M. Häfner, J. C. Cuevas, and P. Nielaba, “Theoretical

analysis of the conductance histograms and structural properties of Ag, Pt, and Ni nanocontacts," *Phys. Rev. B - Condens. Matter Mater. Phys.*, vol. 74, no. 23, pp. 1–21, 2006.

[157] M. R. Calvo, J. Fernández-Rossier, J. J. Palacios, D. Jacob, D. Natelson, and C. Untiedt, "The Kondo effect in ferromagnetic atomic contacts," *Nature*, vol. 458, no. 7242, pp. 1150–1153, 2009.

[158] J. B. Beaufrand, J. F. Dayen, N. T. Kemp, A. Sokolov, and B. Doudin, "Magnetoresistance signature of resonant states in electromigrated Ni nanocontacts," *Appl. Phys. Lett.*, vol. 98, no. 14, pp. 1–3, 2011.

[159] S. F. Shi, K. I. Bolotin, F. Kuemmeth, and D. C. Ralph, "Temperature dependence of anisotropic magnetoresistance and atomic rearrangements in ferromagnetic metal break junctions," *Phys. Rev. B - Condens. Matter Mater. Phys.*, vol. 76, no. 18, pp. 1–5, 2007.

[160] A. L. V. De Parga *et al.*, "Electron resonances in sharp tips and their role in tunneling spectroscopy," *Phys. Rev. Lett.*, vol. 80, no. 2, pp. 357–360, 1998.

[161] M. Uda, A. Nakamura, T. Yamamoto, and Y. Fujimoto, "Work function of polycrystalline Ag, Au and Al," *J. Electron Spectros. Relat. Phenomena*, vol. 88–91, pp. 643–648, 2003.

[162] R. Schuster, J. V. Barth, J. Wintterlin, R. J. Behm, and G. Ertl, "Distance dependence and corrugation in barrier-height measurements on metal surfaces," *Ultramicroscopy*, vol. 42–44, no. PART 1, pp. 533–540, 1992.

[163] C. A. Szafranski, W. Tanner, P. E. Laibinis, and R. L. Garrell, "Surface-enhanced Raman spectroscopy of aromatic thiols and disulfides on gold electrodes," *Langmuir*, vol. 14, no. 13, pp. 3570–3579, 1998.

[164] R. G. Nuzzo, B. R. Zegarski, and L. H. DuBois, "Fundamental Studies of the Chemisorption of Organosulfur Compounds on Au(111). Implications for Molecular Self-Assembly on Gold Surfaces," *J. Am. Chem. Soc.*, vol. 109, no. 3, pp. 733–740, 1987.

[165] F. K. Huang, R. C. Horton, D. C. Myles, and R. L. Garrell, "Selenolates as Alternatives to Thiolates for Self-Assembled Monolayers: A SERS Study," *Langmuir*, vol. 14, no. 17, pp. 4802–4808, 2002.

[166] A. Mishchenko *et al.*, "Influence of conformation on conductance of biphenyl-dithiol

single-molecule contacts," *Nano Lett.*, vol. 10, no. 1, pp. 156–163, 2010.

[167] M. Carini *et al.*, "High conductance values in π-folded molecular junctions," *Nat. Commun.*, vol. 8, no. 15195, 2017.

[168] J. M. Beebe, B. Kim, J. W. Gadzuk, C. D. Frisbie, and J. G. Kushmerick, "Transition from direct tunneling to field emission in metal-molecule-metal junctions," *Phys. Rev. Lett.*, vol. 97, no. 2, pp. 1–4, 2006.

[169] J. M. Beebe, B. Kim, C. D. Frisbie, and J. G. Kushmerick, "Measuring Relative Barrier Heights in Transition Voltage Spectroscopy," *ACS Nano*, vol. 2, no. 5, pp. 827–832, 2008.

[170] H. B. Akkerman and B. De Boer, "Electrical conduction through single molecules and self-assembled monolayers," *J. Phys. Condens. Matter*, vol. 20, no. 1, 2008.

[171] E. H. Huisman, C. M. Guédon, B. J. Van Wees, and S. J. Van Der Molen, "Interpretation of transition voltage spectroscopy," *Nano Lett.*, vol. 9, no. 11, pp. 3909–3913, 2009.

[172] S. Guo, J. Hihath, I. Díez-Pérez, and N. Tao, "Measurement and statistical analysis of single-molecule current-voltage characteristics, transition voltage spectroscopy, and tunneling barrier height," *J. Am. Chem. Soc.*, vol. 133, no. 47, pp. 19189–19197, 2011.

[173] C. A. Brito Da Silva, F. A. De Araujo Pinheiro, and J. Del Nero, "Organic nano-devices composed by carbon nanotube/oligophenylenes/carbon nanotube junctions: Transition-voltage spectroscopy, applications and chirality versus geometry," *J. Nanosci. Nanotechnol.*, vol. 16, no. 9, pp. 9771–9778, 2016.

[174] C. A. Brito Silva, S. J. S. Da Silva, E. R. Granhen, J. F. P. Leal, J. Del Nero, and F. A. Pinheiro, "Electronic transport in biphenyl single-molecule junctions with carbon nanotubes electrodes: The role of molecular conformation and chirality," *Phys. Rev. B - Condens. Matter Mater. Phys.*, vol. 82, no. 8, pp. 14–17, 2010.

[175] C. A. Brito Silva, S. J. S. Da Silva, J. F. P. Leal, F. A. Pinheiro, and J. Del Nero, "Electronic transport in oligo-para-phenylene junctions attached to carbon nanotube electrodes: Transition-voltage spectroscopy and chirality," *Phys. Rev. B - Condens. Matter Mater. Phys.*, vol. 83, no. 24, pp. 1–6, 2011.

[176] M. Araidai and M. Tsukada, "Theoretical calculations of electron transport in molecular junctions: Inflection behavior in Fowler-Nordheim plot and its origin," *Phys. Rev. B - Condens. Matter Mater. Phys.*, vol. 81, no. 23, pp. 1–7, 2010.

[177] K. Wu, M. Bai, S. Sanvito, and S. Hou, “Quantitative interpretation of the transition voltages in gold-poly(phenylene) thiol-gold molecular junctions,” *J. Chem. Phys.*, vol. 139, no. 19, pp. 1–7, 2013.

[178] J. Chen, T. Markussen, and K. S. Thygesen, “Quantifying transition voltage spectroscopy of molecular junctions: Ab initio calculations,” *Phys. Rev. B - Condens. Matter Mater. Phys.*, vol. 82, no. 12, pp. 2–5, 2010.

[179] C. Bruot, J. Hihath, and N. Tao, “Mechanically controlled molecular orbital alignment in single molecule junctions,” *Nat. Nanotechnol.*, vol. 7, no. 1, pp. 35–40, 2012.

[180] S. T. Schneebeli *et al.*, “Single-molecule conductance through multiple π-π-stacked benzene rings determined with direct electrode-to-benzene ring connections,” *J. Am. Chem. Soc.*, vol. 133, no. 7, pp. 2136–2139, 2011.

[181] J. D. Slinker, N. B. Muren, S. E. Renfrew, and J. K. Barton, “DNA charge transport over 34 nm,” *Nat. Chem.*, vol. 3, no. 3, pp. 228–233, 2011.

[182] Z. Zhang, H. Huang, X. Yang, and L. Zang, “Tailoring electronic properties of graphene by π-π Stacking with aromatic molecules,” *J. Phys. Chem. Lett.*, vol. 2, no. 22, pp. 2897–2905, 2011.

[183] S. Wu *et al.*, “Molecular junctions based on aromatic coupling,” *Nat. Nanotechnol.*, vol. 3, no. 9, pp. 569–574, 2008.

[184] H. Song, Y. Kim, Y. H. Jang, H. Jeong, M. A. Reed, and T. Lee, “Observation of molecular orbital gating,” *Nature*, vol. 462, no. 7276, pp. 1039–1043, 2009.

[185] P. Masárová *et al.*, “Spin crossover and high spin electroneutral mononuclear iron(III) Schiff base complexes involving terminal pseudohalido ligands,” *New J. Chem.*, vol. 39, no. 1, pp. 508–519, 2015.

[186] M. Bernien *et al.*, “Spin crossover in a vacuum-deposited submonolayer of a molecular iron(II) complex,” *J. Phys. Chem. Lett.*, vol. 3, no. 23, pp. 3431–3434, 2012.

[187] B. Warner *et al.*, “Temperature- and light-induced spin crossover observed by X-ray spectroscopy on isolated Fe(II) complexes on gold,” *J. Phys. Chem. Lett.*, vol. 4, no. 9, pp. 1546–1552, 2013.

[188] T. Jasper-Toennies, M. Gruber, S. Karan, H. Jacob, F. Tuczek, and R. Berndt, “Robust and

Selective Switching of an FeIIISpin-Crossover Compound on Cu2N/Cu(100) with Memristance Behavior," *Nano Lett.*, vol. 17, no. 11, pp. 6613–6619, 2017.

[189] Z. J. Donhauser *et al.*, "Conductance switching in single molecules through conformational changes," *Science (80-.).*, vol. 292, no. 5525, pp. 2303–2307, 2001.

[190] R. A. Wassel, R. R. Fuierer, N. Kim, and C. B. Gorman, "Stochastic Variation in Conductance on the Nanometer Scale: A General Phenomenon," *Nano Lett.*, vol. 3, no. 11, pp. 1617–1620, 2003.

[191] H. He, J. Zhu, N. J. Tao, L. A. Nagahara, I. Amlani, and R. Tsui, "A conducting polymer nanojunction switch," *J. Am. Chem. Soc.*, vol. 123, no. 31, pp. 7730–7731, 2001.

[192] C. C. Kaun and T. Seideman, "Current-driven oscillations and time-dependent transport in nanojunctions," *Phys. Rev. Lett.*, vol. 94, no. 22, pp. 1–4, 2005.

[193] G. K. Ramachandran, T. J. Hopson, A. M. Rawtett, L. A. Nagahara, A. Primak, and S. M. Lindsay, "A bond-fluctuation mechanism for stochastic switching in wired molecules," *Science (80-.).*, vol. 300, no. 5624, pp. 1413–1416, 2003.

[194] A. H. Jaafar, A. Gee, and N. T. Kemp, "Nanorods vs Nanoparticles: A Comparison Study of Au/ZnO-PMMA/Au Non-volatile Memory Devices showing the importance of Nanostructure Geometry on Conduction Mechanisms and Switching Properties," *IEEE Trans. Nanotechnol.*, 2019.

[195] N. Baadji, M. Piacenza, T. Tugsuz, F. Della Sala, G. Maruccio, and S. Sanvito, "Electrostatic spin crossover effect in polar magnetic molecules," *Nat. Mater.*, vol. 8, no. 10, pp. 813–817, 2009.

[196] K. Scheil *et al.*, "Switching of an Azobenzene-Tripod Molecule on Ag(111)," *J. Phys. Chem. Lett.*, vol. 7, no. 11, pp. 2080–2084, 2016.

[197] G. J. Ashwell *et al.*, "Synthesis of covalently linked molecular bridges between silicon electrodes in CMOS-based arrays of vertical Si/SiO 2/Si nanogaps," *Angew. Chemie - Int. Ed.*, vol. 50, no. 37, pp. 8722–8726, 2011.

[198] V. Shalabaeva *et al.*, "Room temperature current modulation in large area electronic junctions of spin crossover thin films," *Appl. Phys. Lett.*, vol. 112, no. 1, p. 013301, 2018.

[199] S. Caneva *et al.*, "Mechanically controlled quantum interference in graphene break

junctions," *Nat. Nanotechnol.*, vol. 13, no. 12, pp. 1126–1131, 2018.

[200] P. Stegmann, B. Sothmann, A. Hucht, and J. König, "Detection of interactions via generalized factorial cumulants in systems in and out of equilibrium," *Phys. Rev. B - Condens. Matter Mater. Phys.*, vol. 92, no. 15, pp. 1–7, 2015.

[201] A. Kurzmann *et al.*, "Optical Detection of Single-Electron Tunneling into a Semiconductor Quantum Dot," *Phys. Rev. Lett.*, vol. 122, no. 24, p. 247403, 2019.

[202] Z. Wen, L. Zhou, J. F. Cheng, S. J. Li, W. L. You, and X. Wang, "Spin crossover and high spin filtering behavior in Co-Pyridine and Co-Pyrimidine molecules," *J. Phys. Condens. Matter*, vol. 30, no. 10, 2018.

[203] Y. Gu, Y. Hu, J. Huang, Q. Li, and J. Yang, "Spin-Crossover and Coherent Transport Behaviors of a Six-Coordinate Iron(II) Complex with a N4O2 Donor Set," *J. Phys. Chem. C*, vol. 123, no. 26, pp. 16366–16372, 2019.

[204] A. Hauser, "Intersystem crossing in the [Fe(ptz)6](BF4)2 spin crossover system (ptz=1-propyltetrazole)," *J. Chem. Phys.*, vol. 94, no. 4, pp. 2741–2748, 2002.

[205] S. Thies *et al.*, "Light-induced spin change by photodissociable external ligands: A new principle for magnetic switching of molecules," *J. Am. Chem. Soc.*, vol. 133, no. 40, pp. 16243–16250, 2011.

[206] M. Enamullah, W. Linert, V. Gutmann, and R. F. Jameson, "Spin-transition behaviour of transition metal complexes with 2,6-bis-(benzimidazol-2'-yl)-pyridine induced by deprotonation of the complex," *Monatshefte für Chemie Chem. Mon.*, vol. 125, no. 12, pp. 1301–1309, 1994.

[207] S. Thies *et al.*, "Coordination-induced spin crossover (CISCO) through axial bonding of substituted pyridines to nickel-porphyrins: σ-Donor versus π-acceptor effects," *Chem. - A Eur. J.*, vol. 16, no. 33, pp. 10074–10083, 2010.

[208] W. S. Caughey, W. Y. Fujimoto, and B. P. Johnson, "Substituted Deuteroporphyrins. II. Substituent Effects on Electronic Spectra, Nitrogen Basicities, and Ligand Affinities," *Biochemistry*, vol. 5, no. 12, pp. 3830–3843, 1966.

[209] N. G. White, H. L. C. Feltham, C. Gandolfi, M. Albrecht, and S. Brooker, "Towards Langmuir-Blodgett films of magnetically interesting materials: Solution equilibria in amphiphilic iron(II) complexes of a triazole-containing ligand," *Dalt. Trans.*, vol. 39, no.

15, pp. 3751–3758, 2010.

[210] M. Quesada *et al.*, “A molecule-based nanoporous material showing tuneable spin-crossover behavior near room temperature,” *Adv. Mater.*, vol. 19, no. 10, pp. 1397–1402, 2007.

[211] M. Ohba *et al.*, “Bidirectional Chemo-Switching of Spin State in a Microporous Framework,” *Angew. Chemie*, vol. 121, no. 26, pp. 4861–4865, 2009.